

NATIONAL BUREAU OF STANDARDS REPORT

9821

INVESTIGATION OF THE DIRECTIONAL EFFECTS IN THE STRESS CORROSION OF ALUMINUM ALLOYS

Final Report

April 22, 1968



U.S. DEPARTMENT OF COMMERCE
NATIONAL BUREAU OF STANDARDS

THE NATIONAL BUREAU OF STANDARDS

The National Bureau of Standards¹ provides measurement and technical information services essential to the efficiency and effectiveness of the work of the Nation's scientists and engineers. The Bureau serves also as a focal point in the Federal Government for assuring maximum application of the physical and engineering sciences to the advancement of technology in industry and commerce. To accomplish this mission, the Bureau is organized into three institutes covering broad program areas of research and services:

THE INSTITUTE FOR BASIC STANDARDS . . . provides the central basis within the United States for a complete and consistent system of physical measurements, coordinates that system with the measurement systems of other nations, and furnishes essential services leading to accurate and uniform physical measurements throughout the Nation's scientific community, industry, and commerce. This Institute comprises a series of divisions, each serving a classical subject matter area:

—Applied Mathematics—Electricity—Metrology—Mechanics—Heat—Atomic Physics—Physical Chemistry—Radiation Physics—Laboratory Astrophysics²—Radio Standards Laboratory,² which includes Radio Standards Physics and Radio Standards Engineering—Office of Standard Reference Data.

THE INSTITUTE FOR MATERIALS RESEARCH . . . conducts materials research and provides associated materials services including mainly reference materials and data on the properties of materials. Beyond its direct interest to the Nation's scientists and engineers, this Institute yields services which are essential to the advancement of technology in industry and commerce. This Institute is organized primarily by technical fields:

—Analytical Chemistry—Metallurgy—Reactor Radiations—Polymers—Inorganic Materials—Cryogenics²—Office of Standard Reference Materials.

THE INSTITUTE FOR APPLIED TECHNOLOGY . . . provides technical services to promote the use of available technology and to facilitate technological innovation in industry and government. The principal elements of this Institute are:

—Building Research—Electronic Instrumentation—Technical Analysis—Center for Computer Sciences and Technology—Textile and Apparel Technology Center—Office of Weights and Measures—Office of Engineering Standards Services—Office of Invention and Innovation—Office of Vehicle Systems Research—Clearinghouse for Federal Scientific and Technical Information³—Materials Evaluation Laboratory—NBS/GSA Testing Laboratory.

¹ Headquarters and Laboratories at Gaithersburg, Maryland, unless otherwise noted; mailing address Washington, D. C., 20234.

² Located at Boulder, Colorado, 80302.

³ Located at 5285 Port Royal Road, Springfield, Virginia 22151.

NATIONAL BUREAU OF STANDARDS REPORT

NBS PROJECT

3120445

April 22 1968

NBS REPORT

9821

Final Report

INVESTIGATION OF THE DIRECTIONAL EFFECTS IN THE STRESS CORROSION OF ALUMINUM ALLOYS

by

J. Kruger - G. M. Ugiansky

J. R. Ambrose

Contributors:

H. L. Logan - S. W. Stiefel

E. Escalante - A. W. Ruff

A. C. Fraker - L. P. Skolnick

for

National Aeronautics and Space Administration

George C. Marshall Space Flight Center

Huntsville, Alabama

Contract H-2151A

Control 1-6-54-01046-01 (1F)

IMPORTANT NOTICE

NATIONAL BUREAU OF STANDARDS
for use within the Government. It
and review. For this reason, the
whole or in part, is not authorized
Bureau of Standards, Washington
the Report has been specifically p

Approved for public release by the
Director of the National Institute of
Standards and Technology (NIST)
on October 9, 2015

accounting documents intended
subjected to additional evaluation
listing of this Report, either in
Office of the Director, National
the Government agency for which
lies for its own use.



U.S. DEPARTMENT OF COMMERCE

NATIONAL BUREAU OF STANDARDS

ABSTRACT

INVESTIGATION OF THE DIRECTIONAL EFFECTS IN THE STRESS CORROSION OF ALUMINUM ALLOYS

Studies of the relative effects of various metallurgical and electrochemical factors on the directional susceptibility to stress corrosion cracking of a 7075-T651 aluminum alloy plate have been conducted. The factors investigated that could have any possible bearing on the directional susceptibility were as follows: 1) preferred orientation; 2) grain morphology; 3) segregation; 4) precipitate and dislocation configuration; and 5) electrochemical effects.

The role of grain morphology was found to be of paramount importance in controlling crack propagation. It was found that a slow rate of propagation along boundaries parallel to the applied stress, and the fact that the intergranular crack must propagate primarily in this direction accounts for the low susceptibility of longitudinally stressed specimens.

This result suggests that the threshold stress for short transverse specimens approximates the stress necessary to crack grain boundaries normal to the applied stress, and the threshold stress for longitudinal specimens approximates the stress needed to crack boundaries parallel to the applied stress.

Preferred orientation was found to be of secondary importance when

compared to the effect of grain morphology. A high degree of preferred orientation, rather than any specific slip plane orientations, was found to increase the susceptibility of specimens with the same grain morphology.

Electrochemical experiments showed that current flow was greater in short transverse stressed specimens than in longitudinal ones showing the creation of more active areas in the former. Polarization effects due to stress were also minor when stressing longitudinally.

No directional effects related to segregation or precipitate or dislocation configurations were found.

ACKNOWLEDGMENTS

We gratefully acknowledge the invaluable contributions of the following: Mrs. M. Giles and Mr. D. Vieth of the National Bureau of Standards for performing the electron probe microanalyses; Dr. H. Frankel and Dr. T.D. Sciacca of the Goddard Space Flight Center of the National Aeronautics and Space Administration for permission to use their X-ray texture diffractometer; and the Japan Electron Optics Co., Ltd., for making available their scanning type electron microscope.

This report was prepared by the Corrosion Section, National Bureau of Standards under Contract No. H-2151A "Investigation of the Directional Effects in the Stress Corrosion of Aluminum Alloys" for the George C. Marshall Space Flight Center of the National Aeronautics and Space Administration. The work was administered under the technical direction of the Propulsion and Vehicle Engineering Laboratory, Materials Division of the George C. Marshall Space Flight Center with D.B. Franklin acting as project manager.

TABLE OF CONTENTS

<u>Chapter</u>	<u>Page</u>
ABSTRACT.....	ii
ACKNOWLEDGMENTS.....	iv
I. INTRODUCTION.....	1
II. MATERIAL EVALUATION.....	4
III. EFFECT OF PREFERRED ORIENTATION ON SUSCEPTIBILITY.....	7
IV. EFFECT OF GRAIN MORPHOLOGY ON SUSCEPTIBILITY.....	17
V. EFFECT OF SEGREGATION ON SUSCEPTIBILITY.....	25
VI. EFFECT OF ELECTROCHEMICAL FACTORS ON SUSCEPTIBILITY...	28
VII. EFFECT OF PRECIPITATES AND DISLOCATION CONFIGURATIONS ON SUSCEPTIBILITY.....	35
VIII. CONCLUSIONS.....	46
LITERATURE CITED.....	48
TABLES.....	52
FIGURES.....	59

Chapter I

INTRODUCTION

Stress corrosion cracking may be defined as a complex interaction between a sustained tensile stress and a corrosive attack resulting in cracking and premature brittle failure of a normally ductile material. The crack may follow either a transgranular (through the grain interiors) or an intergranular (through the grain boundaries) path. In the aluminum alloys, the crack path is characteristically intergranular.

During the fabrication of some wrought, high strength aluminum alloy products, the grains become very elongated and do not significantly recrystallize on further heat treatments (Figure 1). These products also retain a high degree of preferred orientation (texture). The reported instances of stress corrosion cracking failures⁽¹⁾ in aluminum alloys have resulted from residual or assembly tensile stresses acting in the short transverse direction relative to the grain structure (Figure 1). Longitudinal tensile stresses, on the other hand, have rarely caused stress corrosion problems. Hence, it is very important to understand in more detail this great dependence of stress corrosion cracking susceptibility on stress direction in the wrought, high strength aluminum alloys

The purpose of the studies described in this report was to determine the reasons for the great dependence in the stress corrosion cracking susceptibility on stress direction in wrought, high strength aluminum

alloys. Most of the studies concentrated on 7075-T6. However, some studies were also carried out on 7075-T73, 2219-T37 and 2219-T87.

The strategy of attack was to explore all possible reasons and factors that could influence the directional effects. This final report describes in different chapters each of these possible sources of directional differences. Many different and powerful tools of modern materials science were required to do this. The possible origins of directionality differences and the tools employed were as follows:

- 1) The effect of preferred orientation--X-ray texture diffractometer.
- 2) The effect of grain morphology--scanning electron microscopy and optical microscopy.
- 3) The effect of segregation--electron probe microanalysis.
- 4) The effect of precipitates and dislocation configurations--thin foil transmission electron microscopy (these studies were carried out by Dr. A. Fraker and Dr. A.W. Ruff, Jr.).
- 5) Electrochemical factors--potentiostatic techniques.

On the basis of these many varied studies it was possible to determine that the most significant factor influencing the directional susceptibility to stress corrosion cracking was the effect of grain morphology. The other factors play no role or, at most, a minor one that is related to grain morphology.

Publications and talks resulting from this work thus far are the following:

Talks

1. Ugiansky, G.M., "Effect of Preferred Orientation on Stress Corrosion Susceptibility" as panel member on Metallurgical Aspects, Work Shop on Stress Corrosion of High Strength Aluminum Alloys, Naval Air Engineering Center, Phila., Pa., June 1967.
2. Ugiansky, G.M., "Directional Effects on the Stress Corrosion of a 7075-T651 Aluminum Alloy Plate", Engineering Materials Seminar, University of Maryland, November 1967 and February 1968.
3. Ugiansky, G.M., Skolnick, L.P., and Stiefel, S.W., "Directional Effects in the Stress Corrosion of a 7075-T651 Aluminum Alloy Plate", AIME Annual Meeting, New York, New York, February 26, 1968.

Publications

1. Ugiansky, G.M., Skolnick, L.P., Kruger, J., and Stiefel, S.W., "The Rate-Controlling Step in Stress Corrosion Cracking", Scripta Metallurgica, in press.
2. Ugiansky, G.M., "Directional Effects in the Stress Corrosion Cracking of a 7075-T651 Aluminum Alloy Plate", M.S. Thesis at University of Maryland, December 1967.

Work is now underway to prepare papers on the following:

1. Preferred orientation and grain morphology results.
2. Precipitate and dislocation studies.
3. The electrochemical studies.

Chapter II

MATERIAL EVALUATION

A. Introduction

In order to confirm that the material had the normal properties for that alloy and heat treatment, both mechanical and stress corrosion properties were checked.

B. Experimental Details

The material used for the research was a 2.5 inch thick plate of 7075-T651 aluminum alloy. The composition of the alloy was: Al, 5.23 Zn, 2.13 Mg, 1.61 Cu, 0.184 Cr, 0.183 Fe, 0.040 Mn, 0.035 Ti, 0.035 Si.

The material was evaluated to confirm both the mechanical properties and the stress corrosion susceptibility of specimens of three orientations (Figure 1) with respect to the rolling direction. For all material evaluation tests, a specimen of dimensions shown in Figure 2 was machined such that the reduced section was from the center of the plate. After machining, the specimens were polished parallel to the axes with number 600 silicon carbide paper as a final preparation before testing.

Mechanical properties were determined for at least two specimens from each direction using a Tinius-Olsen tensile test machine at a constant strain rate of 0.005 in/min. Plotting of the engineering stress-strain curves was done automatically utilizing an extensometer attached to the reduced section of the specimen. After testing, the 0.2% offset yield strength was determined from the stress-strain curves and the ultimate tensile strength from the maximum load.

In order to determine the stress corrosion susceptibility of the material, specimens were dead loaded to 75% Y.S. (0.2% offset) to eliminate any variation in susceptibility due to differences in mechanical properties and exposed to an aqueous solution containing 0.3% NaCl, 3.0% $K_2Cr_2O_7$ and 3.0% CrO_3 in distilled H_2O , solution pH = 0.9⁽¹⁶⁾. Specimens were coated* so that only the reduced section was left exposed. The procedure followed was to pour the solution into the glass cell surrounding the specimen just prior to loading. Failure times were registered on a lapsed time indicator controlled by a microswitch placed beneath the load weights.

C. Results and Discussion

Table 1 shows that the maximum change in mechanical properties with specimen orientation with respect to the rolling direction is only 10%, whereas Table 2 shows a maximum difference of greater than two orders of magnitude on the times to failure (t_f) of the stress corrosion specimens. This high dependence of stress corrosion susceptibility on specimen orientation is normal⁽¹⁷⁾ and as mentioned earlier, it was the purpose of this research to explain why.

Incidentally, no failure occurred after 10,000 minutes for a longitudinally stressed specimen that had been room temperature aged for

*SP-5 Strippable Coating
Chemical Coatings & Engineering Co., Inc.
Media, Pennsylvania

approximately one year before testing (shown in Table 2). The tests of longitudinal specimens at various levels in the plate (discussed in the next section) also showed a decrease in susceptibility after room temperature aging. These specimens did fail, however, probably due to the higher testing temperature. Higher temperature overaging of the 7075 alloy is known to produce immunity to cracking in 7075-T73⁽¹⁾, but the great effect of room temperature aging has not been, to the authors' knowledge, discussed previously. It is suggested that any future quantitative stress corrosion test of aluminum alloys be done so that the precipitation in the alloy is held at a minimum after the specified heat treatment is completed. This could easily be done by keeping specimens refrigerated after aging and before subsequent tests are carried out.

Chapter III

EFFECT OF PREFERRED ORIENTATION ON SUSCEPTIBILITY

A. Introduction

Over the years, many theories have been postulated to explain the stress corrosion cracking of aluminum alloys⁽²⁻²¹⁾. The theories differ widely from totally electrochemical to totally mechanical with various combinations of the two in between.

One prominent theory is that promoted by Robertson and Tetelman⁽⁵⁾ and later by Parkins⁽⁶⁾, in which it is stated that dislocation pile ups at grain boundaries increase the stress level locally and, therefore, favor cracking at grain boundaries. Parkins has stated that "In some cases these pile ups assist stress corrosion by producing bursts of mechanical crack propagation, in others they may be the cause, directly or indirectly, of intense electrochemical activity, whilst in between there may be circumstances in which both mechanisms help toward the total failure." Convincing evidence has recently been presented by Holl⁽⁸⁾ and by Speidel⁽⁹⁾ which supports a dislocation pile up mechanism for stress corrosion cracking of the aluminum alloys.

The localized stresses at grain boundaries due to dislocation pile ups is directly related to the orientation of the slip planes with respect to the grain boundary. Robertson, et al, have pointed out through an analysis made by Stroh⁽¹²⁾ that the stresses normal to the grain boundary due to pile ups are maximized when the slip planes make

an angle of 70.5° with the plane of the grain boundary. This angle was later substantiated by Smith and Barnby⁽¹³⁾ although they indicated a much lower dependence of stress on angle.

Because the normal stresses at the grain boundaries due to pile ups are dependent on slip plane orientation, susceptibility to stress corrosion cracking is expected to be related to any preferred orientation of slip planes. (NOTE: Pole figures, as plotted in previous reports, were found to be in error and were corrected for this report.)

B. Experimental Details

In order to determine the effect of preferred orientation on susceptibility, it was necessary to obtain specimens with different textures, but with all other variables (grain morphology, composition and mechanical properties) constant. In order to keep the grain morphology constant, the stress direction with respect to rolling (specimen orientation) had to be held constant because of the highly elongated grain structure. Preferred orientation was then determined as a function of distance from the plate surface and other variables determined with depth for constancy.

For the texture studies, disc shaped specimens (1.550 in. diameter x 0.125 in. thick) were machined with their flat surface parallel to the rolling plane from various levels of the plate. The specimens were polished on numbers 220, 320, 400 and 600 silicon carbide paper and

number 600 microcut paper^{*} followed by an electropolish in a solution of 20 ml. 70% perchloric acid and 100 ml. 95% ethanol (@ 0°C) to remove the mechanically deformed surface layer. Each specimen was polished using five 10-sec. bursts (total 50 sec.) at 20 volts and 1 amp/cm².

For comparison purposes, a specimen having random crystal orientations was prepared by pouring a mixture of finely powdered aluminum and parlodin into a mold to produce a disc shaped specimen of the same dimensions given above.

The actual texture studies were made by the reflection method using a Siemens Texture Diffractometer^{**}. The complete X-ray installation was comprised of the Kristalloflex 4 X-ray unit, the instrument cabinet with radiation counting equipment and Kompensograph potentiometer recorder, the texture diffractometer, and detector. When the entire angle range was scanned (0 to 90°), the potentiometer recorded a curve, which represented the reflection intensities in relation to the inclination angle α and aximuth ψ . This curve was then evaluated in accordance with stereographic projection.

Figure 3 shows the specimen used to determine stress corrosion susceptibility as a function of specimen depth in the plate. The surface preparation was identical to that of the specimens described above.

*Buehler, Ltd., Evanston, Illinois

**Siemens & Halske Aktiengesellschaft, Germany

Masking off of all but 1/8 inch of the reduced section was carried out using the coating mentioned earlier so that there was a maximum variation of only 1/8 inch in plate depth on any one specimen.

The method of stressing was identical to that mentioned previously. Short transverse specimens were stressed to 50% Y.S. and longitudinal specimens to 75% Y.S. (mechanical properties were determined as mentioned earlier). As it was not necessary to compare failure times of short transverse specimens with those of longitudinal specimens, stress levels were used that gave convenient failure times. However, the stresses were held at a constant fraction of yield strength within the groups to eliminate any differences in mechanical properties. The specimen cell arrangement is shown in Figure 4 and the constant temperature system in Figure 5. The complete system including the loading frame is shown in Figure 6. A tubing pump^{*} was used to circulate 250 ml. of solution, which was discarded after each test, through the cell at the rate of 400 ml/min. and return it to the constant temperature system. The solution temperature was held constant^(17,18) at $35.0 \pm 0.1^\circ\text{C}$ at the specimen and was allowed to circulate around the specimen for 60 seconds before

*Variable Speed Masterflex Tubing Pump
Cole Parmer Co.
Chicago, Illinois

loading. When failure occurred circulation of the solution was stopped and automatically drained from the cell in order to prevent any further corrosion. The lapsed time indicator also registered the time to failure. A statistical analysis of variance was employed to determine whether or not there was a significant change in susceptibility with depth in the plate.

To determine changes in grain morphology with depth, specimens were taken from various depths in the plate. Surfaces examined included both the short transverse-long transverse and the short transverse-longitudinal planes. The specimens were polished using standard metallographic techniques (through number 600 microcut paper and magomet* abraded polishing cloth) and etched with Keller's Etch to reveal the grain structure. Grain boundary intercept distances (grain sizes) were determined by several people independently to eliminate any prejudices.

Emission spectrographic analysis of composition was made on material taken from several levels within the plate.

C. Results and Discussion

As seen in Figures 7 through 11, the (111) pole figures changed markedly with distance from the surface of the plate. The material changed from nearly randomly oriented near the surface to the typical

*Buehler, Ltd., Evanston, Illinois

aluminum rolling texture⁽¹⁹⁾ at the center of the plate.

Mechanical properties and stresses used for testing stress corrosion cracking susceptibility at various levels in the plate are given in Table 3.

The stress corrosion susceptibility of short transverse specimens increases toward the plate center (Table 4) with an exception of 3/8" below the surface. (This deviation from the trend will be discussed later.) Table 5 shows that the susceptibility of longitudinal specimens also increases at the plate center. The geometric mean of endurance time is reported as suggested by Booth, et al^(20,21). These data are shown plotted in Figure 12. The statistical analysis of variance showed in both cases that the above conclusions were significant.

Robertson, et al⁽⁵⁾, have suggested that intergranular cracking will occur through boundaries approximately normal to the stress at which slip planes make an angle of approximately 70°. This angle was derived from the Stroh relationship⁽¹²⁾, which shows that the stress, due to dislocation pile ups, normal to a plane making an angle θ with the slip plane is proportional to $\sin \theta \cos 1/2 \theta$. This function has its maximum at $\theta = 70.5^\circ$. It seemed logical that the preferred orientation could have oriented more grains such that $\theta \sim 70^\circ$. This, however, was not the case as determined from the pole figures.

A careful analysis of the possible variations in slip plane orientations with respect to any particular crack plane showed that there will

always be at least one slip plane (111) making an angle between 54.74° and 90.0° to the crack plane. This leads to a possible variation of only 10% in the function $\sin \theta \cos 1/2 \theta$. Furthermore, Smith and Barnby⁽¹³⁾ have shown that the stress normal to the plane, θ degrees from the slip plane, depends much less on θ than indicated by Stroh. They have shown that the tendency for cracking varies little when $0 < \theta < 90^\circ$. Any change in susceptibility due to preferred orientation, then, cannot be explained by a higher or lower fraction of grains being oriented such that their slip planes make angles of approximately 70° to the crack plane. Further evidence of this is shown by Logan⁽²²⁾. He has seen that in α -brass, which is susceptible to intergranular cracking, both the angles between the (111) and the crack plane and the angles between the (111) and the stress direction are completely random. This shows that there is no relationship between slip plane orientation and crack plane, and that the resolved shear stress on the slip planes is also relatively unimportant. Therefore, any change in resolved shear stress due to preferred orientation also could not account for the change in susceptibility.

Robertson⁽²³⁾, however, has suggested that because a material having a high degree of preferred orientation consists of lower energy grain boundaries (lower angle) the corrosion rate and, therefore, the susceptibility to stress corrosion cracking would be less than for a material

consisting of randomly oriented crystals. Logan has also shown that cracking, in fact, does occur primarily at grain boundaries where the misorientation between slip planes is at least 13° .

Contrary to the above, the results of this research show that stress corrosion cracking susceptibility increases with an increasing degree of preferred orientation. It is believed that the following will clarify this.

Davis and co-workers⁽²⁴⁾ have shown that for slip band continuity across grain boundaries on aluminum bicrystals, the active slip planes in the component crystals had to intersect the boundary on lines that diverged by no more than approximately 15° . This angle correlates approximately with the angle below which Logan observed no cracking in α -brass.

It is believed, therefore, that material having a high degree of preferred orientation, because it will contain more low angle grain boundaries, will allow significantly more slip across grain boundaries than material with random crystal orientations. Hence, the total distance (L) between dislocation source and barrier (some high angle boundary) will be greater in the oriented than in the random material. Since (L) is a measure of the total number of dislocations piled up at the boundary and the number, in turn, determines the magnitude of the stress concentration, it is expected that material in which (L) is greatest will be most susceptible to stress corrosion cracking. That

is, material with a high degree of preferred orientation would be expected to be more susceptible than material with randomly oriented grains.

In other words, preferred orientation makes some grain boundaries approach being sub-grain boundaries or disappearing completely, thus simulating material of larger grain size, greater (L), and greater susceptibility. The above explanation of the dependence of susceptibility on (L) has already been used to explain the greater susceptibility of larger grained specimens⁽⁵⁾.

Logan's data⁽²²⁾ can also be explained by the slip band continuity across low angle boundaries. Since dislocation pile ups are believed to be responsible for cracking, grain boundaries at which dislocations do not pile up (low angle boundaries) would be immune to cracking.

Other variables (composition, mechanical properties, and grain size) were also checked with depth in the plate to be sure that they did not effect the stress corrosion susceptibility. Composition of the alloy did not change significantly with depth, Table 6, and was ruled out as a variable. Mechanical properties were also ruled out as a variable because of the slight changes with depth seen in Table 3. In all tests, however, any effects due to differences in mechanical properties were minimized by testing at a constant fraction of yield strength. Grain size and shape were constant throughout most of the plate interior, but were not at 3/8" below the surface of the plate (Figure 13). This would

account for the relative high susceptibility of the short transverse specimens taken from the 3/8" level. Grain intercept distances in the short transverse direction for different levels in the plate are given in Table 7. This seemingly great dependence of susceptibility on grain size led to the studies of the effects of grain morphology on susceptibility explained in the next chapter.

Chapter IV

EFFECT OF GRAIN MORPHOLOGY ON SUSCEPTIBILITY

A. Introduction

Another factor thought to be important was the component of applied stress normal to the grain boundaries which is dependent on orientation of grains with respect to the stress. In a material having an elongated grain structure, this is of particular importance.

Prestley⁽¹⁴⁾, assuming that the susceptibility to stress corrosion cracking is dependent upon the average resolved tensile stress acting normal to the faces of an idealized grain, derived a mathematical model to predict the variation in susceptibility to stress corrosion cracking with the orientation of the test specimen in material having an elongated grain structure. Haynie, et al⁽¹⁵⁾, expanding Prestley's two-dimensional model to a three-dimensional model based on an ideal elongated octahedral grain, analyzed stress corrosion data for two aluminum alloys. They concluded that there is no significant difference in stress corrosion cracking susceptibility of specimens stressed in the long transverse and short transverse directions when the stress component normal to the grain boundaries is the same. They also suggested that observed differences as a function of stress direction are related to grain shape rather than other metallurgical factors. However, as Haynie et al pointed out, changes in other metallurgical factors were minimized by the use of thin plate and sheet in their tests. Sprowls and Brown⁽¹⁰⁾ have pointed out that

Haynie's results should be regarded as tentative until other metallurgical variables are adequately investigated.

Therefore, it was the purpose of the research in this section to investigate the relative importance of the component of applied stress normal to the grain boundary (grain morphology), which could affect the susceptibility to stress corrosion cracking of a wrought, high strength aluminum alloy.

B. Experimental Details

The specimen used for the effects of grain morphology studies (Figure 14) was designed specifically to fit into the specimen chamber of a scanning electron microscope. The specimens were extracted from the center of the 7075-T651 plate such that the stressed face was in the short transverse-longitudinal plane and the stress direction parallel to the longitudinal direction. This particular orientation was chosen because it is the grain morphology most immune to stress corrosion cracking, and is ideal for observing crack initiation in an elongated grain structure.

After a final light machine cut, the specimens were polished on numbers 320, 400 and 600 silicon carbide paper, number 600 microcut paper, on a magomet abraded polishing wheel and finally electropolished for 30 seconds in the solution of perchloric acid and ethanol under the conditions stated previously.

A small strain gage was then attached to the surface of the specimen (Figure 15) to be stressed so that the relationship between strain and deflection at the screw could be obtained. After obtaining the strain-deflection curve, the stress-deflection curve (Figure 16) was plotted with the help of previously obtained stress-strain curves. Other specimens were then stressed to 75% Y.S. (0.2% offset) (56,500 psi) and masked to leave only a 2mm square area exposed (Figure 17) to the corrodent. These specimens were then corroded for various times from 30 seconds to 16 hours in the chromate solution. Non-corroded stressed and corroded unstressed specimens were also examined for comparison. Surface features were then observed in a scanning type electron microscope.* In some cases after cracking was observed, the stress on the specimen was released (by removing the screw) so that cracks could be positively identified.

Studies were also carried out with a high purity 7075 alloy forging received from The Aluminum Company of America. Chemical analysis: 5.85 Zn, 2.57 Mg, 1.77 Cu, 0.25 Cr, 0.04 Ti, 0.01 Si, 0.00 Fe, 0.00 Mn.

After the miniature tuning fork specimens were machined from the forging, they were heat treated to produce the -T6 condition (solution treated to 900°F for 45 minutes in a salt bath, quenched in ice water,

*JSM Scanning Type Electron Microscope
Japan Electron Optics Lab., Ltd.

aged at 250°F for 26 hours).

These specimens were machined from the forging to produce longitudinal and short transverse type specimens. After heat treatment, specimens were given a minimum amount of mechanical polish, then electropolished as previously described.

Longitudinal and short transverse specimens were stressed at levels ranging from 10 ksi to 70 ksi and corroded in the chromate solution for times from 30 seconds to 10 minutes and observed with an optical microscope.

C. Results and Discussion

Observation of the surface condition of stress corroded specimens utilizing the scanning electron microscope enabled study of the crack initiation and propagation processes in the 7075-T651 alloy. Cracks were seen to initiate in as short a time as 30 seconds in the longitudinally stressed specimens (Figure 18) although the same specimen was not cracked while in the stressed but uncorroded condition. Successively longer exposure times produced cracking as shown in Figures 19 through 24. This cracking was found to occur primarily at the ends of the elongated grain boundaries, normal to the applied stress as shown in Figure 20. This Figure also points out the difficulty in studying early cracking at low magnification. The same crack can clearly be seen in Figure 21 at the higher magnification easily obtainable in the scanning electron microscope. Cracking after 7 minutes exposure (Figures 22a and 23a) was confirmed by releasing the stress on the specimens and observing closure of the crack (Figure 22b and 23b). Stress corrosion cracks on the surface of specimens exposed for 5 to 7 minutes were seen to have propagated to approximately

the same extent as cracks on a specimen exposed for 16 hours (Figure 24).

Cracking was also observed optically in 30 seconds on both short transverse and longitudinal specimens of the high purity 7075-T6 stressed at 60 ksi. (Figure 25 shows this for 1 min. exp.) Cracking observed in the short transverse and longitudinal specimens was found to be always normal to the applied stress at stresses as high as 70 ksi (Figure 26).

As found before, cracking proceeded along boundaries normal to the applied stress and stopped when a boundary parallel to the stress was met (unfavorable boundary), see Figure 27. At the lower levels of stress studied, cracking was also seen to be present. On the longitudinal specimen corroded for 10 minutes at a stress of 20 ksi, cracking was observed (Figure 28). Cracking was not as severe (pitting was more severe) as on specimens stressed to a higher level, but it was significant because 20 ksi is well below the threshold stress for failure of a longitudinal specimen.

Thus, cracking occurs at grain boundaries normal to the applied stress in a short time (virtually instantaneously) regardless of the type of specimen (i.e., short transverse and longitudinal). Cracking occurs at these normal boundaries at low stress levels even on a longitudinal specimen. In the corrodent used, short transverse specimens failed in approximately 5 minutes and longitudinal specimens in 24 hours. Since crack initiation is, however, very rapid for longitudinally stressed specimens, on those boundaries normal to the stress direction, its long time to failure must be due to the fact that crack propagation is difficult because most of the crack path lies along boundaries parallel to the stress direction. Thus, an elongated grain structure would be much more susceptible when stressed normal than when

stressed parallel to the principal axis of the grains. Figure 29, based on the sort of crack initiation and propagation observed shows this schematically. Actual micrographs of typical failures are shown in Figure 30. The similarity between this figure and Figure 25 is clearly seen.

In the short transverse direction, the propagation can always occur in a plane essentially perpendicular to the stress direction. However, when stress is in the longitudinal direction, initiation occurs on short grain boundary segments perpendicular to the stress direction, but then the crack must somehow propagate along a direction parallel to the stress before it can then connect another very short segment that is perpendicular to the stress direction.

In summary, then, it is a combination of the facts that grain boundaries parallel to the applied stress have a very low susceptibility and that in the longitudinal specimens the crack must propagate almost entirely along these paths of low susceptibility that accounts for the relative low susceptibility of material stressed parallel to the longitudinal direction. However, in short transverse specimens the crack may propagate with very little deviation from boundaries perpendicular to the stress (i.e., highly susceptible boundaries). Therefore, material stressed in the short transverse direction is highly susceptible.

It is believed, then, that the threshold stresses for the different grain morphologies⁽²⁾ (different specimen orientations in a highly elongated grain structure) can be related to the applied stress

necessary to crack grain boundaries at various angles to the stress direction. If this is true, then the threshold stress for short transverse specimens approximates the stress necessary to crack grain boundaries normal to the applied stress and the threshold stress for longitudinal specimens approximates the stress needed to crack boundaries parallel to that stress. Evidence for this is given by the fact that boundaries normal to the applied stress crack at stress levels as low as 20 ksi on either type of specimen.

The high susceptibility of short transverse specimens from 3/8" below the plate surface (Figure 12) can be explained in light of the grain size. Stress corrosion cracking is influenced by the amount that the crack plane must deviate from a plane normal to the applied stress in order to propagate through the specimen. Since the grains are smaller along the stress axis at 3/8" below the surface (Table 7), the crack may deviate less from a plane normal to the stress for specimens from the 3/8" level than for specimens from deeper levels. Therefore, the material at 3/8" below the surface would be expected to be more susceptible than material at lower levels in the plate.

Figures 31 through 33 show surfaces of unstressed specimens exposed for 10 seconds and 5 minutes. General pitting has occurred to a much greater extent on the unstressed specimens than on the stressed specimens seen earlier (Figures 18 through 24). The stifling of general pitting on specimens undergoing stress corrosion cracking may be due to the grain

areas which are cracking becoming more anodic than those areas normally susceptible to pitting attack. The net effect would be inhibition of general corrosion by an "internal cathodic protection mechanism." That is, when the specimen is unstressed, small areas, e.g. weak sites in the passive film, on the surface of the specimen are the anodes and become pits. When stressed, the grain boundary becomes more anodic than the interior of the grain (including the original weak areas in the film). It thus acts as an anode that cathodically protects the rest of the surface and stops pitting.

Chapter V

EFFECT OF SEGREGATION ON SUSCEPTIBILITY

A. Introduction

In 1940, Dix⁽²⁾ discussed the effect of segregation of alloy elements on the stress corrosion of aluminum alloys. The larger precipitates in the grain boundaries were thought to provide a susceptible path for the stress corrosion crack. Since then the theory has been modified by many investigators as discussed by Sprowls and Brown⁽¹⁰⁾.

It was the intention of this part of the investigation to determine by electron probe microanalysis whether or not there was any variation in segregation with orientation with respect to the rolling plane. That is, this investigation was directed at determining the part that segregation plays in the directional susceptibility of the alloys tested.

B. Experimental Details

Flat, polished specimens were prepared from both the 7075-T651 and -T73 material for electron probe microanalysis. Specimens were taken perpendicular to the rolling plane from the center and from near the surface of the plate. At each level, specimens were taken from both the short transverse-long transverse and short transverse-longitudinal planes.

Electron probe microanalysis was also made of the vicinity of a

crack on a flat specimen which had undergone stress corrosion cracking in the previously mentioned chromate solution.

C. Results and Discussion

The target current images of areas with inclusions are shown in Figure 34 for the specimens near the surface of both the 7075-T6 and -T73 conditions. The light areas indicate inclusions of lower atomic number and the dark indicates inclusion of higher atomic number than the matrix. In Figure 35, the magnesium X-ray images, the light areas are high in magnesium content. These areas correspond to the light particles in Figure 34 and, as determined by other X-ray images, are also high in silicon. It was also determined that the dark inclusions of Figure 34 were low in magnesium and silicon.

Figure 36, the iron X-ray images, shows iron to be highly segregated at the dark particles of Figure 34. Copper and manganese were also segregated at these inclusions. Aluminum and zinc were found to be depleted at all inclusions.

The chromium X-ray image, Figure 37, shows that there are zones depleted of chromium that do not correspond to the inclusions of Figure 34.

Titanium, not shown, also follows the chromium. These depleted zones are seen to be more prominent in the 7075-T651 than in the -T73 material and are believed to correspond to subgrain boundaries and may be somewhat responsible for the higher susceptibility of 7075-T651.

No major differences could be found between the two planes of material examined. The only difference found in the electron probe microanalysis between the material from the center and from near the surface of the plate was that the inclusions and zones near the surface were approximately twice as large as those near the surface. This is believed to be due to the more highly deformed nature of the material near the surface. No relation, whatsoever, could be found between any segregation and the direction of rolling of the plate.

Electron probe microanalysis of the crack vicinity on the stress corrosion specimen revealed a significant increase in chromium concentration in the vicinity of the crack, Figure 38. However, further studies with specimens cracked in the chromium-free chloride ion corrodent revealed no such effects. That is, no relationship could be found between the crack path and any previous segregation of alloy elements.

Chapter VI

EFFECT OF ELECTROCHEMICAL FACTORS ON SUSCEPTIBILITY

A. Introduction

The purposes of these studies were: 1) to learn something about which factors in the environment control cracking, such as pH, solution composition, and potential, so that some sort of cracking mechanism can be arrived at and related to directionality; and 2) to measure corrosion rates under stress and without stress with respect to direction and to learn if there is enhancement of corrosion rate depending on direction and stress, as measured by current flow.

B. Experimental Results

Three specimen designs were used: 1) 0.75 x 0.75 x 0.030-inch square specimens (Figure 39), capable of being stressed parallel to either axis in a given plane; 2) tuning fork specimen (Figure 40) with a 0.375 x 0.500-inch face; 3) miniature tuning fork specimens of the same design as those used in the scanning electron microscopy studies (Figure 14). In each instance, specimens were machined from the center portion of the plate in order to eliminate those effects resulting from the variation in stress corrosion susceptibility with plate depth.

The procedure for surface preparation of the specimens prior to exposure has been previously mentioned in this report.

Square specimens were clamped in a stainless steel bracket (Figure 39)

and all but an 1/8-inch square area in the center of the specimen coated with electroplater's stop-off lacquer. Tuning fork specimens were stressed before mounting in the support bracket and coated with stop-off lacquer. Specimen assemblies were then placed in the appropriate electrochemical cell (Figures 39, 40b, and 41).

Two cell systems were used during the course of the investigation. The initial design consisted of a pyrex glass body with a built-in Luggin capillary and platinized platinum counter electrode. The cell was later modified so that self-stressed tuning fork specimens could be used. In addition, the Luggin capillary of the reference electrode could be positioned to within 0.1mm of the specimen surface to minimize IR drop in the electrolyte. The potential of the specimen surface was maintained at a selected value by means of a potentiostat. Current measurements were then made as a function of specimen potential. During the course of exposure, the corrodent (500 ml) was circulated at a constant flow rate of 600 ml per minute and directed at the specimen surface to sweep away gas bubbles which would interfere with current measurements.

Electrochemical studies of the role of environment were made using the three corrodents: 1) a 0.3% NaCl, 3.0% $K_2Cr_2O_7$, 3.0% CrO_3 solution whose pH was 0.9; 2) 3.5% sodium chloride, and 3) a 1.0N sodium nitrate solution, both of whose pH was adjusted to 0.9 with hydrochloric and nitric acid, respectively. These solutions were adjusted to these low pH values because initial experiments showed that excessive film would

build up on the specimen surface in the neutral solutions during anodic polarization.

The effects of applied stress and chloride additions to a normally non-aggressive environment upon longitudinal and short-transverse stressed specimens were studied using the miniature tuning fork specimens.

A 1/8" diameter aluminum rod threaded at one end and simulating the tightening screw was inserted into the specimen, thereby permitting application of stress external to the electrochemical cell. All but the polished surface of the specimen was coated with successive layers of "Glyptal" lacquer and electroplaters stop-off lacquer.

Specimens were exposed for five minutes to environments of 500 ml of 1.0N sodium nitrate (0.02N in aluminum nitrate) which also contained from zero to 100 ppm chloride ion. Solutions were recirculated at the flow rate of 600 ml/minute at room temperature. Specimens were stressed to 75% of yield either prior to exposure to the environment or within the environment after electrically steady-state conditions were obtained. In either case, optical micrographs were made before and after exposure, and current measurements in polarized systems were made during the course of exposure. In each environment, open circuit corrosion potential measurements were made on both stressed and unstressed specimens.

Specimens were polarized to +0.100 volts vs SCE which correspond to a potential within the active region of the polarization curve, where

film growth could be expected to occur.

C. Results and Discussion

Studies were carried out to measure the corrosion current associated with crack propagation both as a function of time and stress direction. A simple experiment for measuring the current and potential drop across a cell composed of two identical tuning fork specimens immersed in the chromate solution--one stressed to 75% of yield, the other unstressed--has been performed.

Results from this measurement of open-circuit current flow in the cell composed of a stressed and unstressed specimen were as follows: for a longitudinal stressed specimen, the current density was 20 microamp/cm² and was relatively constant over the exposure period. Regular fluctuations were noted, but these could be due to hydrogen evolution which would cause changes in the electrode surface area. Current measured in the short transverse cell system rose steadily from an initial level of 20 microamp/cm² to 80 microamp/cm² over a 4 minute period until failure occurred. Since the current is some measure of the amount of surface available for reaction, this experiment shows that the short transverse specimen, as expected from the microscopic studies, has more of its grain boundaries favorably oriented for such reactions than the longitudinal.

Polarization curves were constructed for the 7075-T651 alloy in each of the environments previously described. The potential was varied in both an anodic as well as a cathodic direction, and current readings were

made only after a steady-state value was reached. At least three sets of data were obtained in each environment. The curves obtained are shown in Figures 42 through 47.

The obtaining of these curves was the first step in our electrochemical studies of the role of directionality on the mechanism of cracking. The open circuit potentials are labeled on these curves for the chromate and for the chloride solutions and cracking does occur at these potentials.

It is well known that specimens of the 7075-T651 alloy exhibit shorter times to failure in the chromate solution, and much less severe general pitting attack, than in the chloride environment. Furthermore, on the basis of the polarization curves for this alloy in these solutions (Figures 42 through 47) it is readily seen that 7075-T651 is considerably more active in the 3.5% NaCl solution. From these observations, and the previously noted stifling of pitting during stress corrosion, it is clear that susceptibility to stress corrosion is not dependent upon general corrosion susceptibility, but in all probability, depends upon stress enhanced breakdown of a passive film (probably at the grain boundary) followed by anodic dissolution at such grain boundaries.

In order to determine whether the role of the chromate under open circuit conditions was to bring the system to a potential where cracking occurs by a mechanism involving the formation of a passive film, potentiostatic studies in nitrate solutions containing no chloride were carried

out. By then setting the potential with the potentiostat at various values, it was hoped that the potential for cracking could be determined. We were unable, however, to obtain any evidence of stress corrosion cracking in short transverse stressed specimens in nitrate solutions under any conditions of applied potential and chloride concentrations up to 100 ppm. However, addition of as little as 5 mg chloride ion (10 ppm solution concentration) shifted the open circuit corrosion potential nearly 400 mv in the active direction. This potential (-0.680 mv vs SCE) corresponds to the corrosion potential in 3.5% NaCl where stress corrosion cracking is known to occur. This observation would lead to the conclusion that although small concentrations of chloride ion are needed to break down the passive film generated on the metal in a nitrate environment, such small concentrations are not sufficient to cause cracking. Further work is necessary in the determination of these conditions of chloride ion concentration and applied potential to cause cracking.

It was also noticed that the level of the corrosion current in specimens, polarized to +0.100V, depended upon the mode of stress application. Although the actual absolute current values were rather unreproducible, the following trends were observed:

1. For specimens stressed prior to immersion, the corrosion current was approximately 50% lower than the unstressed short transverse specimens.
2. For specimens stressed, in situ, the current was perhaps 10%

greater than non-stressed specimens.

The explanation of this observation is unclear at this time, and further experiments are necessary to elucidate this behavior.

Because it has not been possible to obtain reproducible results in these electrochemical experiments, we were not able to tie them in to optical and scanning electron observations of the surface to relative electrochemical parameters to the difference in directional susceptibility, as originally planned.

Chapter VII

EFFECT OF PRECIPITATES AND DISLOCATION CONFIGURATIONS ON SUSCEPTIBILITY

A. Introduction

The purpose of this part of the study was to examine the dislocations, precipitate and grain boundary microstructures in various commercial 7075 aluminum alloys and to see if these were related in any way to susceptibility differences. Two tempers of this alloy were studied, the T651 susceptible temper and the T73 resistant temper. The technique applied was that of transmission electron microscopy of thin metal sections taken from stress corrosion specimens of these alloys. Both corroded and uncorroded specimens were examined in three different sections, namely the longitudinal, long transverse, and short transverse directions. It was hoped that these direct microstructural studies would indicate possible explanation for differences observed in directional stress corrosion susceptibility in this system, and at the same time reveal any microstructural changes involved in the development of stress corrosion resistance after suitable heat treatments.

Several recent studies of stress corrosion in alloys have concentrated on the dislocation and precipitate microstructures. It was shown by Swann⁽²⁵⁾ that alloys with cellular dislocation arrangements are resistant to transgranular stress corrosion failure while alloys which exhibit planar dislocation arrays are highly susceptible. Although aluminum fails inter-

granularly in stress corrosion, the studies of Holl⁽⁸⁾ showed that susceptible underaged Al-Mg-Zn alloys do have planar dislocation bands after plastic deformation. This type of dislocation arrangement is missing if the alloys are given a further heat treatment which produces immunity to stress corrosion cracking. [This observation also was made by Ryum et al⁽²⁶⁾ who studied brittleness vs. microstructure in Al-Mg-Zn alloys.] Hornbogen⁽²⁷⁾ has also emphasized the importance of dislocation glide bands, and has discussed the shearing of coherent precipitates with reference to the earlier work of Gleiter and Hornbogen⁽²⁸⁾. Speidel⁽²⁹⁾ has elaborated on the idea that particle-shearing and dislocation pile-up enhance stress corrosion cracking and he presents some supporting experimental results. Earlier work by Thomas and Nutting⁽³⁰⁾ dealt with zone formation, hardening, and with the importance of precipitate-free zones adjacent to grain boundaries in certain alloys. Much of the earlier literature in this field is reviewed by Robertson and Tetelman⁽⁵⁾. Jacobs⁽³¹⁾ concluded that stress corrosion resistance is lowered by an increased density of precipitates or dislocations with the precipitate density being the most important factor. The stress corrosion studies of Jacobs show electron micrographs of corroded surfaces. He has also studied glide band structures in 7075 alloys and electron microscope fractographs of cracked specimens.

B. Experimental Results

Samples were taken from the as-received commercially produced slabs

and from stress corrosion tuning fork shaped specimens which in some cases had undergone stress corrosion testing at 75% of the yield stress. No attempt has yet been made, however, to prepare foil specimens which retain an original stress corroded surface. Wafers approximately 0.5mm thick were cut from the stress corroded specimens by a spark discharge slicer. These wafers were then spark planed to a uniform thickness of 0.3mm and electropolished in a 1:2 nitric acid-methanol solution -25°C and 8.5 volts to produce thin foils suitable for transmission electron microscope studies. Foils taken from these specimens were mounted in a rotating-tilting goniometer holder in the electron microscope and examined at 100kv accelerating potential. Selected area diffraction pattern identification of precipitates was accomplished using the alloy matrix diffraction spots as a local diffraction standard.

C. Results and Discussion

Grain Shape Anisotropy: As reported earlier, after optical microscope examination of different sections of these alloys, a strong grain shape anisotropy was found in the thin foil sections. Figure 48 is an electron micrograph of a sample taken in the long transverse section from the T651 treatment. In this low magnification micrograph the grain shape anisotropy is shown, the grains being elongated parallel to longitudinal direction of the material. In other sections of these alloys similar observations are made although the amount of anisotropy varies with the section and location in the slab. As shown by the roughly equiaxed grain in this

figure some variation in grain shape is noted in all sections. No attempt has been made to determine lattice orientations from grain to grain. The procedures which would involve selected area electron diffraction are straight-forward but tedious. Previous X-ray diffraction studies have indicated the nature of the preferred orientation in these materials and presumably those results would be substantiated by single grain studies of this type. In comparing the precipitate and dislocation structures observed in the various sections (to be discussed later in greater detail) it is clear that the high degree of grain shape anisotropy has not led to corresponding differences in these aspects of the microstructure. For example, the precipitate density and dislocation density in elongated grains do not appear appreciably different from the values found in equiaxed grains in any of the sections. The degree of precipitation along the grain boundaries does not appear to vary significantly between short and long boundary lengths at the ends and sides, respectively, of the elongated grains. These details will be illustrated in the thin foil micrographs and discussion which follows.

Dislocation and Precipitate Structures: In examining thin foils made from various sections of these alloys we have employed bright field transmission electron microscope techniques by tilting the area of interest in order to control the diffraction contrast. Two general conditions are of interest. First, by tilting the area away from the Bragg diffraction

condition, no contrast is developed at dislocations within the area, however, precipitate contrast remains enabling one to determine precipitate sizes, shapes and densities. Figure 49 taken from a longitudinal section of T651 at a relatively low magnification illustrates predominantly "precipitate contrast". That is, in only relatively few areas are the diffraction conditions suitable for reviewing dislocations. One of these areas is indicated in the photograph. This condition is emphasized to avoid misunderstandings concerning the distribution of dislocations in the samples. Areas which appear to contain no or few dislocations may in fact be unsuitably oriented for the diffraction process required. This situation is usually indicated by somewhat reduced contrast within those areas. The second technique involves tilting rather near the Bragg diffraction condition to reveal dislocation lines and at the same time reveal precipitate particles. This condition is generally employed in high magnification studies due to the considerable variation in lattice orientation in these polycrystalline specimens. The plate-like habit of the intermediate size precipitates and the tendency for orientation is evident in Figure 49. The fine distribution of small precipitates cannot be resolved at this magnification. We have identified these precipitates and many of the larger ones to be MgZn_2 in agreement with the results of other workers. These precipitates are known to be anodic with respect to the matrix. Precipitate growth along the grain boundaries is obvious in many areas and these grain boundary precipitates

tend to be somewhat larger than those within the grains. No striking examples of precipitate-free zones adjacent to the boundaries are found.

A thin foil section taken of the long transverse plane is shown in Figure 50. The grain shape anisotropy is shown together with precipitate structures in several grains and the dislocation and precipitate structures in others. At this somewhat higher magnification the fine distribution of small precipitates can be seen in the background. A particularly interesting feature associated with this area concerns the boundary at A. Selected area diffraction patterns taken on opposite sides of this boundary show a very small if any lattice rotation. This feature is apparently a low angle subgrain boundary oriented nearly orthogonal to the long axis of the longitudinal grain structure. The inset to this photograph shows a higher magnification view of this particular area indicating several precipitates growing immediately adjacent to this boundary. Structures of this type could represent structural weaknesses in a material under the influence of an applied stress. Since it has been previously reported that boundaries normal to the longitudinal stress direction are generally sites of crack initiation, a feature of this kind would be particularly suspect.

Another area taken from a long transverse section of the T651 alloy is shown in Figure 51. Two separate photographs have been obtained in different contrast by tilting the sample. In Figure 51a the grain region

to the lower right shows only precipitate contrast while in Figure 51b the dislocations in this same area are revealed along with the precipitates. It is interesting to note that the intermediate size precipitates do serve as effective barriers for dislocations in this material. The fine distribution of small precipitates is of course the primary hardening constituent and its effect on the dislocation lines is shown here as a general ragged appearance of the dislocation images. Two triple grain boundary junctions are shown in this area with advanced precipitation present at the boundaries. Several of the grain boundaries are nearly orthogonal to the foil plane and offer the opportunity to examine for precipitate-free zones adjacent to them. One such boundary is shown at A in the figures and the small precipitates appear to be present at a uniform density at all distances from this boundary. In general, precipitate-free zones adjacent to grain boundaries were not observed in any of the specimens examined here, although occasionally such regions were observed. Further examples of dislocation and precipitate structures in the long transverse section of the T651 alloy are shown in Figures 52 and 53. In Figure 52 at A, a dislocation is shown bowed around an intermediate size particle indicating that the particle has disturbed the normal glide process of the dislocation. A second example of this type of interaction is shown at B and many other instances can be located in this field. The two grain boundaries contained within this area can be seen to serve as effective

barriers for dislocation motion although the general dislocation arrangement is random and uniform. No tendency is observed for dislocation groups or planar arrays to form in the vicinity of these boundaries. The large magnification of Figures 52 and 53 show clearly the interactions between dislocations and the small precipitates in the matrix. In Figure 53 two large dislocation loops are indicated at A. These loops presumably arise as the dislocations attempt to move through the lattice under the influence of stress and interact with the precipitate structures. Again there is lack of indication of glide band formation in this region. Strong interactions between the dislocations and grain boundaries are not observed.

A foil section taken in a short transverse plane is shown in predominantly precipitate contrast in Figure 54. Several grains are included in this region of the specimen and a considerable variation in precipitate density is observed within the grains. Grain boundary precipitation is indicated at several locations in this micrograph taken from a specimen with the T73 treatment. The small hardening precipitates appear to have grown considerably as a result of the thermal treatments applied to this material in a comparison with the T651 treatment. The dislocation density in this specimen and all others with the T73 treatment was appreciably smaller than that with the T651 treatment.

A higher magnification view of this specimen is shown in Figure 55, a region illustrating a triple grain boundary junction. The small

precipitate distribution is clearly resolved in this case and for the first time an orientation tendency is noticed among these precipitates. Somewhat advanced precipitation at the grain boundaries is indicated. As observed in the T651 specimens, precipitate free zones adjacent to the grain boundaries do not develop with the T73 treatment. This particular region has been tilted away from the diffraction condition so that dislocations contained within it are not in contrast. Another example of a grain boundary region in this type of specimen is shown in Figure 56. There are regions along this particular grain boundary where the small precipitate density in the matrix is somewhat reduced and other regions where there is no observable effect. Again the dislocation contrast has been suppressed in this figure.

The interactions between dislocations and the precipitates in the T73 temper are illustrated in Figure 57 which is also taken from a short transverse section. This micrograph is at a sufficiently high magnification to clearly resolve individual precipitates in the background which have grown appreciably as a result of the thermal treatments applied to the alloy. There are many areas showing interactions between the dislocations and the small precipitates and further interactions also with the intermediate size precipitates. The dislocation distribution within the grains is reasonably random and no planar arrays are observed. Not only is the dislocation density of the T73 treated

alloys much lower than that in the T651 treated alloys, but the dislocation lines appear straighter and less ragged possibly indicating a reduced interaction with the precipitates. In view of the reduced strength associated with alloys having undergone a T73 treatment these observations are not surprising since they indicate that the precipitate distribution is much less effective as a barrier to dislocation motion.

Conclusions from the microstructural studies of the commercial 7075 aluminum alloys used in this investigation are as follow. Both the T651 and the T73 treated specimens have high precipitate densities and electron diffraction studies show that the majority of the intermediate sized and small sized precipitates are MgZn_2 . The precipitates are randomly dispersed throughout the grains and grain boundaries, and grain boundary precipitation is only moderately advanced. The morphology of grains and grain boundaries has not influenced the precipitate density or distribution. Sizeable precipitate-free zones adjacent to the boundaries are not a distinguishing feature in these materials are were rarely observed. The principal differences in the T651 and T73 processed alloys are the dislocation density and arrangement and the size of the small precipitates. The dislocation density is much greater after the T651 treatment than after the T73. Dislocations are tangled and ragged in the T651 type material while they are straighter after the T73 treatment. Dislocations in the T73 specimen are few in number and are not easily observed. Growth of the very small precipitates of the T651 specimen has occurred after the

T73 treatment. In the latter material, the formation of small directional platelets showing the growth relation of these precipitates to the matrix is especially evident.

Thin foil sections taken normal to each of the three principal directions showed no appreciable differences in dislocation density, dislocation arrangements, or in precipitate density and distribution. Therefore, the observed directional sensitivity in these alloys cannot be explained in terms of these microstructural variables. The most likely explanation still refers to the angle the grain boundaries make with the applied stress direction as discussed earlier in this report.

Chapter VIII

CONCLUSIONS

A. The role of grain morphology was found to be of paramount importance in controlling crack propagation. Observations of cracking in as short a time as 30 seconds at grain boundaries normal to the applied stress on the surface of longitudinally stressed specimens show conclusively that it is the slow rate of crack propagation along boundaries parallel to the applied stress that accounts for the low susceptibility of longitudinally stressed specimens. These results suggest that the threshold stress for short transverse specimens approximates the stress necessary to crack grain boundaries normal to the applied stress, and the threshold stress for longitudinal specimens approximates the stress needed to crack boundaries parallel to the applied stress.

B. Preferred orientation was found to increase the susceptibility to stress corrosion cracking in the 7075-T651 alloy by increasing the stress at grain boundaries due to dislocation pile ups. However, its effect on susceptibility is of secondary importance when compared to the effect of grain morphology. A high degree of preferred orientation, rather than any specific slip plane orientations, was found to increase the susceptibility of specimens with the same grain morphology.

C. The electrochemical experiments showed that current flow was greater in short transverse stressed specimens than in longitudinal ones showing

the creation of more active areas in the former. Polarization effects due to stress were also minor when stressing longitudinally.

D. No directional effects related to segregation or precipitate or dislocation configurations were found.

E. Pitting corrosion was found to occur to a much greater extent on unstressed than on stressed (undergoing stress corrosion cracking) specimens. This phenomenon is explained by what is termed an "internal cathodic protection mechanism."

LITERATURE CITED

- (1) Sprowls, D.O. and Brown, R.H., "Resistance of Wrought High-Strength Aluminum Alloys to Stress Corrosion", Technical Paper 17, Aluminum Company of America, Alcoa Research Laboratories, New Kensington, Pennsylvania (1962).
- (2) Dix, E.H., Jr., "Acceleration of the Rate of Corrosion by High Constant Stresses", Trans. AIME, 137, 11 (1940).
- (3) Mears, R.B., Brown, R.H. and Dix, E.H., Jr., "A Generalized Theory of Stress Corrosion of Alloys", Symposium on Stress Corrosion Cracking of Metals, 329 (1944), ASTM-AIME.
- (4) Logan, H.L., "Film Rupture Mechanism of Stress Corrosion", J. Research NBS, 48, 99 (1952), RP 2291.
- (5) Robertson, W.D. and Tetelman, A.S., "A Unified Structural Mechanism for Intergranular and Transgranular Corrosion Cracking", Strengthening Mechanisms in Solids, 217 (1962), ASM.
- (6) Parkins, R.N., "Stress Corrosion Cracking", Metallurgical Reviews 9, 35, 201 (1964).
- (7) Haynie, F.H. and Boyd, W.K., "Stress Corrosion Cracking of Aluminum Alloys", DMIC Report 228 (1966), Defense Metals Information Center, Battelle Memorial Institute, Columbus, Ohio.
- (8) Holl, H.A., "Deformation Substructure and Susceptibility to Intergranular Stress Corrosion Cracking in an Aluminum Alloy", Corrosion 23, 6, 173 (1967).

- (9) Speidel, M.O., "Interaction of Dislocations with Precipitates in High Strength Aluminum Alloys and Susceptibility to Stress Corrosion Cracking", Paper presented at the International Conference on Fundamental Aspects of Stress Corrosion Cracking (1967), The Ohio State University.
- (10) Sprowls, D.O. and Brown, R.H., "Stress Corrosion Mechanisms for Aluminum Alloys", Paper presented at the International Conference on Fundamental Aspects of Stress Corrosion Cracking (1967), The Ohio State University.
- (11) Jacobs, A.J., "The Mechanism of Stress Corrosion Cracking in 7075 Aluminum", Paper presented at the International Conference on Fundamental Aspects of Stress Corrosion Cracking (1967), The Ohio State University.
- (12) Stroh, A.N., "The Formation of Cracks as a Result of Plastic Flow", Proc. Roy. Soc. 223, 404 (1954).
- (13) Smith, E. and Barnby, J.T., "Crack Nucleation in Crystalline Solids", Metal Science J., 1, 56 (1967).
- (14) Prestley, J.S., Jr., "Effect of Specimen Orientation on Resistance to Stress Corrosion Cracking of Aluminum Alloys--A Mathematical Model", STP-425, Symposium of Stress Corrosion Testing (1967), ASTM.
- (15) Haynie, F.H., Vaughan, D.A., Phalen, D.I., Boyd, W.K., and Frost, P.D., "A Fundamental Investigation of the Nature of Stress Corrosion Cracking in Aluminum Alloys", Technical Report AFML-TR-66-267, Jan. 1967, Contract

AF 33(6150-171), sponsored by the U.S. Air Force Materials Laboratory, Wright-Patterson AFB, Ohio.

- (16) Sprowls, D.O., Lifka, B.W., King, W., Shumaker, M.B., Kelsey, R.A., and Vandenburg, D.G., "Investigation of the Stress Corrosion Cracking of High Strength Aluminum Alloys", Summary Report for the Period of May 6, 1963 to July 6, 1965, Contract NAS 8-5340, sponsored by the George C. Marshall Space Flight Center of the NASA, Huntsville, Alabama.
- (17) Romans, H.B. and Craig, H.L., Jr., "Environmental Factors Affecting the Stress Corrosion Cracking Behavior of an Aluminum-Zinc Magnesium Alloy", STP-425, Symposium on Stress Corrosion Testing (1967), ASTM.
- (18) Helfrich, W.J., "Influence of Stress and Temperature on Short-Transverse Stress Corrosion Cracking of an Al-4.2 Zn-2.5 Mg Alloy", STP-425, Symposium on Stress Corrosion Testing (1967), ASTM.
- (19) Barrett, C.S. and Massalski, T.B., "Structure of Metals", 556 (1966), McGraw-Hill.
- (20) Booth, F.F., Tucker, G.E.G., and Godard, H.P., "Statistical Distribution of Stress Corrosion Endurance", Corrosion, 19, 11, 390t (1963).
- (21) Booth, F.F. and Tucker, G.E.G., "Statistical Distribution of Endurance in Electrochemical Stress Corrosion Tests", Corrosion, 21, 5, 173 (1965).
- (22) Logan, H.L., "Relationship Between Crystal Orientation and Stress Corrosion Cracking in Alpha and Beta Brasses", J. Research NBS, 56, 159 (1956), RP 2662.
- (23) Robertson, W.D., "Preferred Orientation as a Factor in Intergranular Corrosion", J. Metals, 188, 790 (1950).

- (24) Davis, K.G., Teghtsoonian, E. and Lu, A., "Slip Band Continuity Across Grain Boundaries in Aluminum", *Acta Metallurgica*, 14, 1677 (1966).
- (25) Swann, P.R., "Dislocation Substructure vs Transgranular Stress Corrosion Susceptibility of Single Phase Alloys", *Corrosion* 19, 102 (1963).
- (26) Ryum, N., Haegland, B., and Lindtveit, T., "Brittleness and Microstructure of Some Al-Mg-Zn Alloys", *Z. Metallkunde* 58, 28 (1967).
- (27) Hornbogen, E., Discussion of reference (26).
- (28) Gleiter, H. and Hornbogen, E., "Theorie der Wechselwirkung von Versetzungen mit Kohärenten geordneten Zonen (I)", *Phys. Stat. Sol.* 12, 235 (1965).
- (29) Speidel, M.O., "Interaction of Dislocations with Coherent Particles and Stress Corrosion Cracking of High-Strength Aluminum Alloys", *Phys. Stat. Sol.* 22, K71 (1967).
- (30) Thomas, G., and Nutting, J., "The Aging Characteristics of Aluminum Alloys", *J. Inst. Metals* 88, 81 (1959).
- (31) Jacobs, A.J., "The Role of Dislocations in the Stress Corrosion Cracking of 7075 Aluminum Alloys", *Trans. ASM* 58, 581 (1965).

TABLE 1
MECHANICAL PROPERTIES AT THE PLATE CENTER (20°C)

<u>Stress Direction</u>	<u>Yield Strength (0.2% offset)</u> (ksi)	<u>Tensile Strength</u> (ksi)
Short Transverse	65.4	78.4
Long Transverse	70.7	83.3
Longitudinal	76.7	87.7

TABLE 2
STRESS CORROSION SUSCEPTIBILITY AT THE PLATE CENTER (20°C)

<u>Stress Direction</u>	<u>Stress (ksi and % Y.S.)</u>		<u>Average Endurance Time</u> (min.)
Short Transverse	49.0	75%	4.8
Long Transverse	53.0	75%	143
Longitudinal	57.5	75%	834*

*No failure after 10,000 minutes for a specimen tested after room temperature aging for 1 year.

TABLE 3
MECHANICAL PROPERTIES VERSUS DEPTH IN THE PLATE (20°C)

<u>Stress Direction</u>	<u>Depth in Plate*</u> (in.)	<u>Yield Strength**</u> (ksi)	<u>Tensile Strength</u> (ksi)	<u>Stresses for Stress Corrosion Tests</u> (ksi) (% Y.S.)	
Short Transverse	0.375	68.5	78.3	35.5	52
	0.625	65.2	75.8	35.7	55
	0.875	66.4	77.4	36.5	55
	1.125	65.6	77.0	36.5	56
	1.375	65.2	74.2	36.2	55
Longitudinal***	0.625	69.0	78.1	53.4	75
	1.250	70.1	75.8	54.1	77

*Distance between surface of plate and center of specimen gage length.

**0.2% offset yield strength.

***Room temperature aged for approximately 1 year before tests.

TABLE 4
SHORT TRANSVERSE STRESS CORROSION ENDURANCE TIMES
VERSUS DEPTH IN THE PLATE (35°C)

	Depth in Plate (inches)				
	<u>0.375</u>	<u>0.625</u>	<u>0.875</u>	<u>1.125</u>	<u>1.375</u>
Endurance Times (minutes)	3.2	7.5	5.7	5.4	4.0
	4.1	8.4	6.3	5.7	4.6
	4.2	12.0	7.0	6.0	4.9
	4.3	12.0	8.2	6.1	5.0
	4.9	12.4	10.6	7.9	5.8
	6.5	19.2	20.0	11.3	5.8
	9.4				
Geometric Mean (minutes)	4.9	11.4	8.7	6.8	5.0
Standard Devia- tion of Log Normal Distribution (minutes)	1.5	3.8	3.7	1.7	0.6

TABLE 5
LONGITUDINAL STRESS CORROSION ENDURANCE TIMES
VERSUS DEPTH IN THE PLATE (35°C)

	Depth in Plate (inches)	
	<u>0.625</u>	<u>1.250</u>
Endurance Times (minutes)	539*	178*
		187*
	820	548
	1551	692
	1601	919
	2412	972
	2540	1074
	<u>3473</u>	<u>1935</u>
	Geometric Mean	1874
		940
Standard Deviation of Log Normal Distribution (minutes)	173	62

*Room temperature aged for approximately 4 months less than remainder of longitudinal specimens.

TABLE 6
COMPOSITION VERSUS DEPTH IN PLATE

Depth in Plate (inches)	<u>Element</u>							
	<u>Zn</u>	<u>Mg</u>	<u>Cu</u>	<u>Cr</u>	<u>Fe</u>	<u>Mn</u>	<u>Ti</u>	<u>Si</u>
	<u>Percent</u>							
0.375	5.17 ±.03	2.14 ±.07	1.62 ±.02	0.182 ±.002	0.188 ±.005	0.040 ±.001	0.033 ±.001	0.035 ±.005
0.625	5.26 ±.04	2.12 ±.03	1.58 ±.03	0.186 ±.002	0.184 ±.006	0.040 ±.001	0.036 ±.002	0.033 ±.006
1.250	5.26 ±.03	2.13 ±.04	1.63 ±.02	0.184 ±.001	0.178 ±.008	0.040 ±.001	0.036 ±.0002	0.036 ±.007
Mean	5.23 ±.02	2.13 ±.03	1.61 ±.01	0.184 ±.001	0.183 ±.004	0.040 ±.001	0.035 ±.0003	0.035 ±.004

Plus and minus values listed under the mean concentrations are the standard deviations of means.

Each determination was run in quadruplicate.

TABLE 7
GRAIN SIZE VERSUS DEPTH IN PLATE

	Depth in Plate (inches)		
	<u>0.375</u>	<u>0.875</u>	<u>1.375</u>
Average number of grains per inch in the short transverse direction*	319	263	257

*Each number is the average of five different counts on each of three specimens from that depth in the plate.

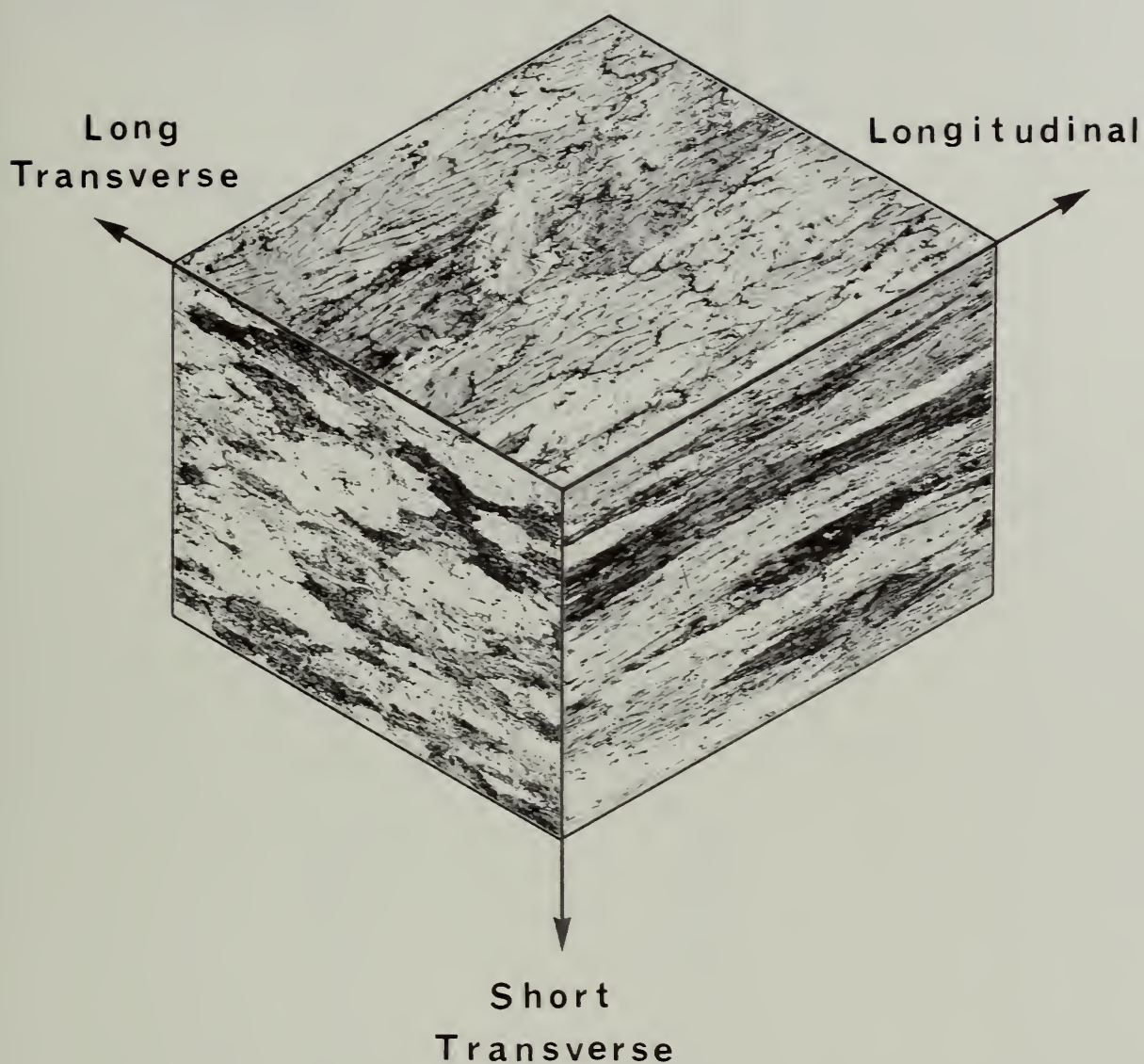


FIGURE 1

Composite photomicrograph of the grain structures in three orientations at the center of a 2.5-inch thick plate of 7075-T651 aluminum alloy. Etched in Keller's etch. X 50

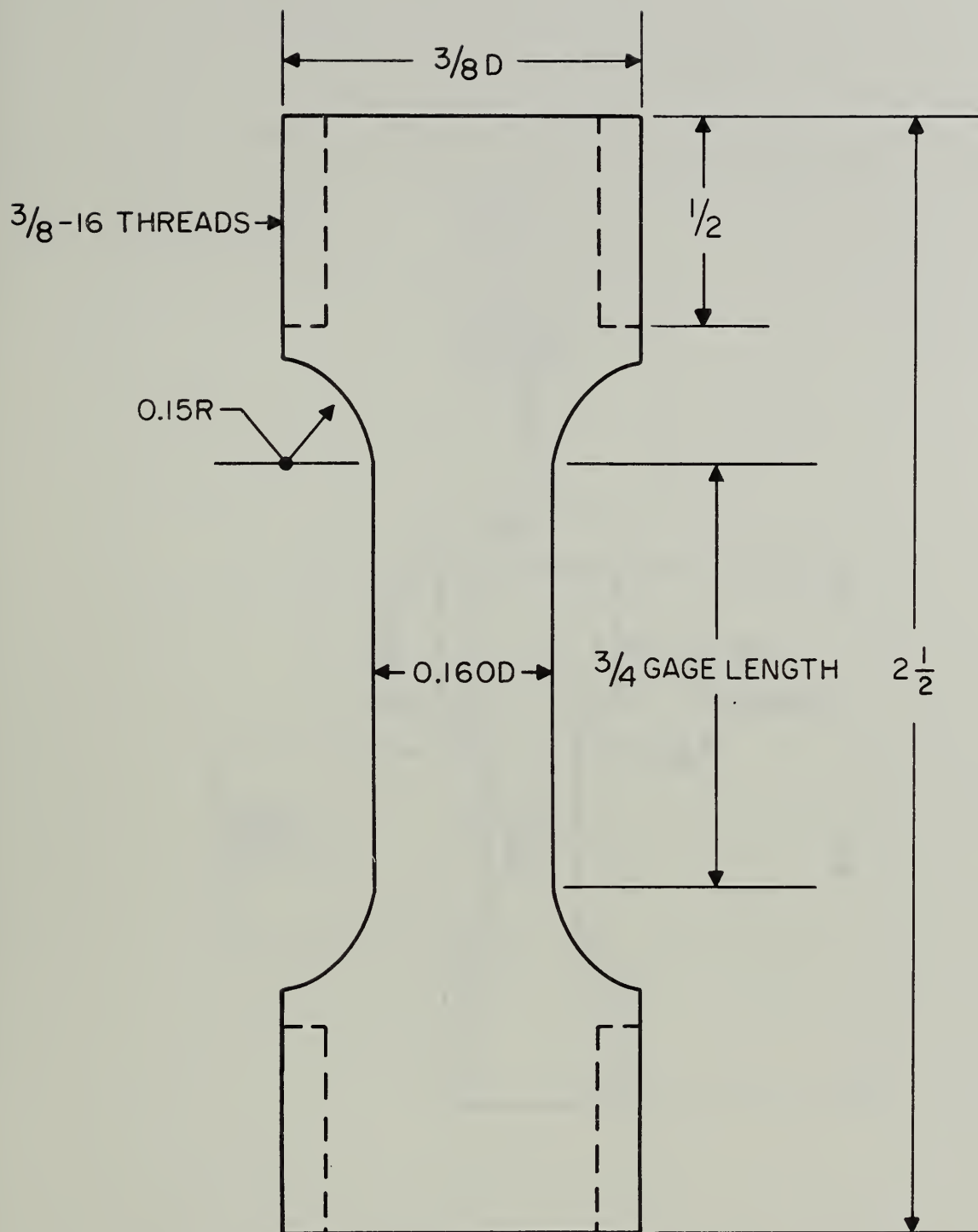


FIGURE 2

Specimen used for the material evaluation studies.

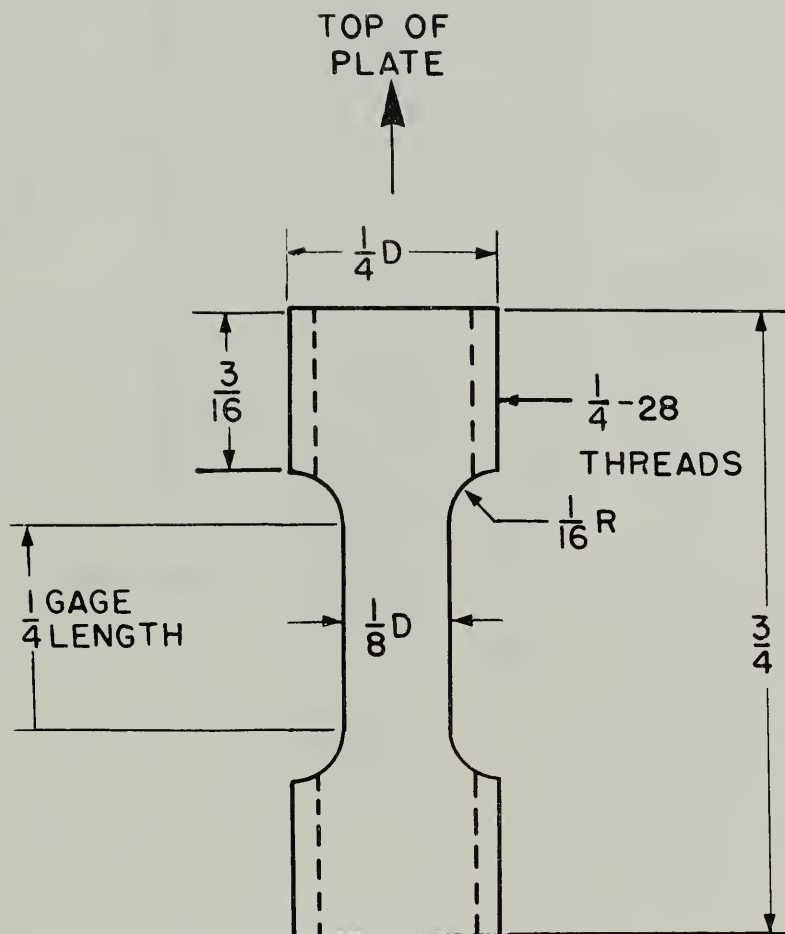


FIGURE 3

Miniature specimen used to determine the mechanical properties and susceptibility to stress corrosion cracking at various depths in the plate of material.

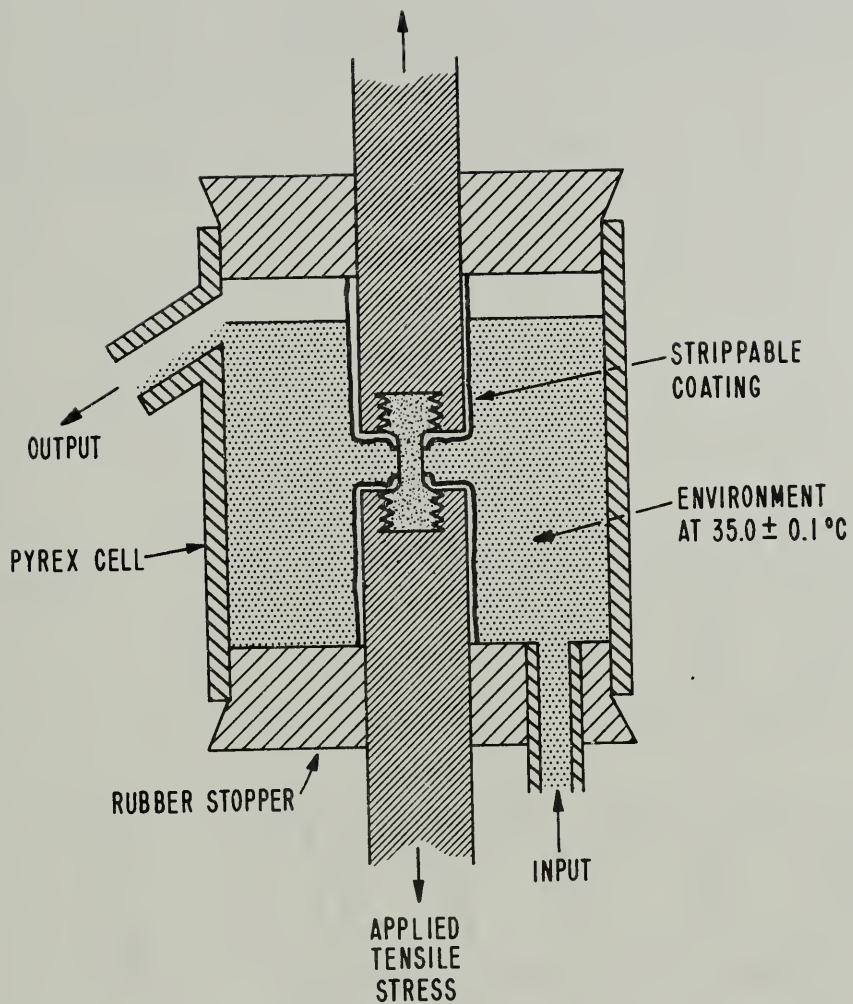


FIGURE 4
Stress corrosion susceptibility testing cell.

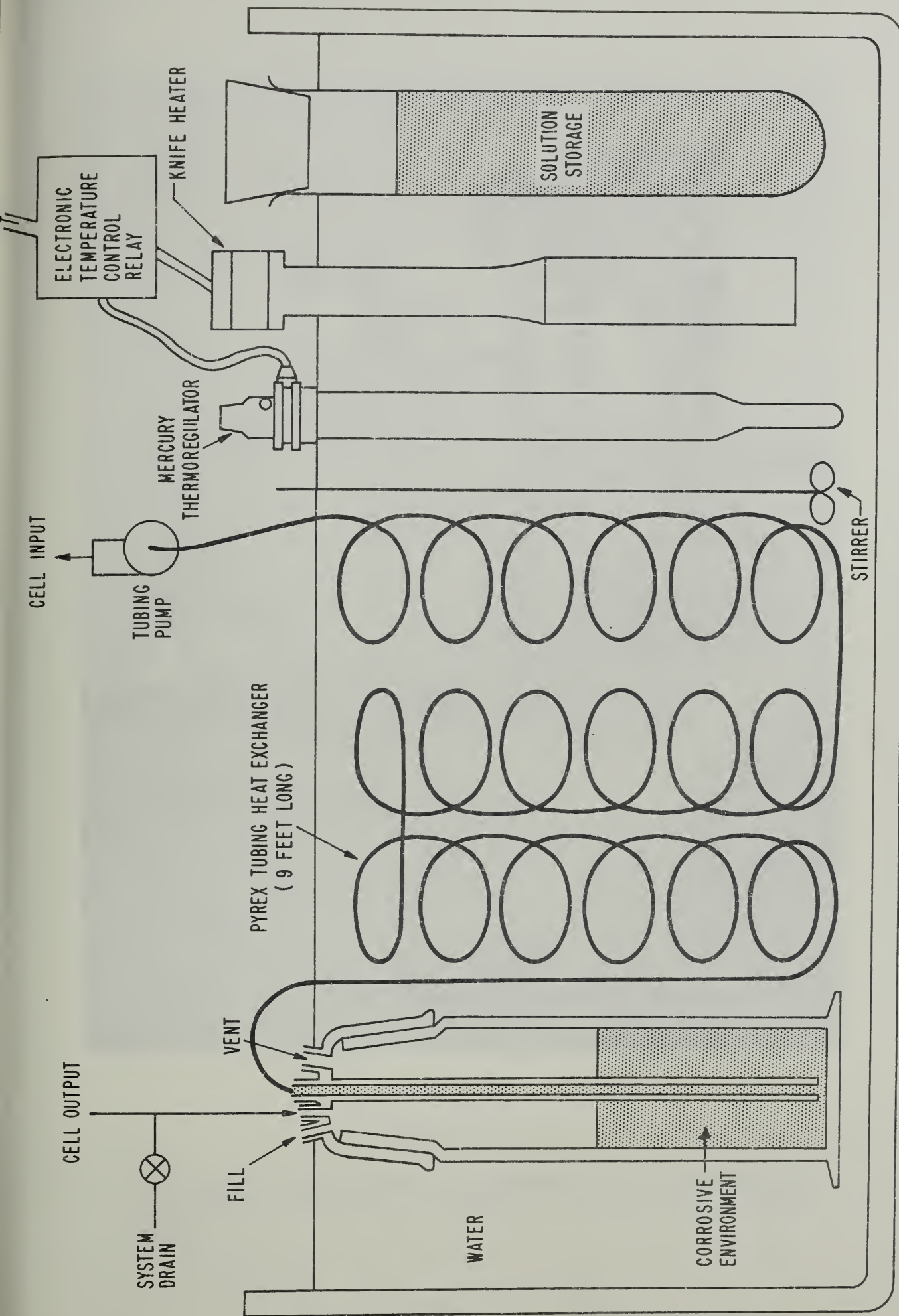


FIGURE 5

Recirculating constant temperature corrosive environment system.

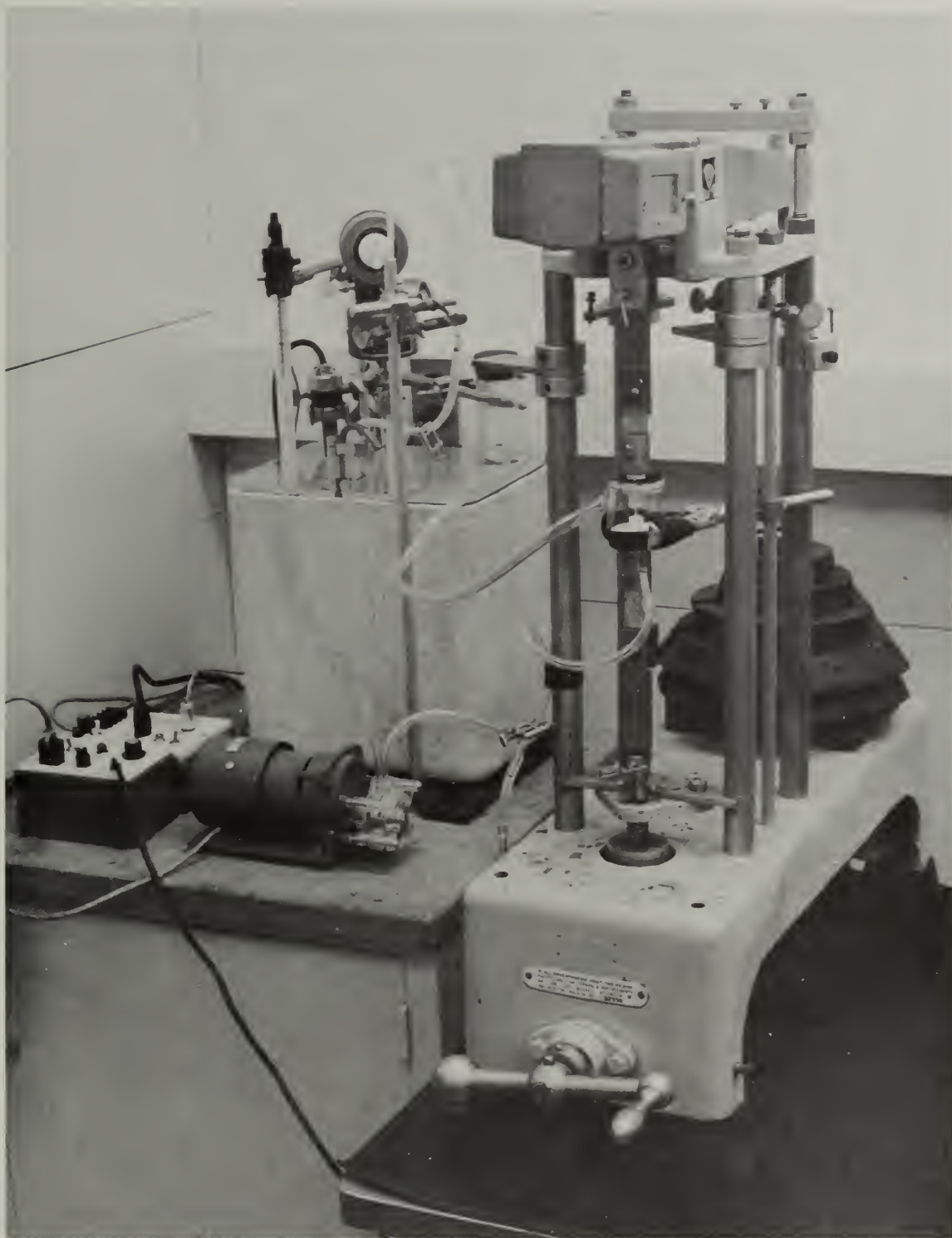


FIGURE 6

The complete stress corrosion susceptibility testing system. Items shown include those in Figures 4 and 5 and the loading frame.

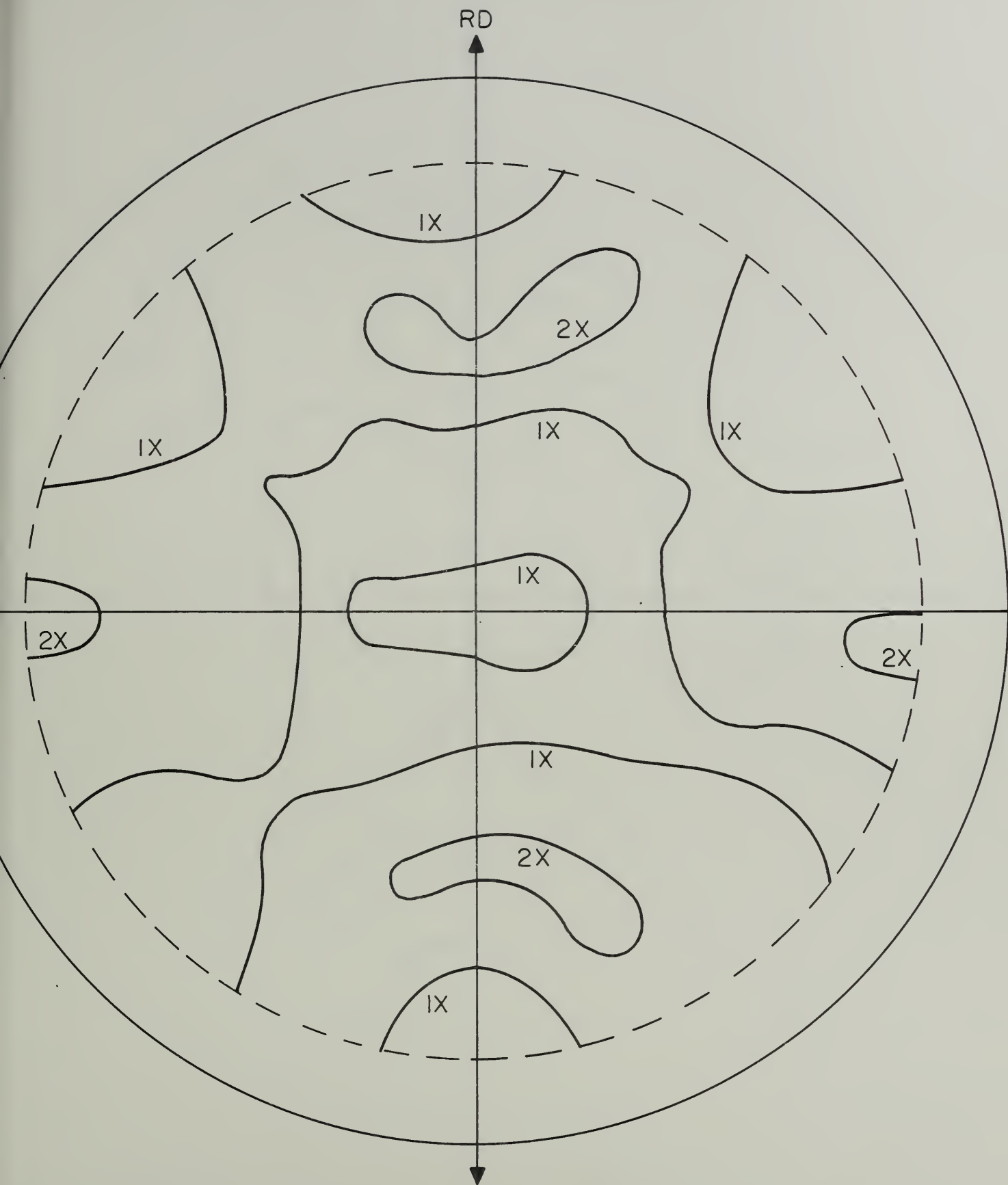


FIGURE 7

Absolute (111) pole figure for a plane of material at 0.26 inches below the surface of the plate. The constant intensity contours are shown as multiples of the intensity of the (111) reflection for a randomly oriented specimen.

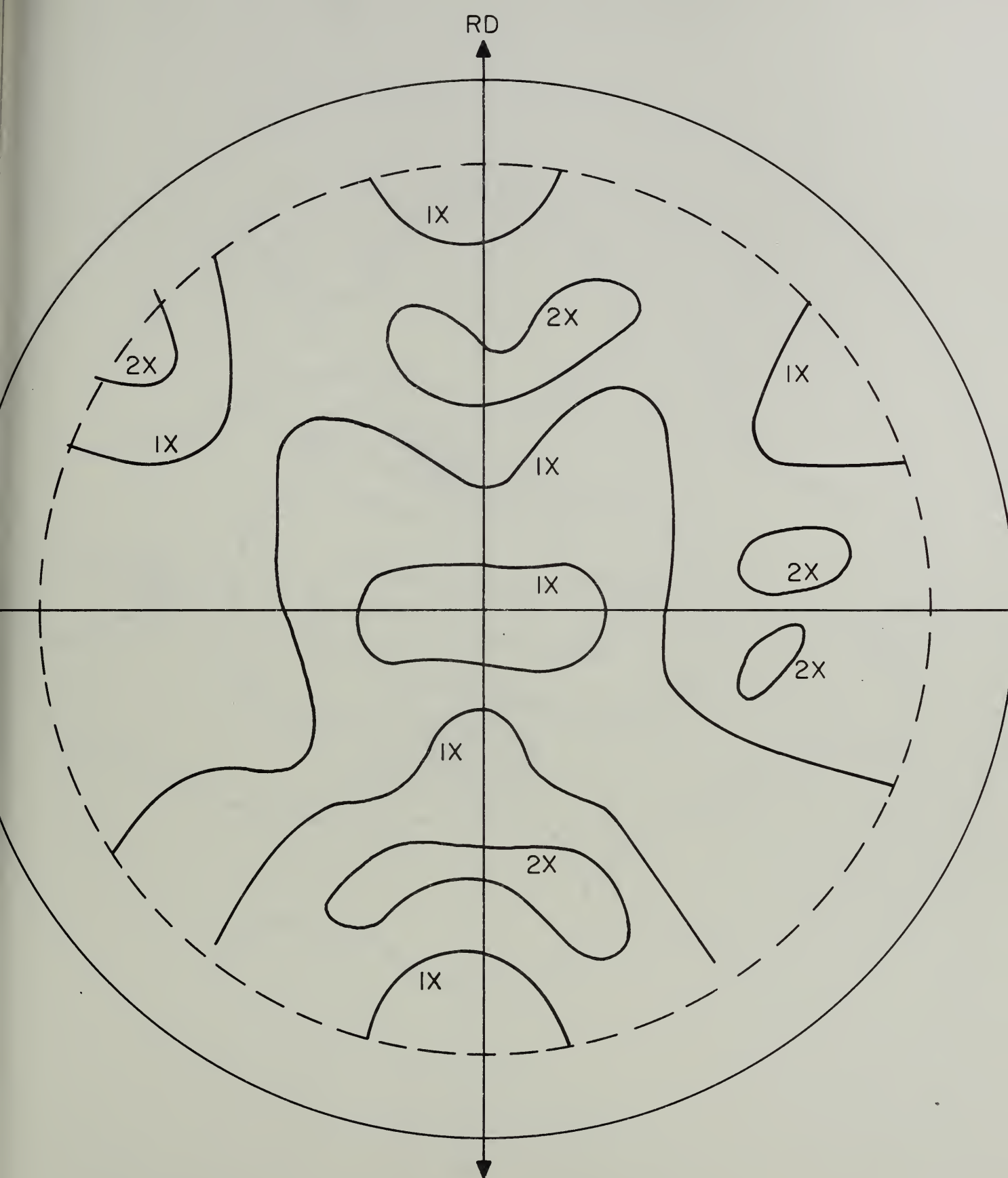


FIGURE 8

Absolute (111) pole figure for a plane of material at 0.57 inches below the surface of the plate. The constant intensity contours are shown as multiples of the intensity of the (111) reflection for a randomly oriented specimen.

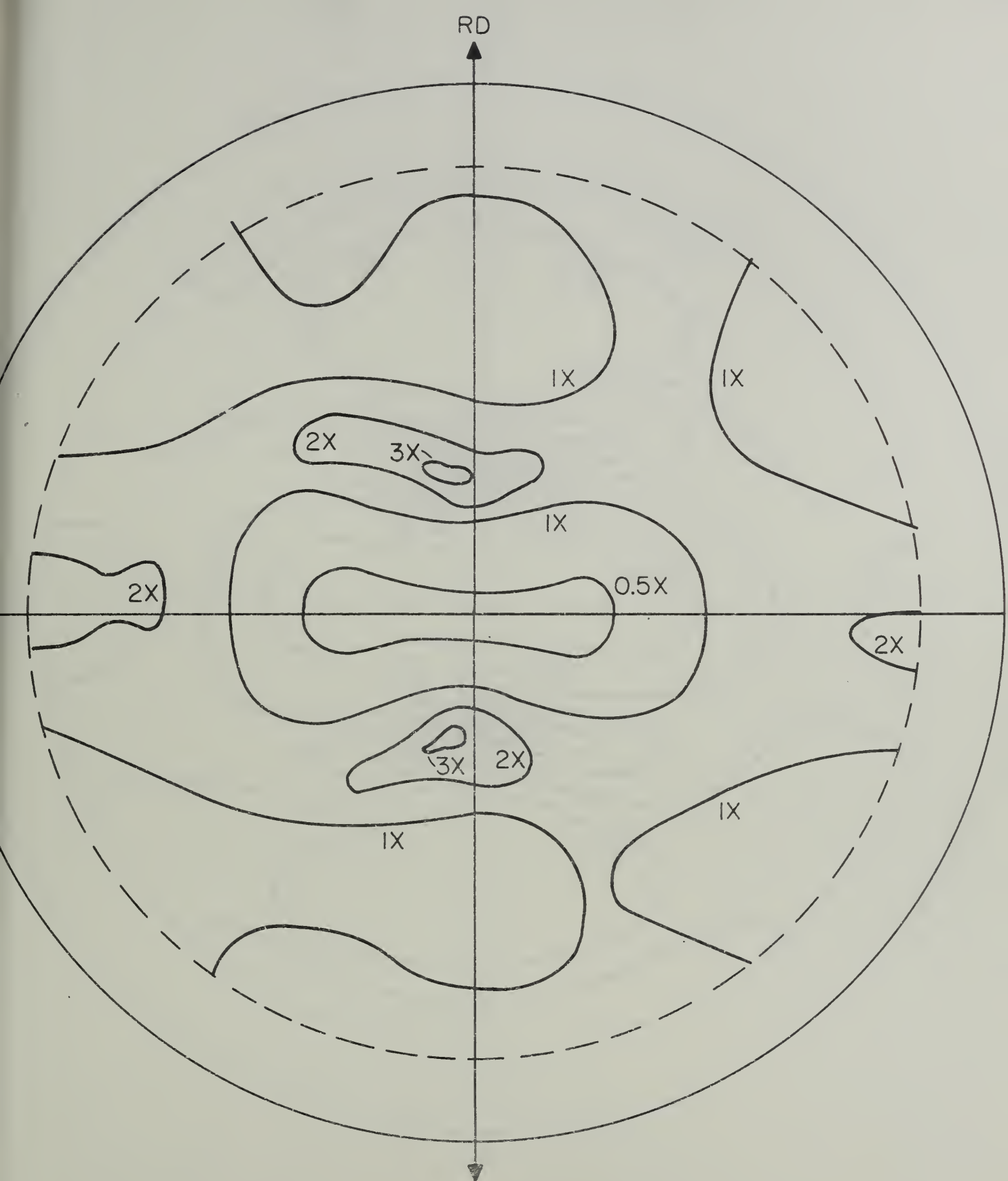


FIGURE 9

Absolute (111) pole figure for a plane of material at 0.73 inches below the surface of the plate. The constant intensity contours are shown as multiples of the intensity of the (111) reflection for a randomly oriented specimen.

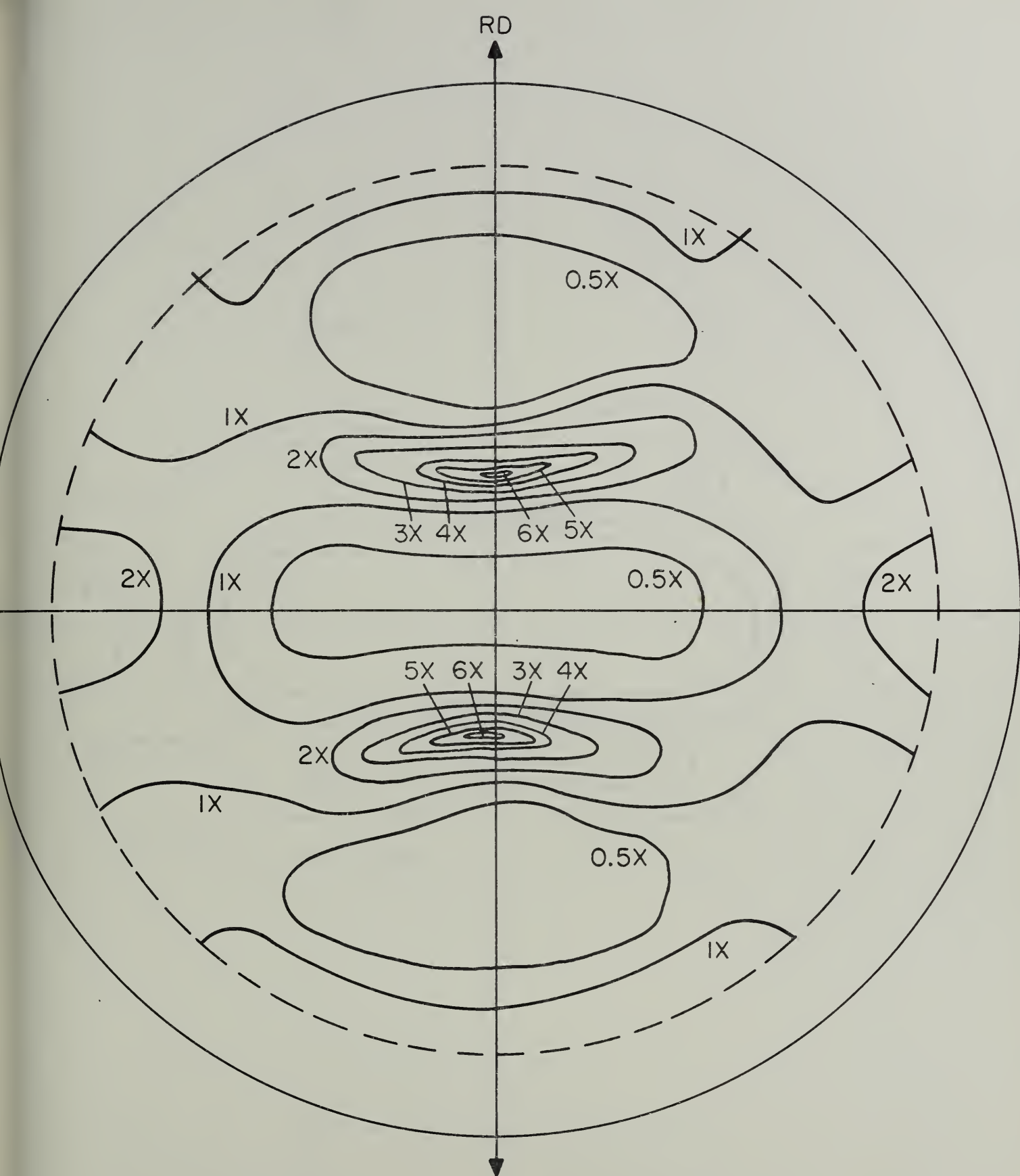


FIGURE 10

Absolute (111) pole figure for a plane of material at 0.89 inches below the surface of the plate. The constant intensity contours are shown as multiples of the intensity of the (111) reflection for a randomly oriented specimen.

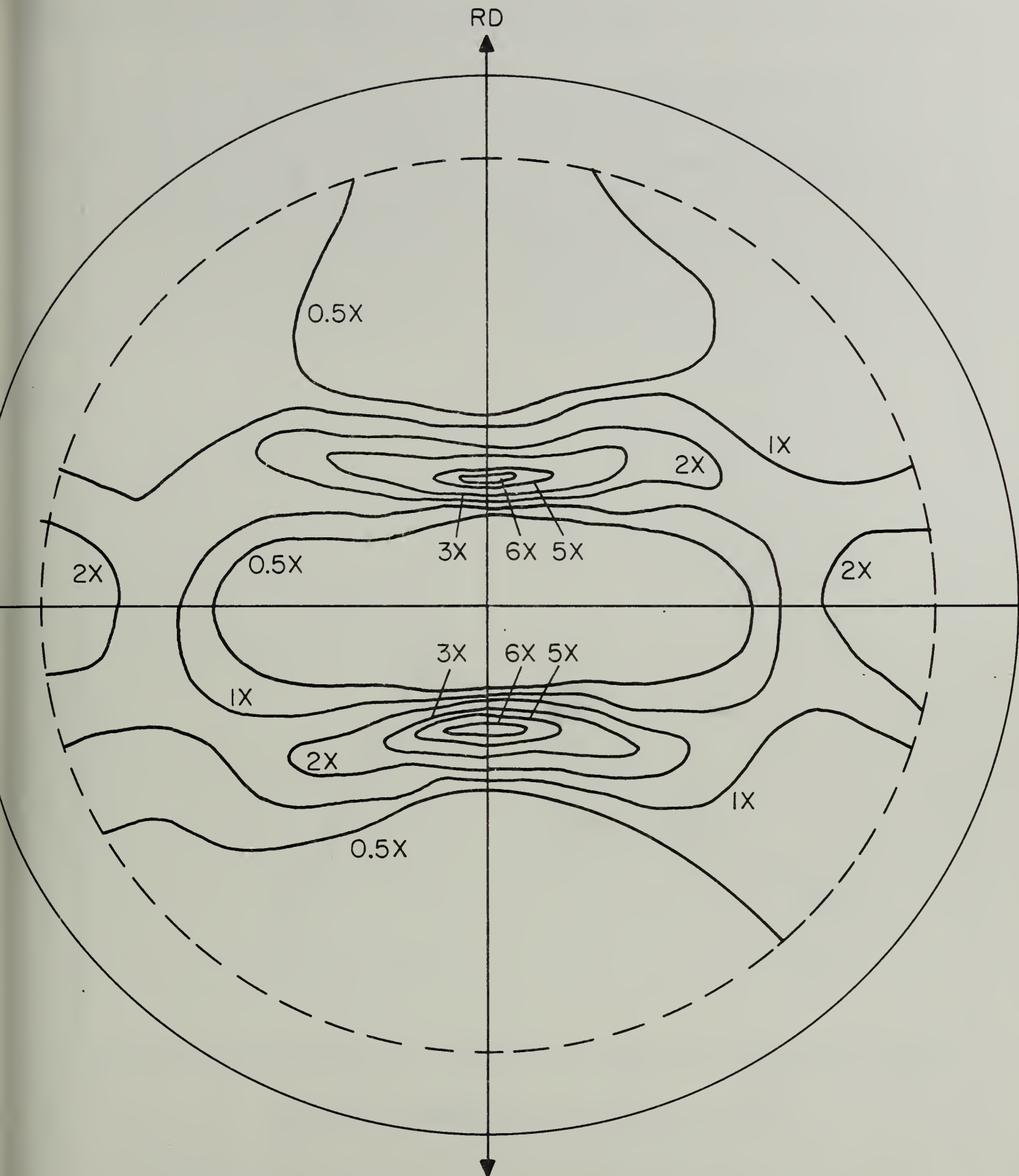


FIGURE 11

Absolute (111) pole figure for a plane of material at 1.20 inches below the surface of the plate. The constant intensity contours are shown as multiples of the intensity of the (111) reflection for a randomly oriented specimen.

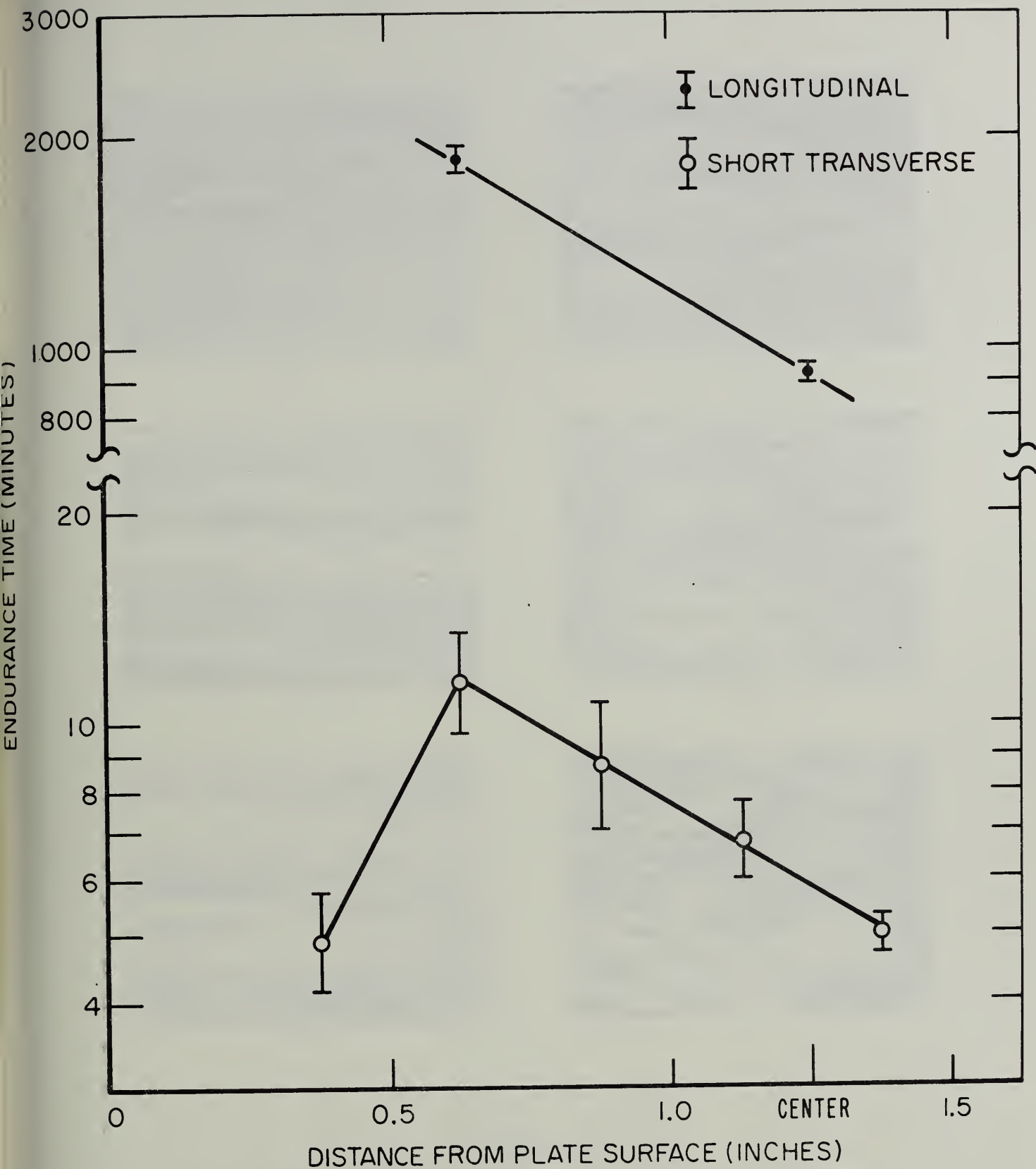
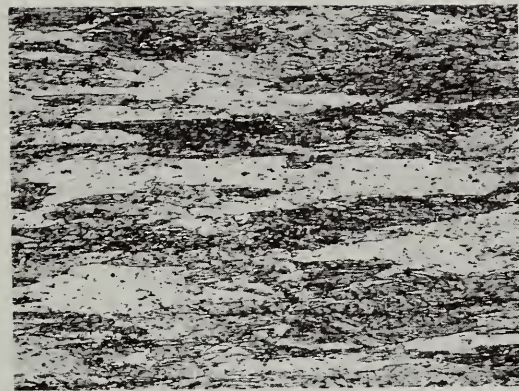


FIGURE 12

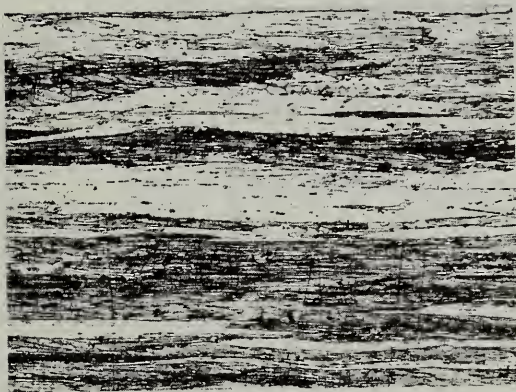
Stress corrosion endurance time versus depth of specimen in the plate for both short transverse and longitudinal specimens. Extremes of data points are the standard deviations based on the logarithms of endurance times.



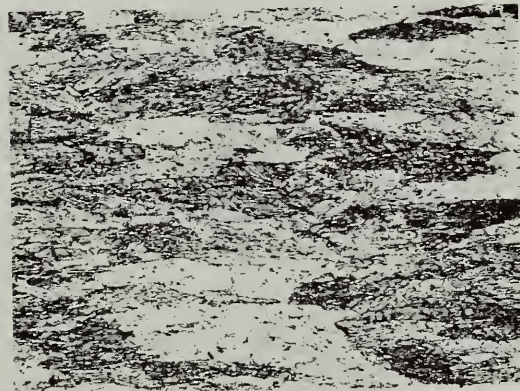
(a)



(b)



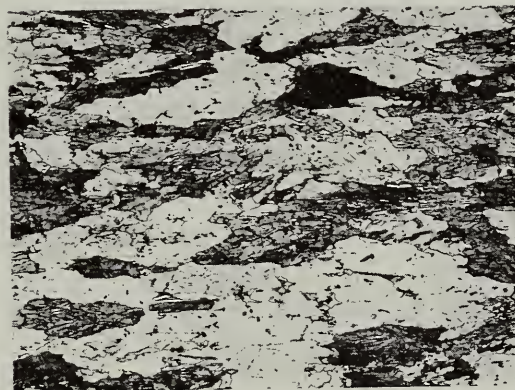
(c)



(d)



(e)

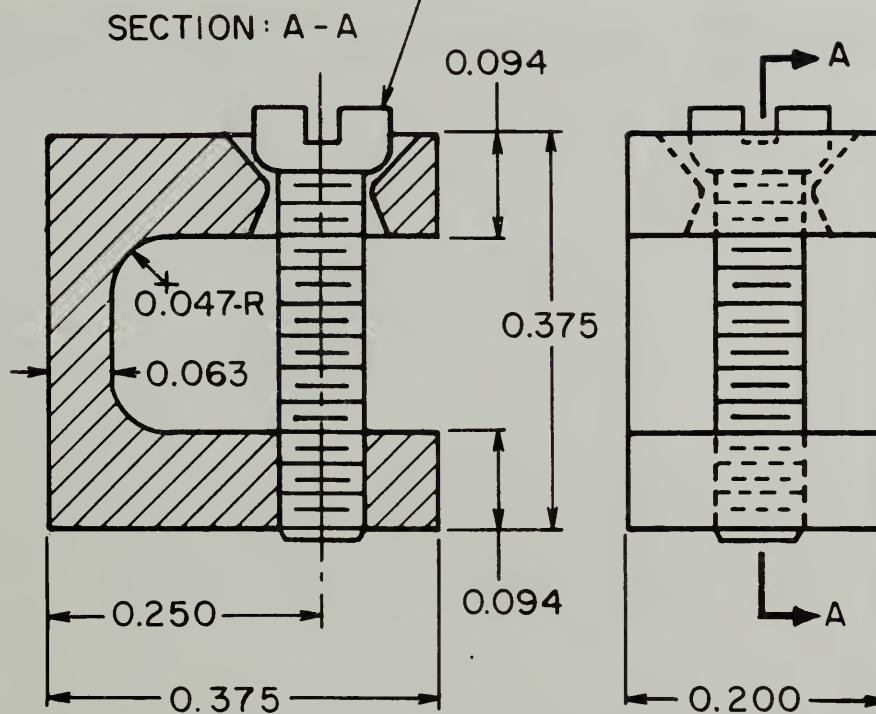


(f)

FIGURE 13

Photomicrographs of both the short transverse-longitudinal plane (a, c & e) and the short transverse-long transverse plane (b, d & f) at $3/8$ (a & b), $5/8$ (c & d), and $1\ 1/4$ (e & f) inches below the surface of the plate. Etched in Keller's etch. X 75

3-48 MACHINE SCREW
(WITH SHOULDER ROUNDED)



ALL DIMENSIONS IN INCHES
TOLERANCE ± 0.001 THROUGHOUT

FIGURE 14

Miniature tuning fork stress corrosion specimen.



FIGURE 15

Miniature tuning fork specimen shown with strain gage in place
on stressed surface. X 5

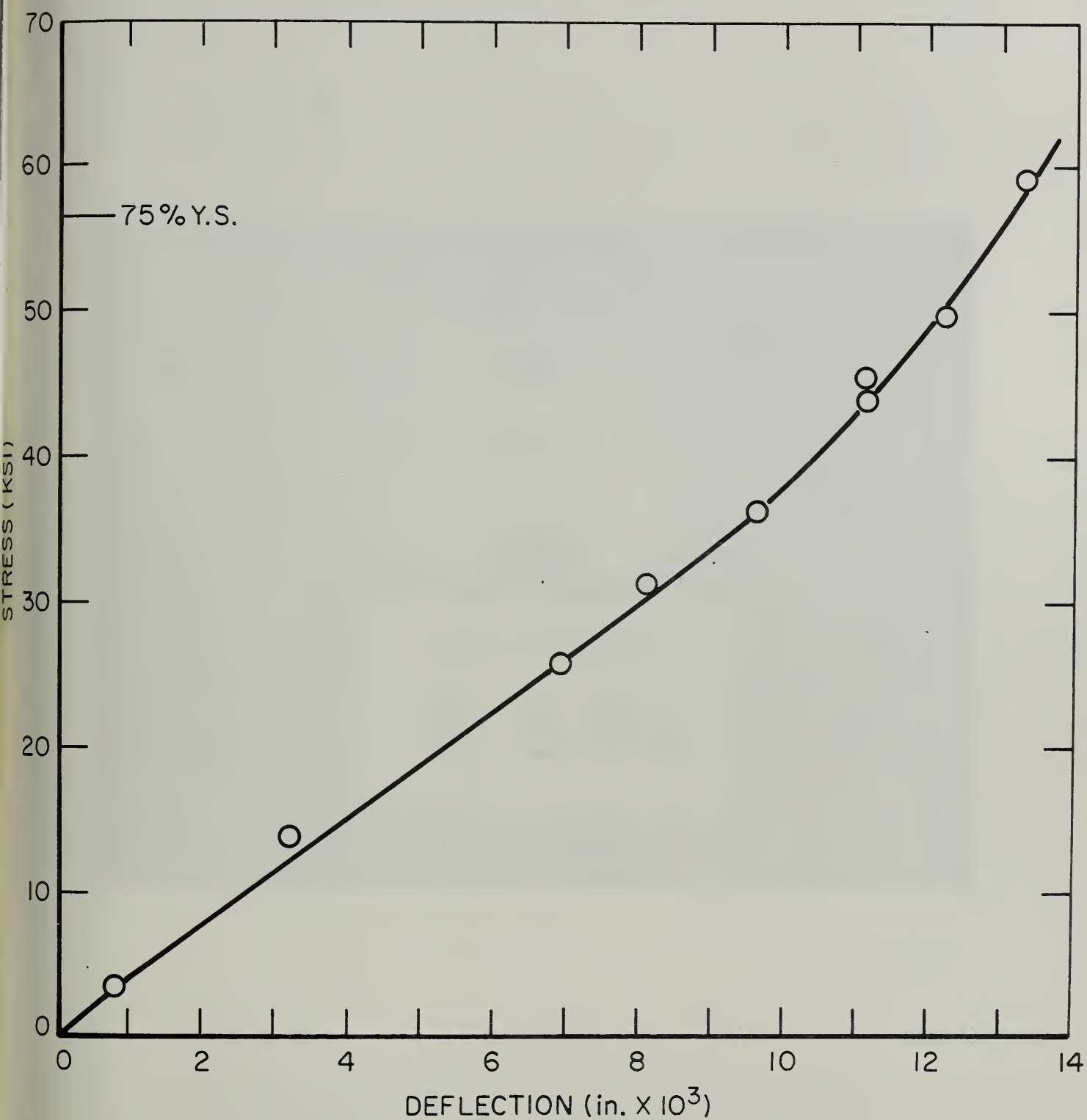


FIGURE 16

Stress-deflection curve showing the stress on the test area of the miniature tuning fork specimen versus the deflection at the screw end of the specimen.

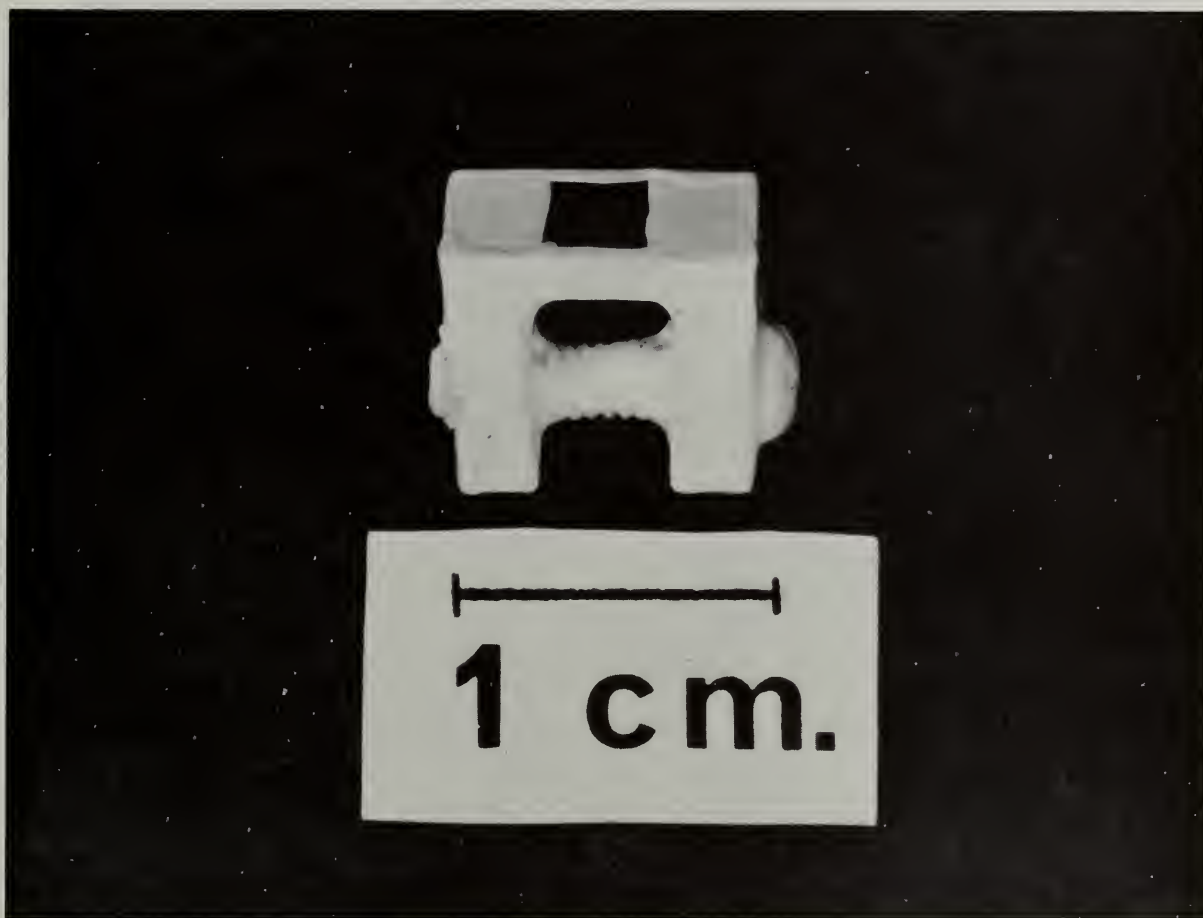


FIGURE 17

Miniature tuning fork specimen with the masking applied to all but a 2mm square area on the stressed surface. X 4

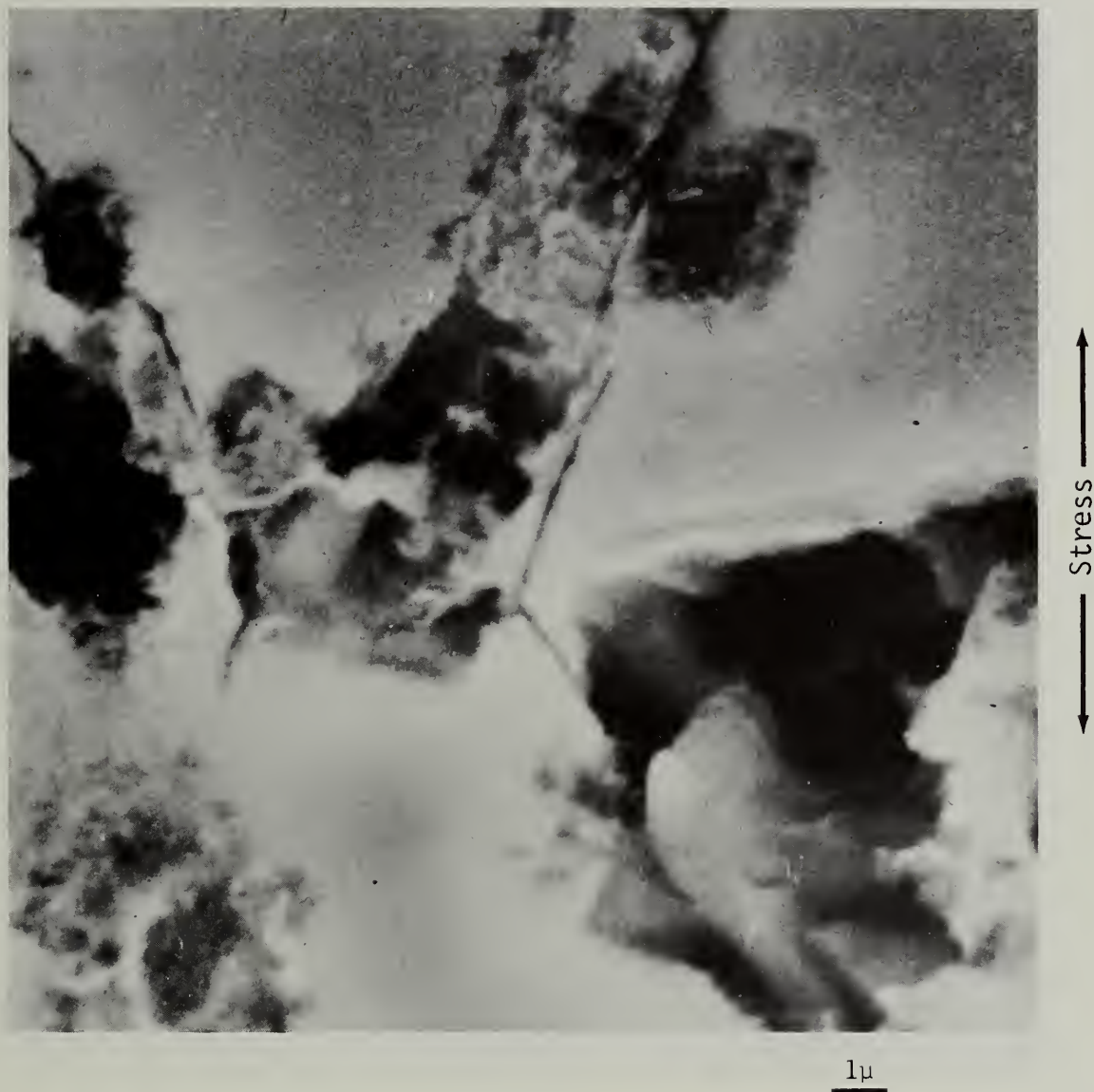


FIGURE 18

Scanning electron micrograph of a longitudinally stressed specimen after 30 seconds exposure to the chromate solution. Note stress corrosion cracks. X 7,500

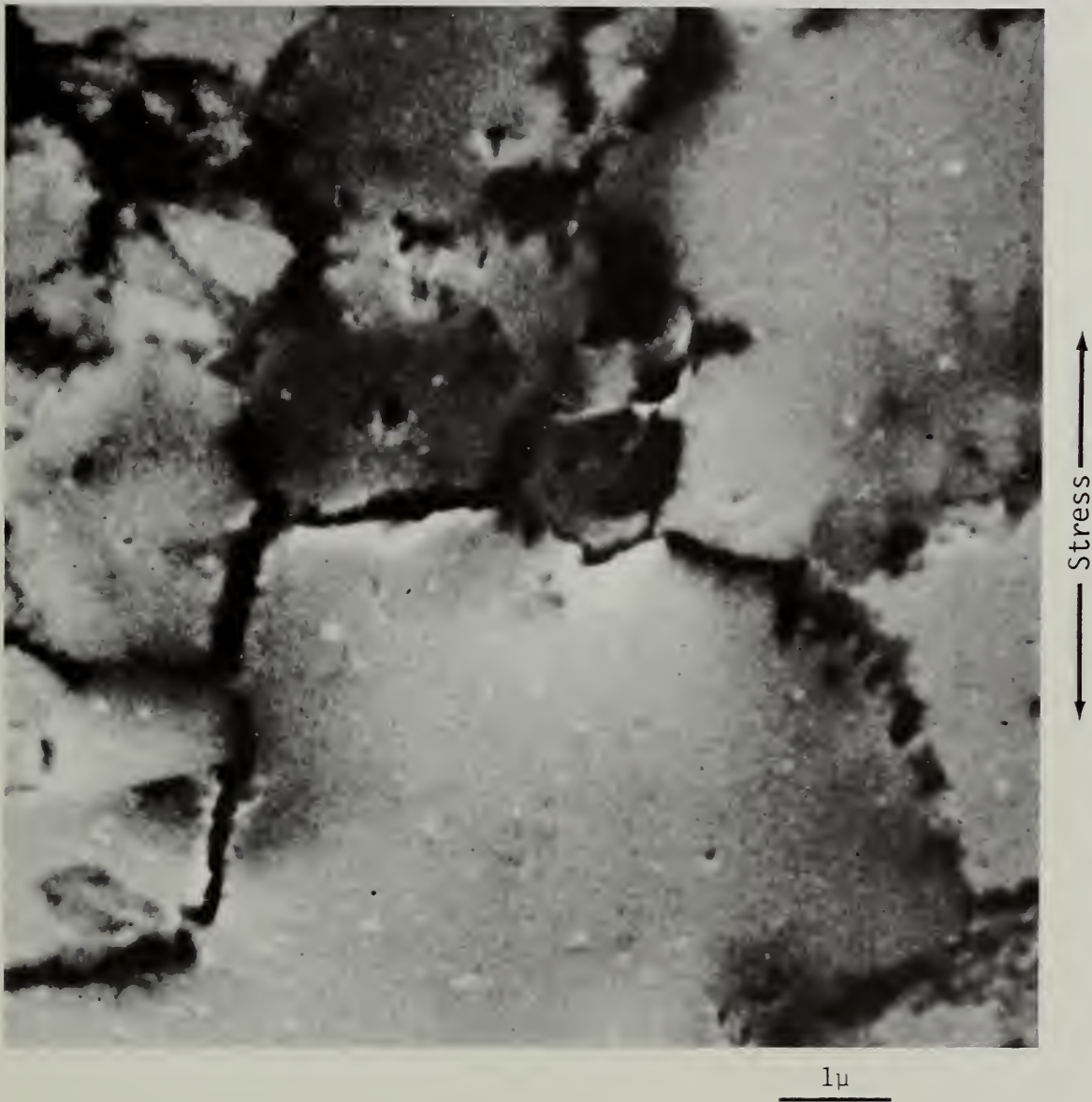


FIGURE 19

Scanning electron micrograph showing stress corrosion cracks on the surface of a longitudinally stressed specimen after 2 minutes exposure to the chromate solution. X 15,000

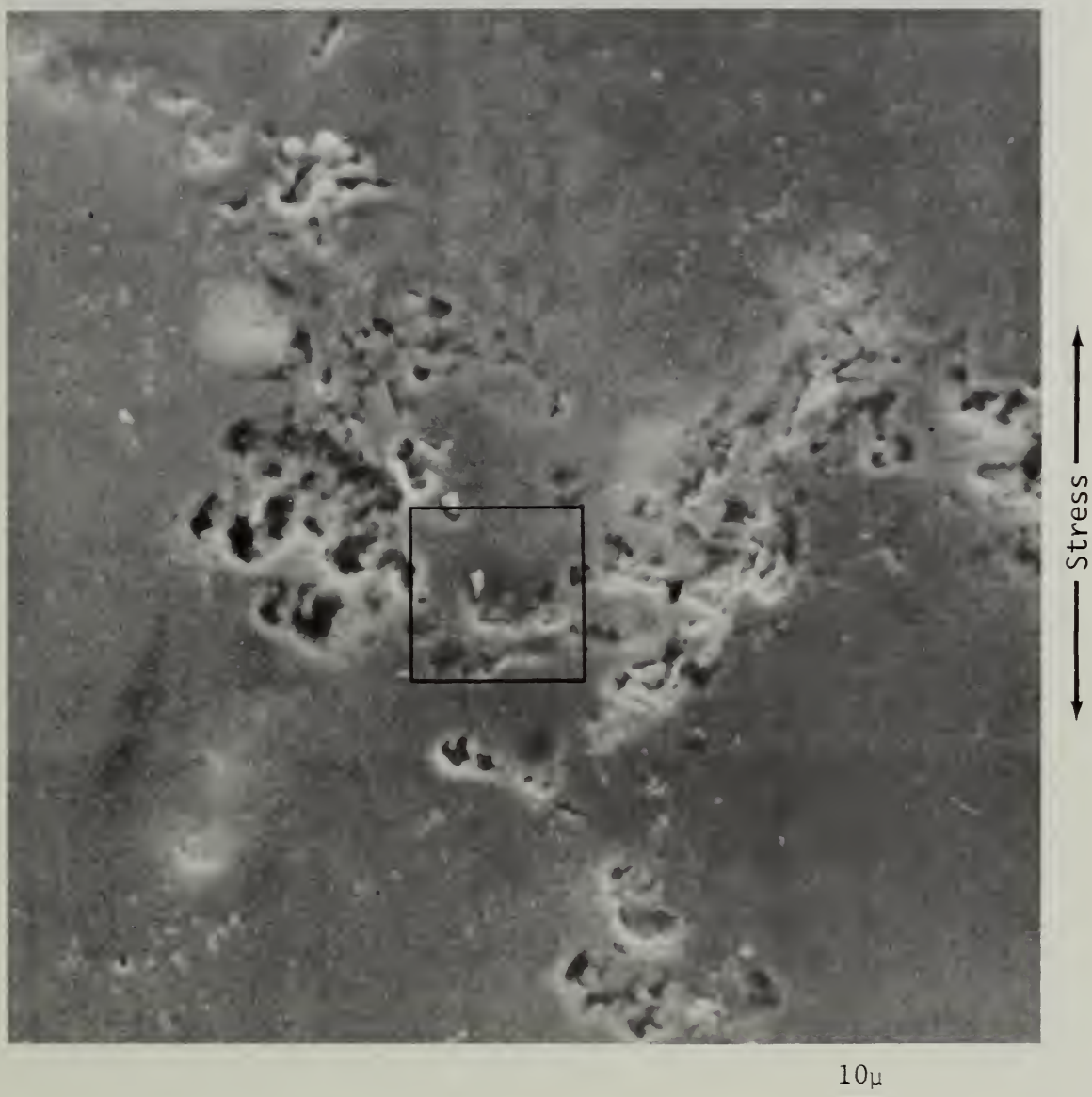


FIGURE 20

Scanning electron micrograph of a longitudinally stressed specimen showing stress corrosion cracks at the end of an elongated grain where the boundary is normal to the applied stress (enclosed area) after 5 minutes exposure to the chromate solution. Note the difficulty in observing the cracks at this low magnification. The enclosed area is shown at a higher magnification in Figure 21. X 750

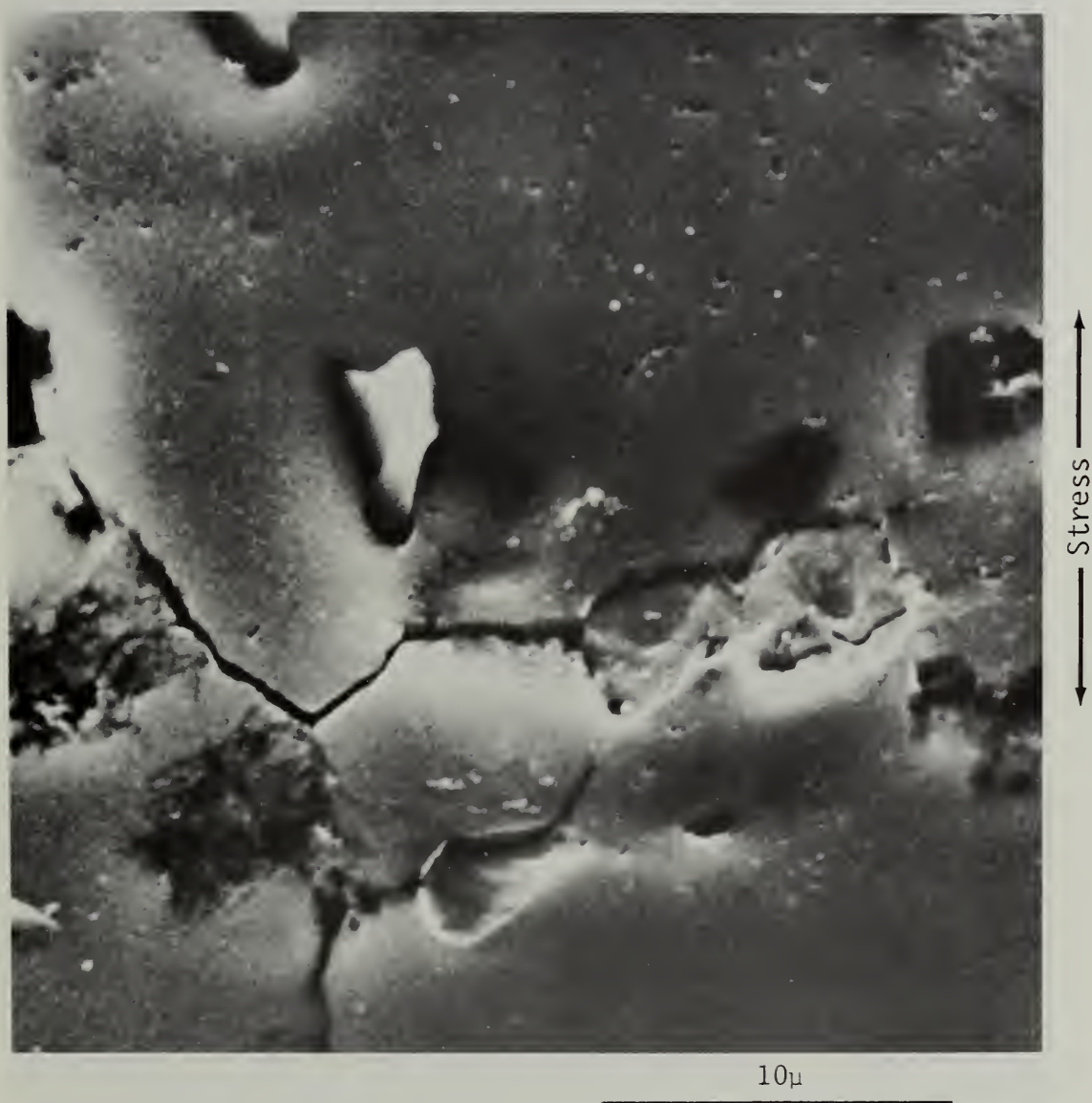


FIGURE 21

Scanning electron micrograph of the area marked off in Figure 20. Note that the cracking is primarily normal to the applied stress. X 4,500



(a)

↑ Stress ↓



(b)

10 μ

FIGURE 22

Scanning electron micrographs of a longitudinally stressed specimen after 7 minutes exposure to the chromate solution. The specimen is shown in both the stressed (a) and unstressed (b) states. Note closure of the crack in (b).
X 4,500



(a)

↑
Stress
↓



(b)

1μ

FIGURE 23

Scanning electron micrographs of areas shown in Figure 22 in the stressed (a) and unstressed (b) states. Note closure of crack in (b). X 15,000

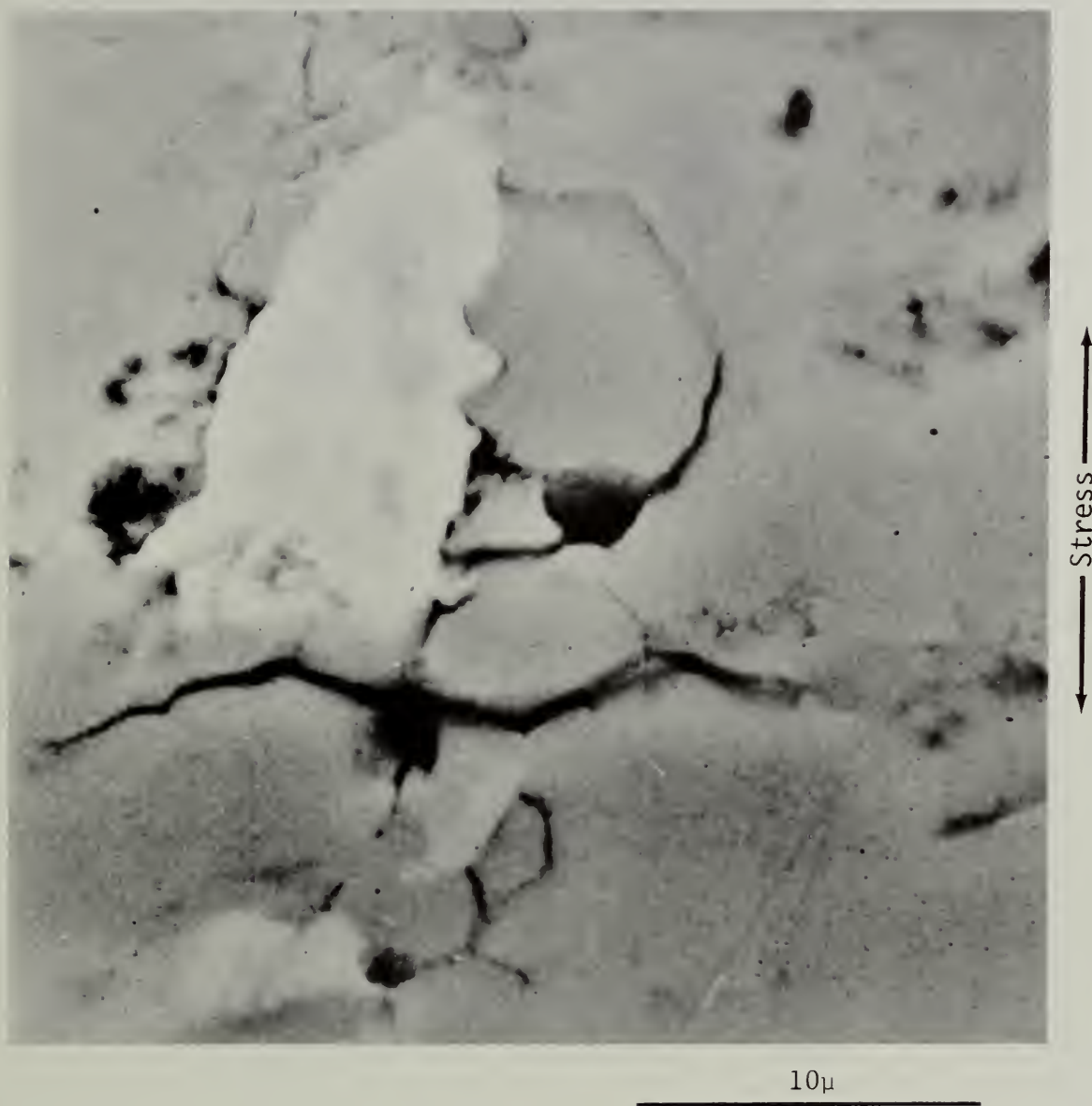
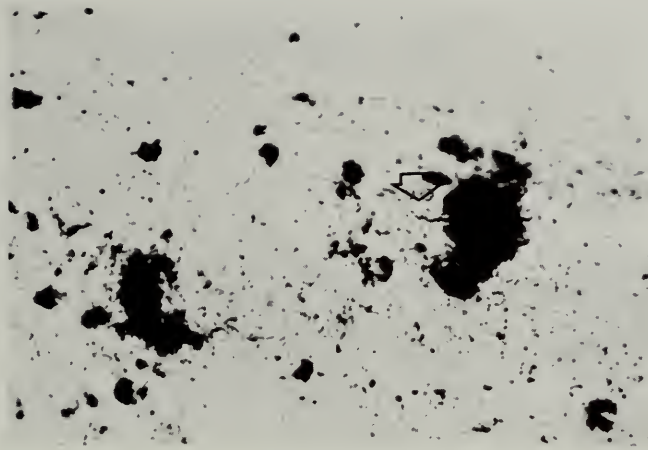


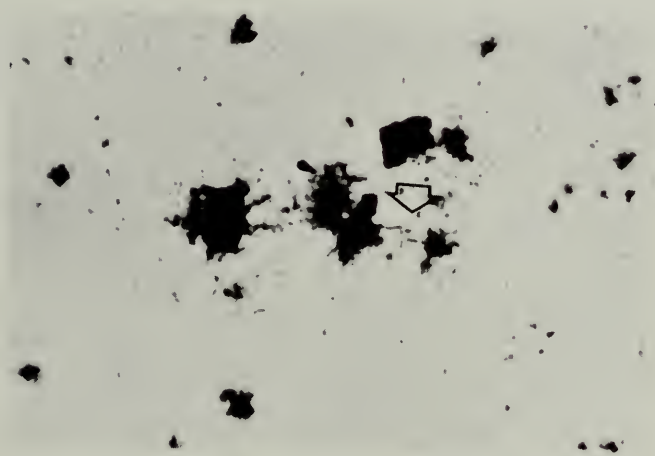
FIGURE 24

Scanning electron micrograph of a longitudinally stressed specimen after 16 hours exposure to the chromate solution. The general condition of the specimen was similar to that of a specimen after 7 minutes exposure with little additional crack propagation. X 4,500



(a)

←Stress→



(b)

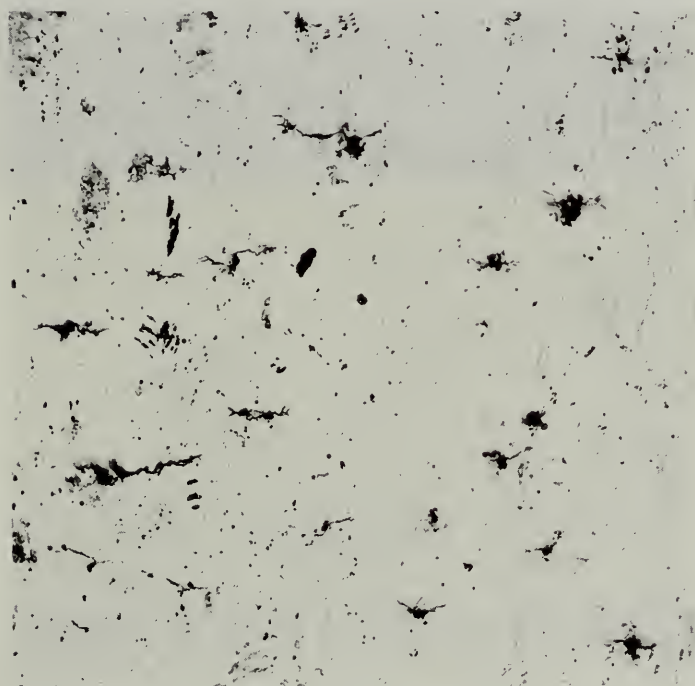
FIGURE 25

Stress corrosion cracks on short transverse (a) and longitudinal (b) specimens after 1 minute exposure to the chromate solution. Applied stress = 60 ksi. (a) - X2,000; (b) - X3,000



(a)

←Stress→



(b)

FIGURE 26

Stress corrosion cracks on short transverse (a) and longitudinal (b) specimens after 10 minutes exposure to the chromate solution. Applied stress = 70 ksi. X50



←Stress→

FIGURE 27

A stress corrosion crack on a longitudinally stressed specimen after 10 minutes exposure to the chromate solution. Note that cracking stops when unfavorable boundary is met. Applied stress = 70 ksi. Keller's etch. X200



FIGURE 28

Stress corrosion cracks on a longitudinal specimen after 10 minutes exposure to the chromate solution. Applied stress = 20 ksi. X400

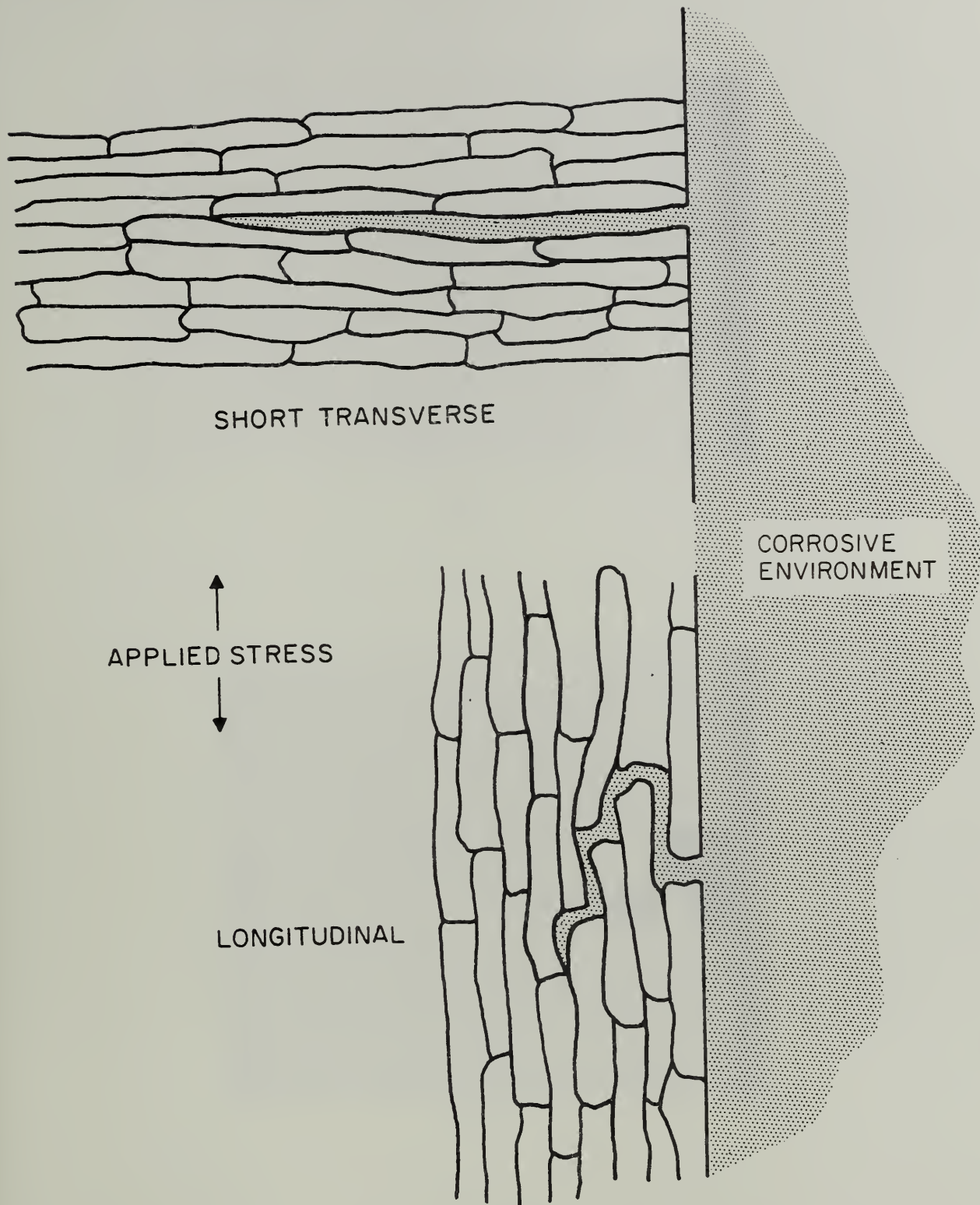
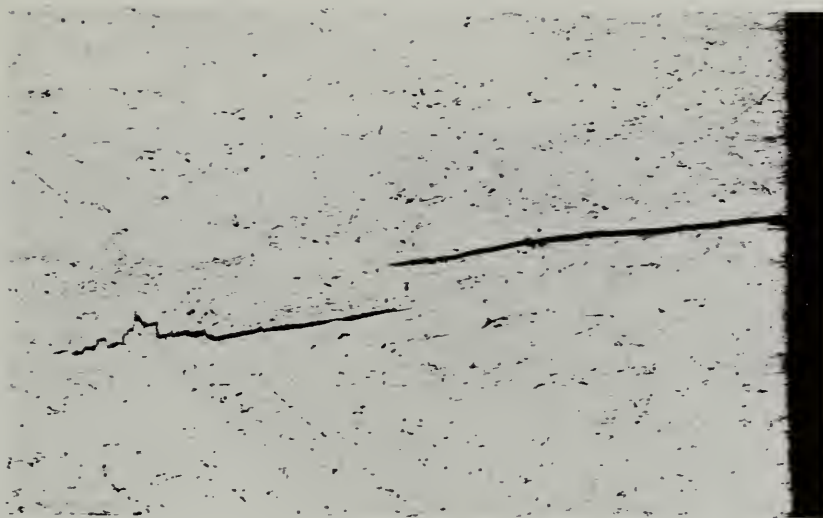


FIGURE 29

Schematic representation of stress corrosion crack propagation through an elongated grain structure when stressed in the short transverse and in the longitudinal directions. Note that in the short transverse specimen the crack may propagate in a plane that deviates very little, while the crack plane in the longitudinal specimen must deviate greatly from a plane normal to the applied stress.



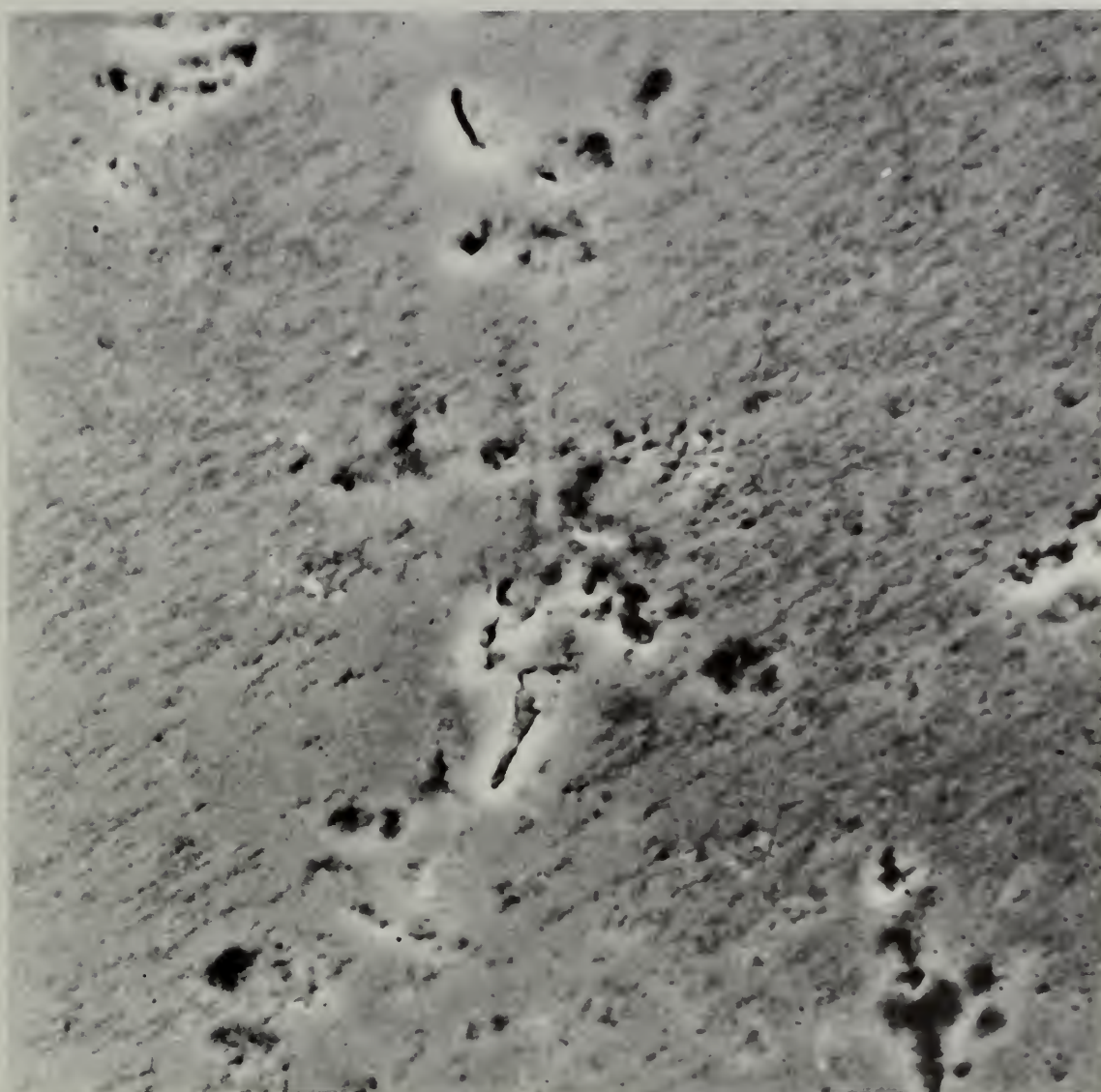
(a)



(b)

FIGURE 30

Photomicrographs of stress corrosion cracks in (a) a short transverse specimen, X75, and (b) a longitudinal specimen, X160. Note similarity to Figure 29.



10μ

FIGURE 31

Scanning electron micrograph of the surface of an unstressed specimen exposed to the chromate solution for 10 seconds. Note the great amount of general pitting as compared to specimens corroded under stress. X 1,500

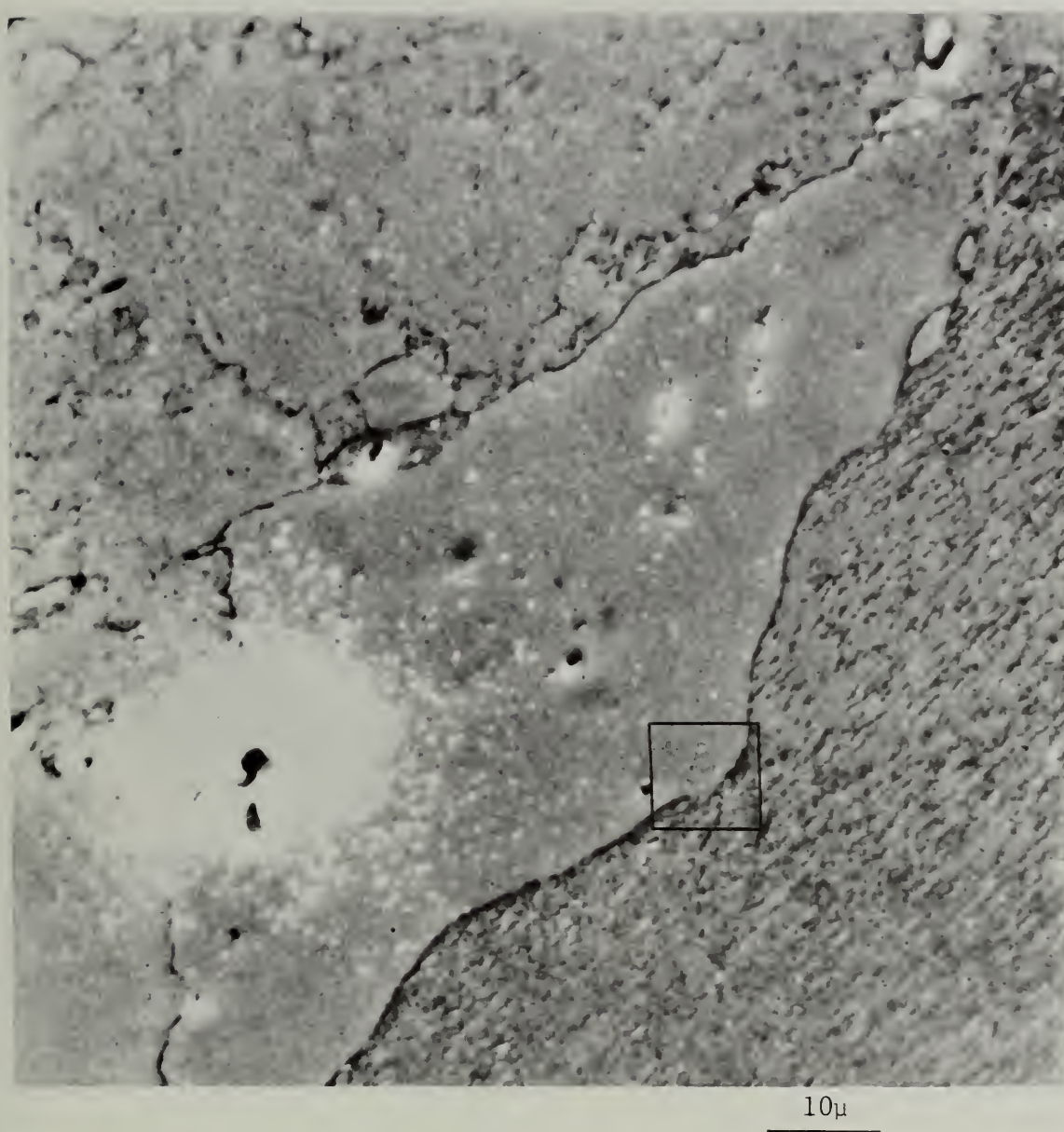


FIGURE 32

Scanning electron micrograph of the surface of an unstressed specimen after 5 minutes exposure to the chromate solution. Note general pitting and intergranular corrosion. See Figure 33 for greater detail of enclosed area. X 1,500

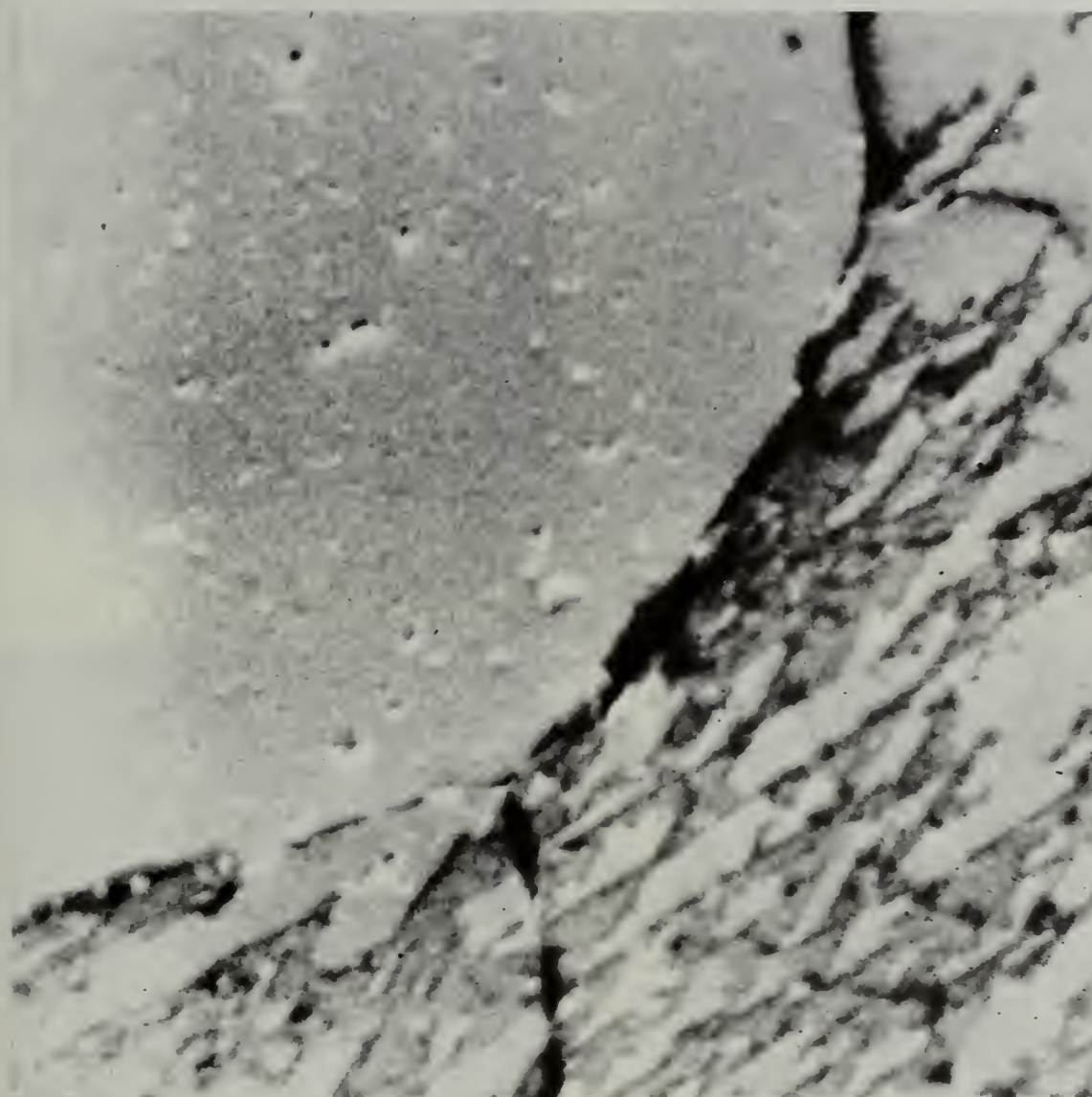
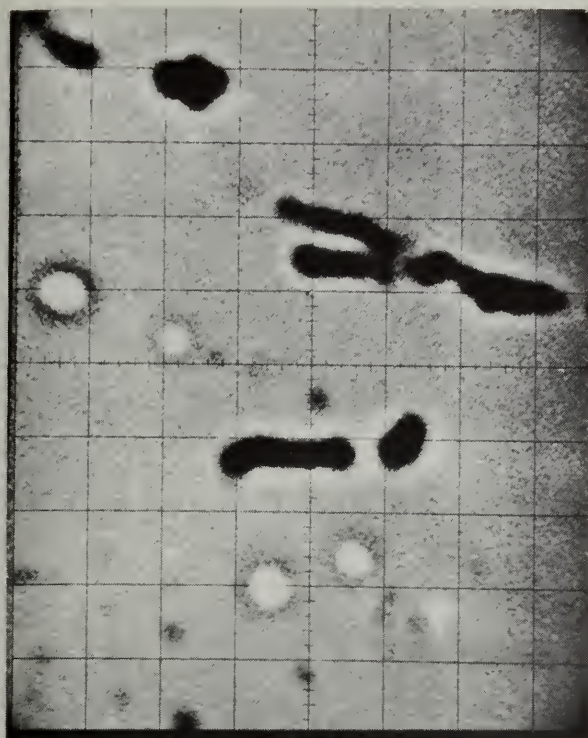
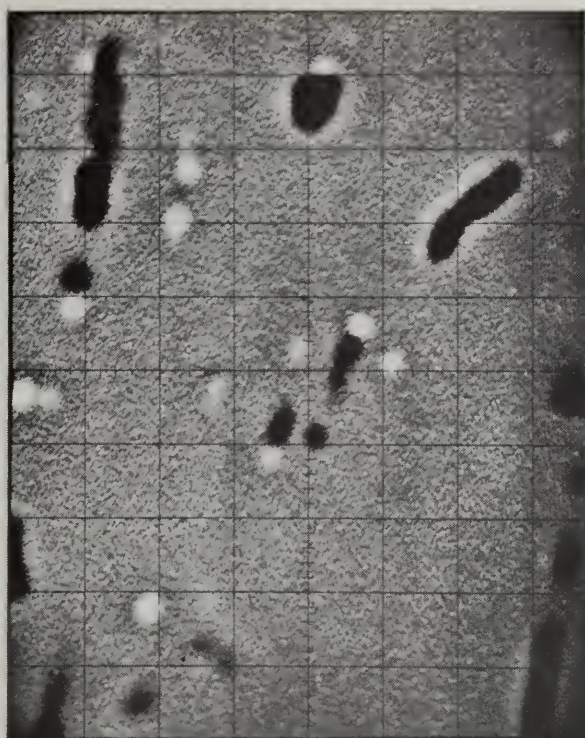


FIGURE 33

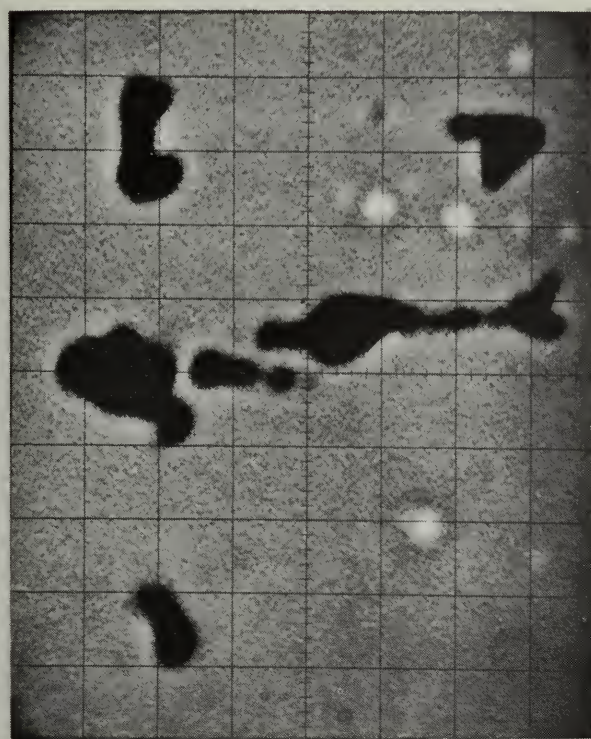
Scanning electron micrograph of the area marked off in Figure 32. Note general pitting and intergranular corrosion. X 15,000



(a)



(b)



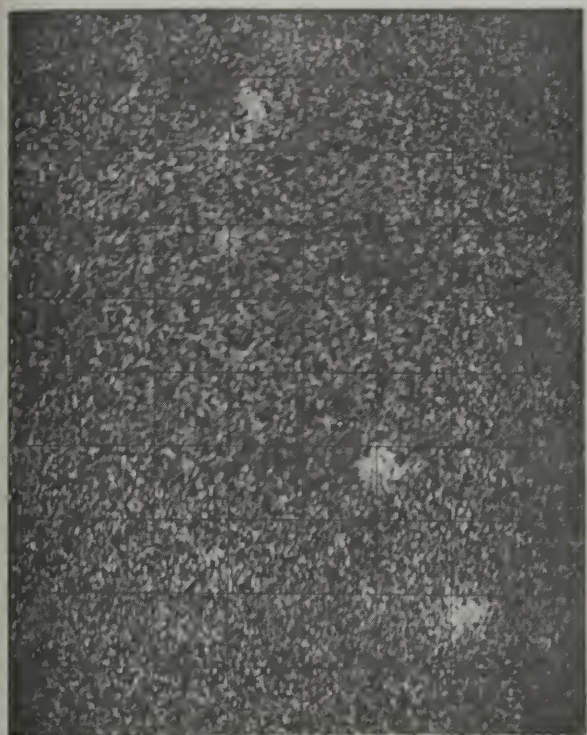
(c)



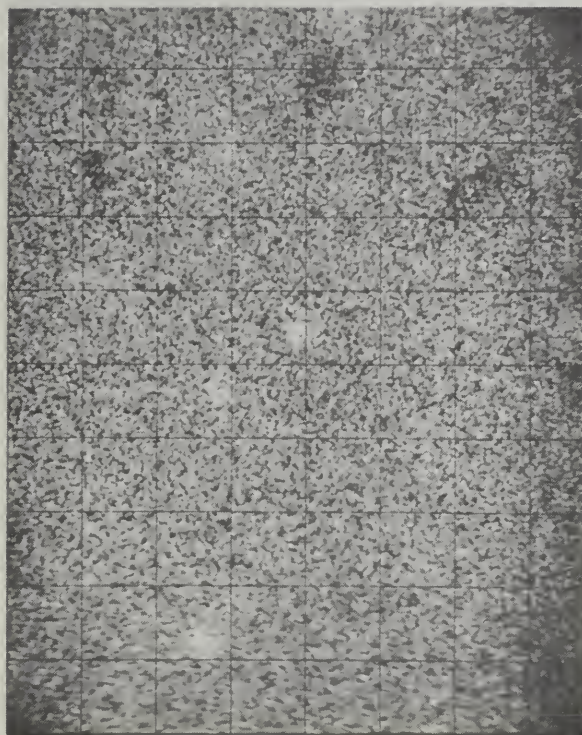
(d)

FIGURE 34

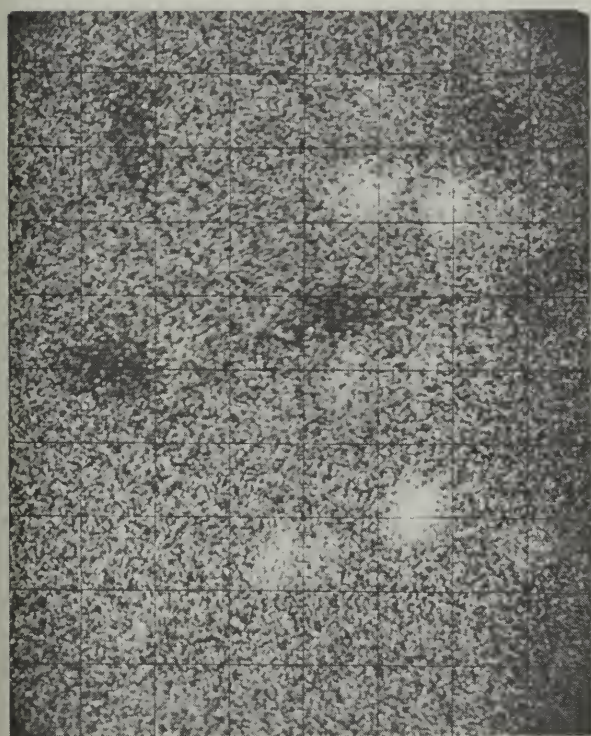
Target current images of areas with inclusions from a 7075 aluminum alloy plate. The light areas indicate inclusions of lower atomic number and the dark areas, inclusions of higher atomic number than the matrix. Both the -T651 (a & b) and the -T73 (c & d) treatments are shown. Areas shown include the short transverse-long transverse plane (a & c) and the short-transverse-longitudinal plane (b & d). $7\mu/\text{div}$.



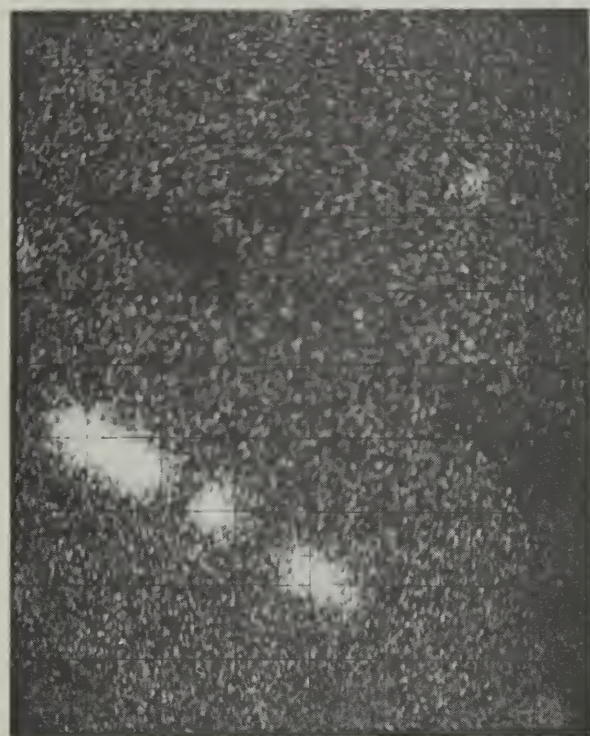
(a)



(b)



(c)



(d)

FIGURE 35

Magnesium X-ray images of areas shown in Figure 34. Light areas are high in magnesium.



(a)



(b)



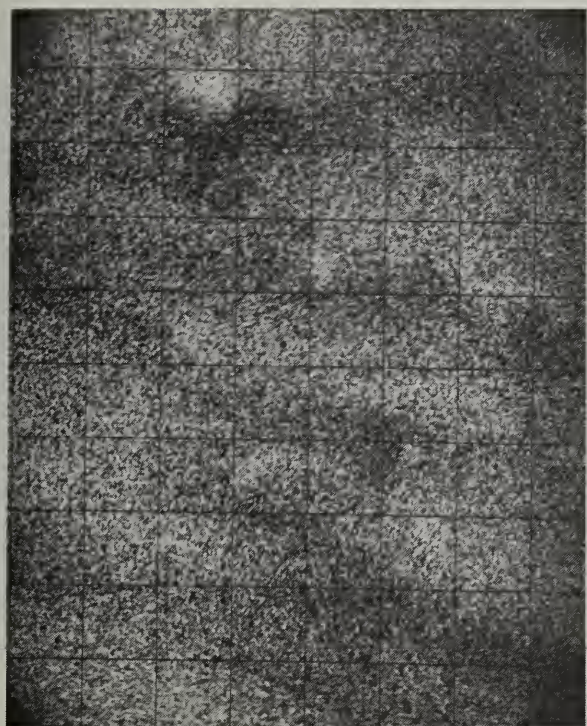
(c)



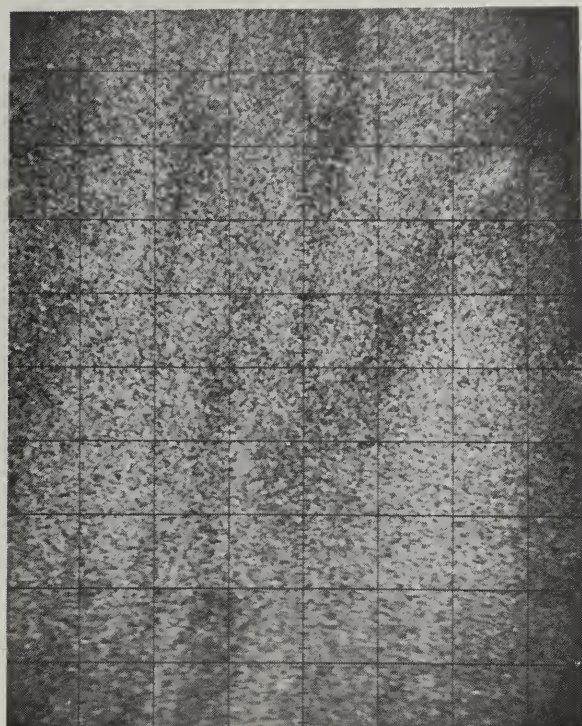
(d)

FIGURE 36

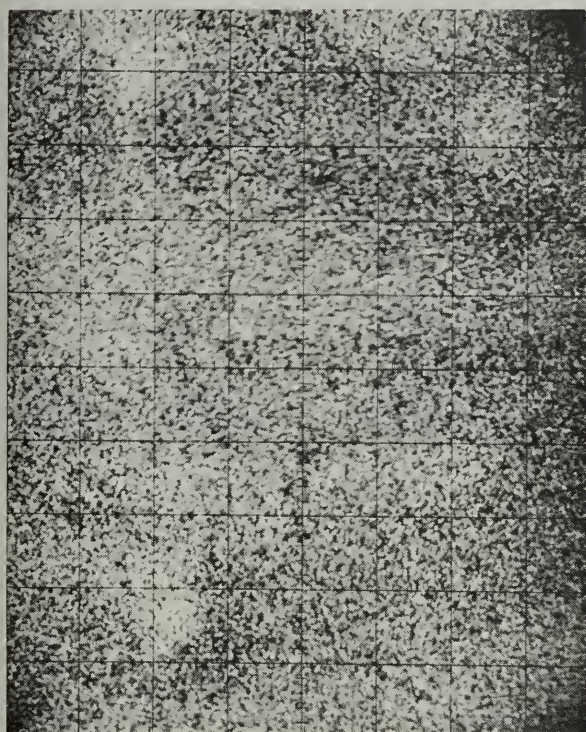
Iron X-ray images of areas shown in Figure 34. Light areas are high in iron.



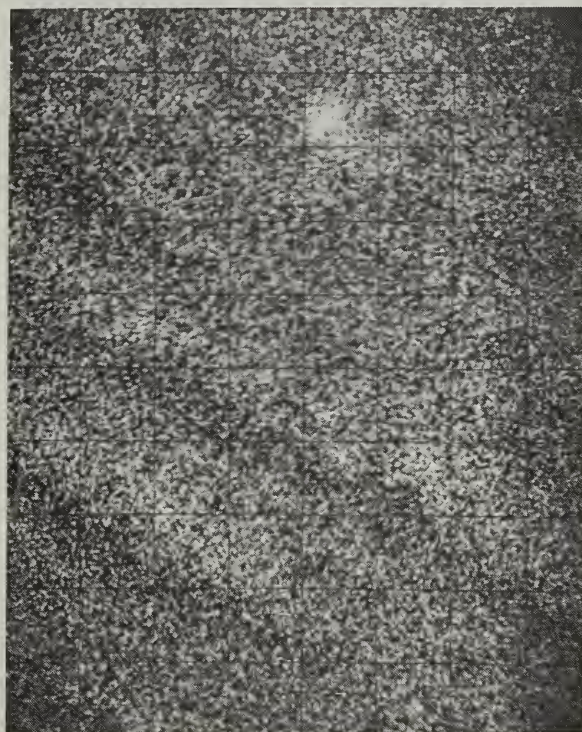
(a)



(b)



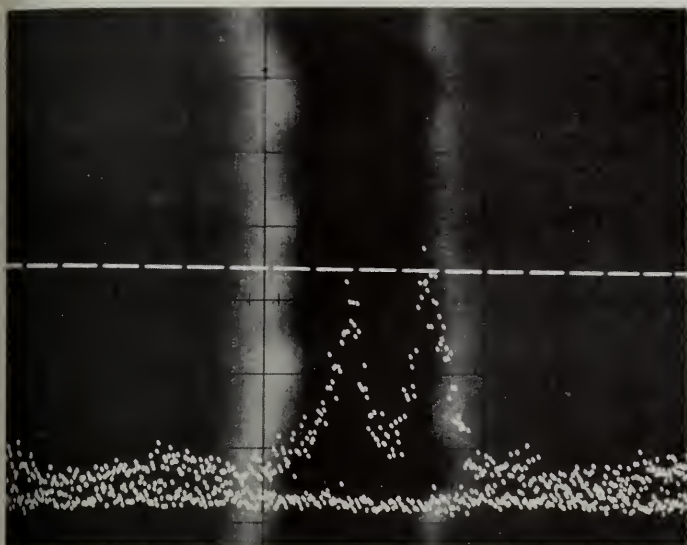
(c)



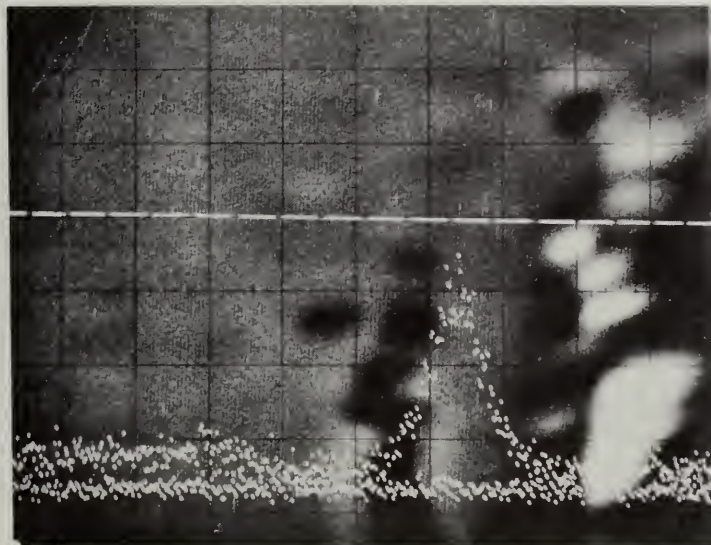
(d)

FIGURE 37

Chromium X-ray images of areas shown in Figure 34. Light areas are high in chromium.



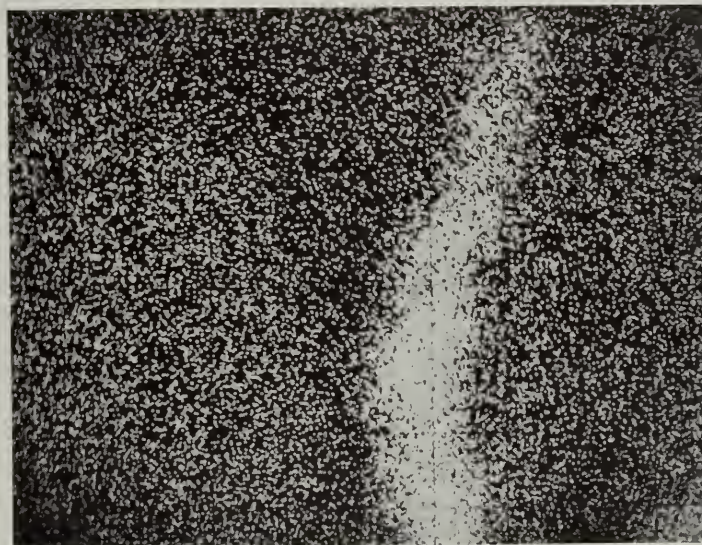
(a) Target Current Plus CrK α



(c) Target Current Plus CrK α



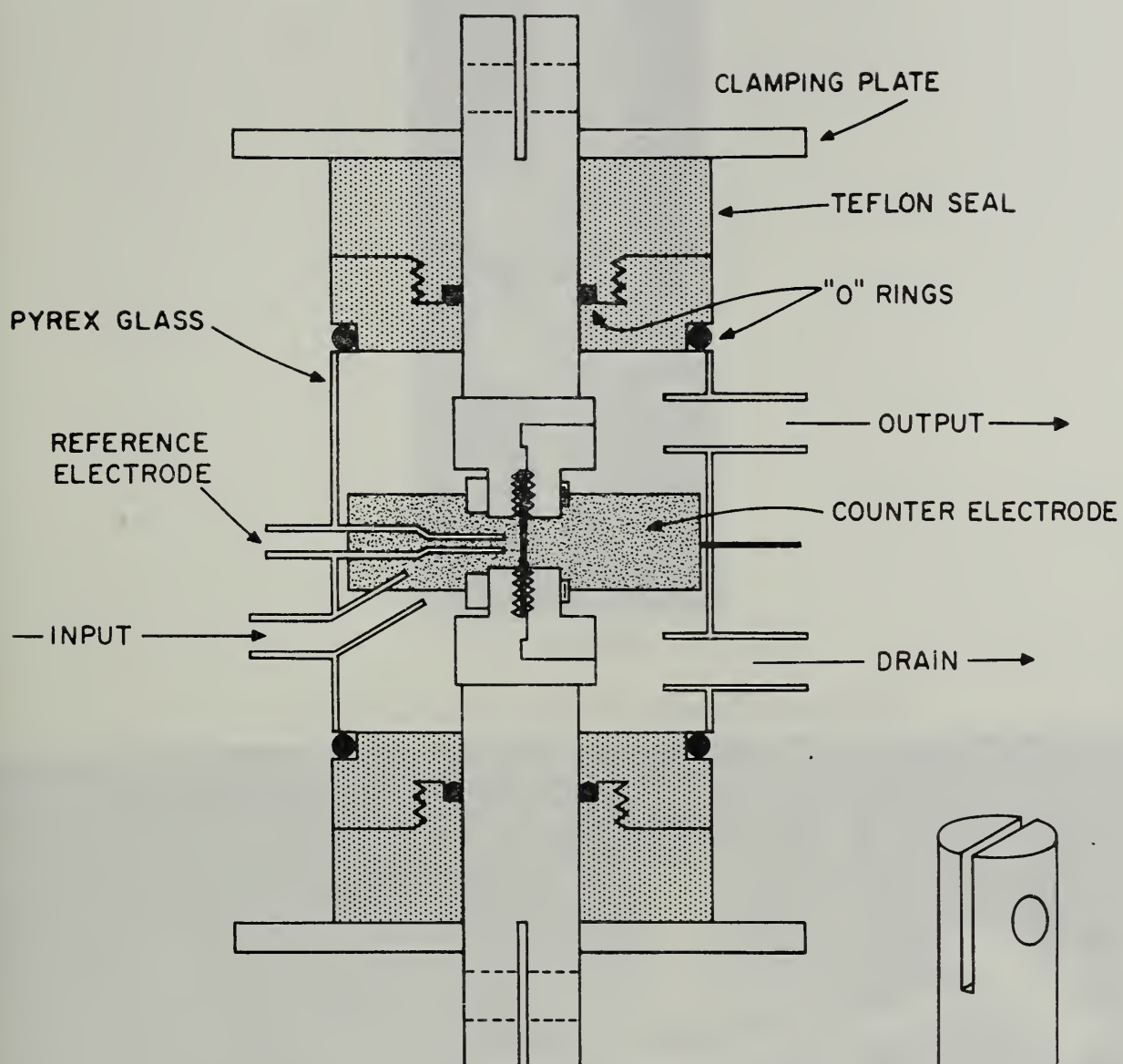
(b) Cr X-ray Scan



(d) Cr X-ray Scan

FIGURE 38

Electron probe microanalysis of areas along the path of crack propagation. Figures (a) and (c) are target current images with the CrK α X-ray rate meter trace superposed on it. The dashed line is the locus of the electron beam as it was swept over the sample. Chromium X-ray area scans are shown in Figures (b) and (d) in which light areas are high in Chromium.



SCALE 1:1

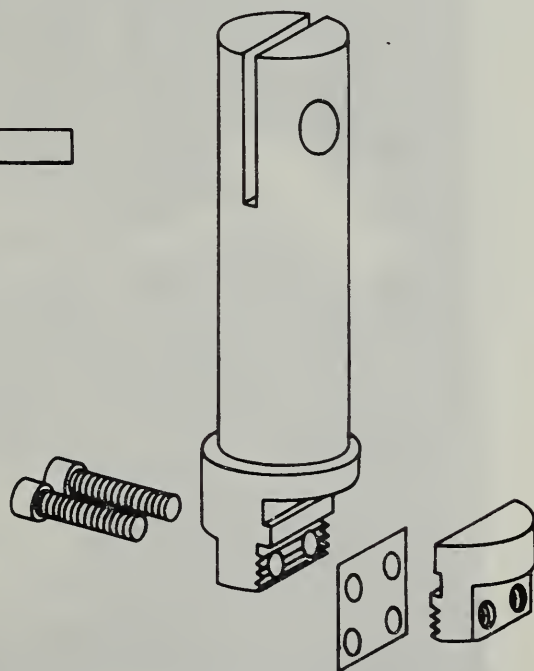


FIGURE 39

Initial electrochemical stress corrosion cell design for externally applied stress on square specimens.

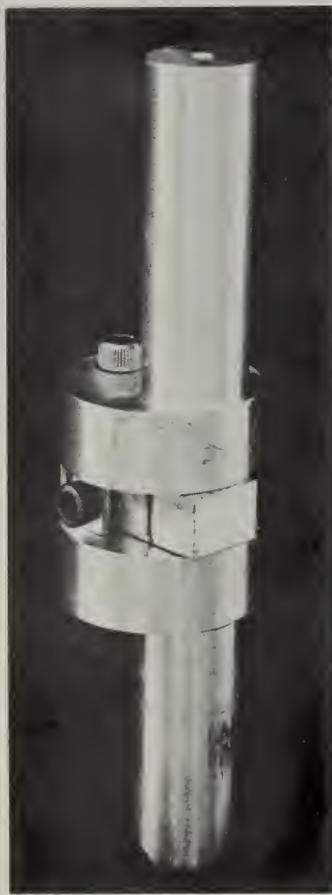


FIGURE 40a

Tuning fork specimen in mounting bracket.

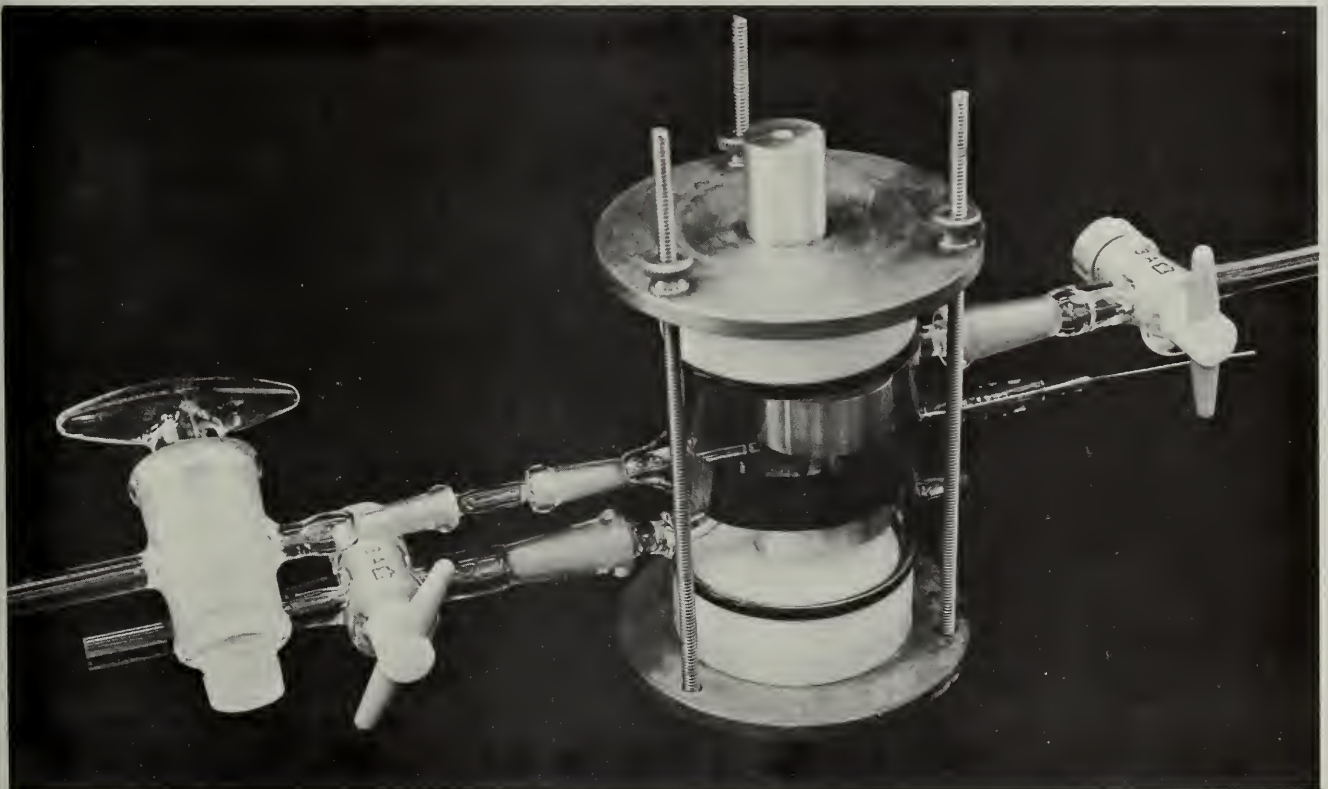


FIGURE 40b

Assembled electrochemical stress corrosion cell for self-stressed tuning fork specimens.

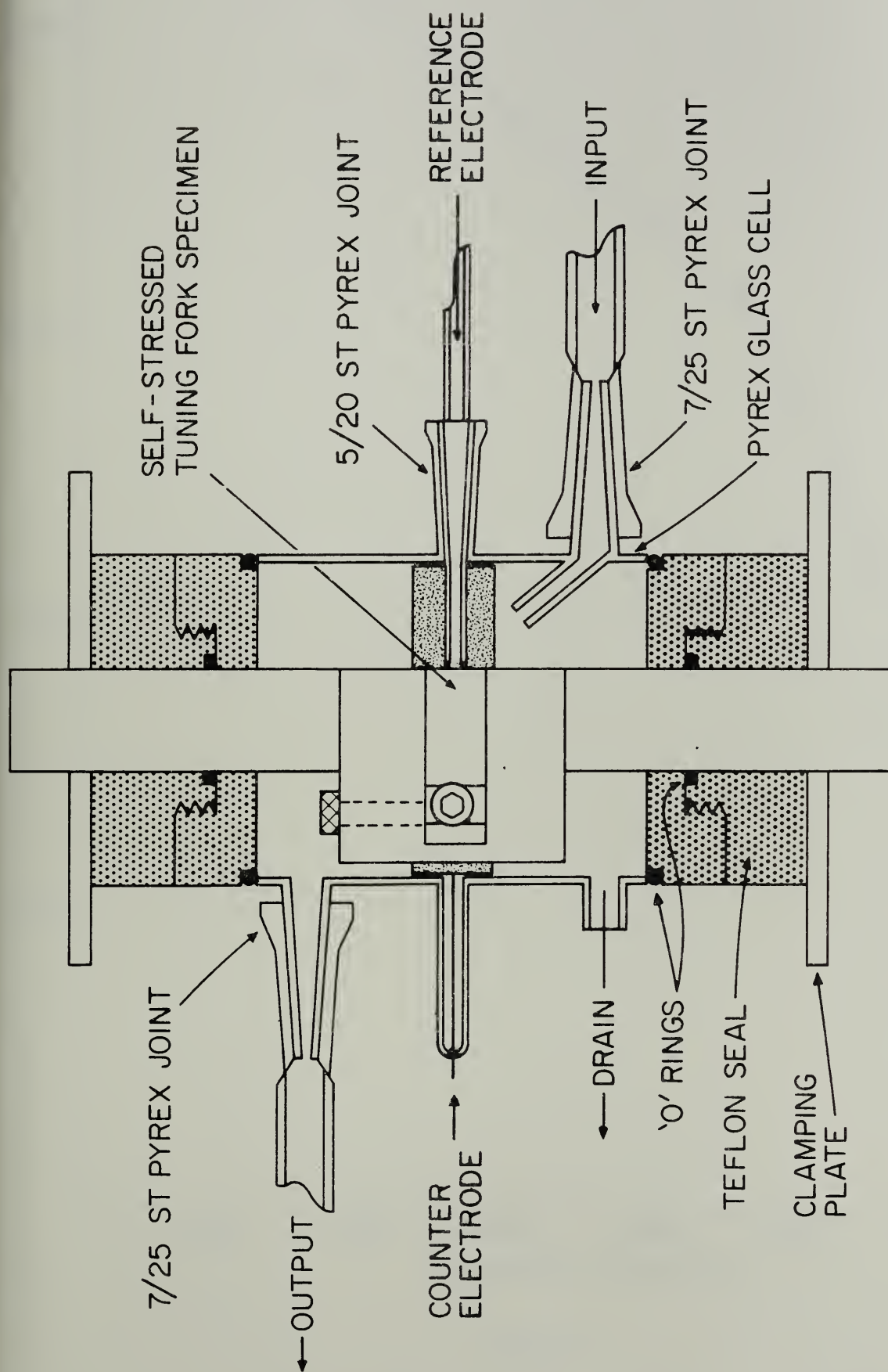


FIGURE 41

Final electrochemical stress corrosion cell design for self-stressed tuning fork specimens.

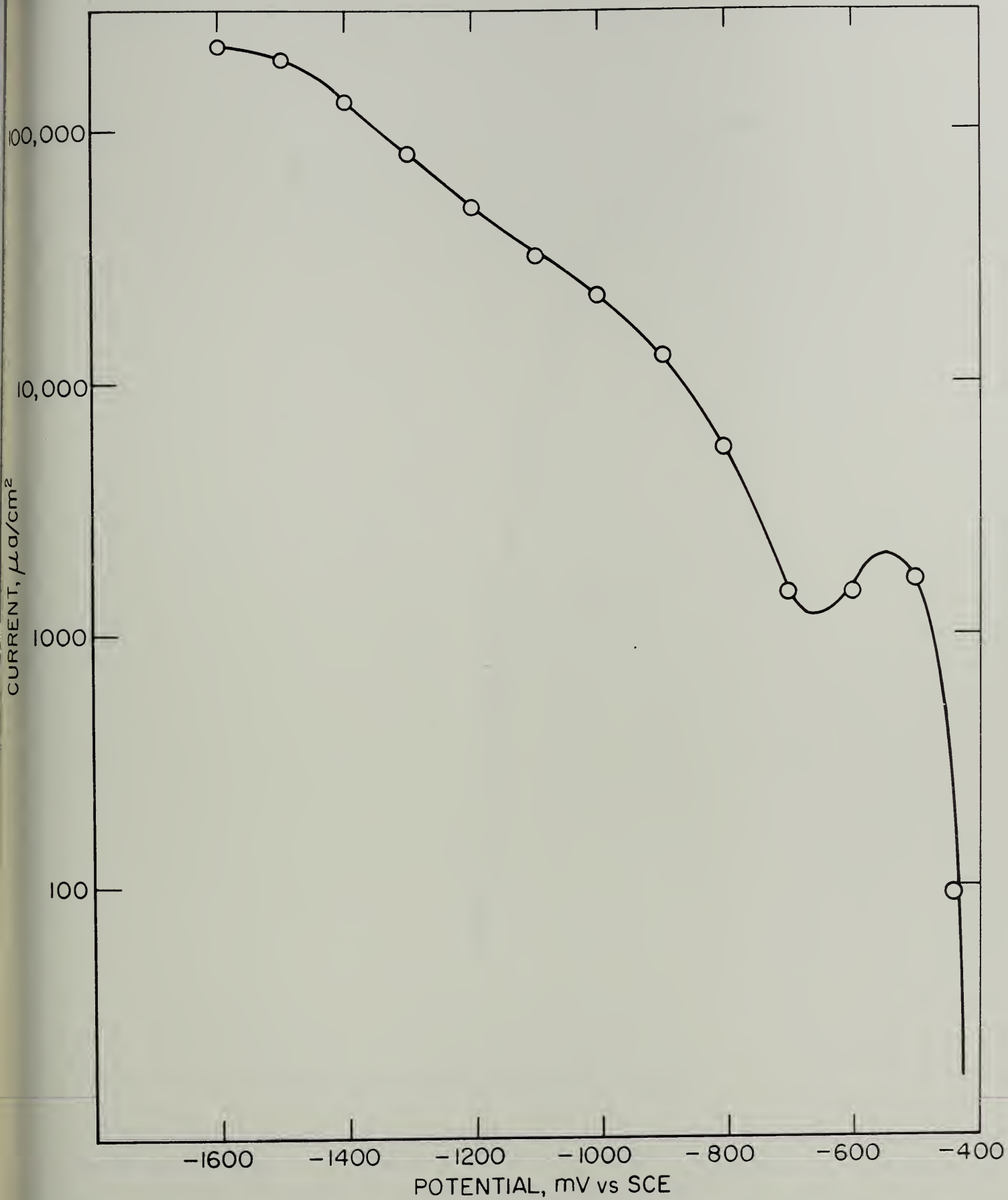


FIGURE 42

Cathodic polarization curve for 7075-T651 in 0.3% NaCl - 3.0% $K_2Cr_2O_7$ - 3.0% CrO_3 . Open circuit EMF = -440 mV vs SCE.

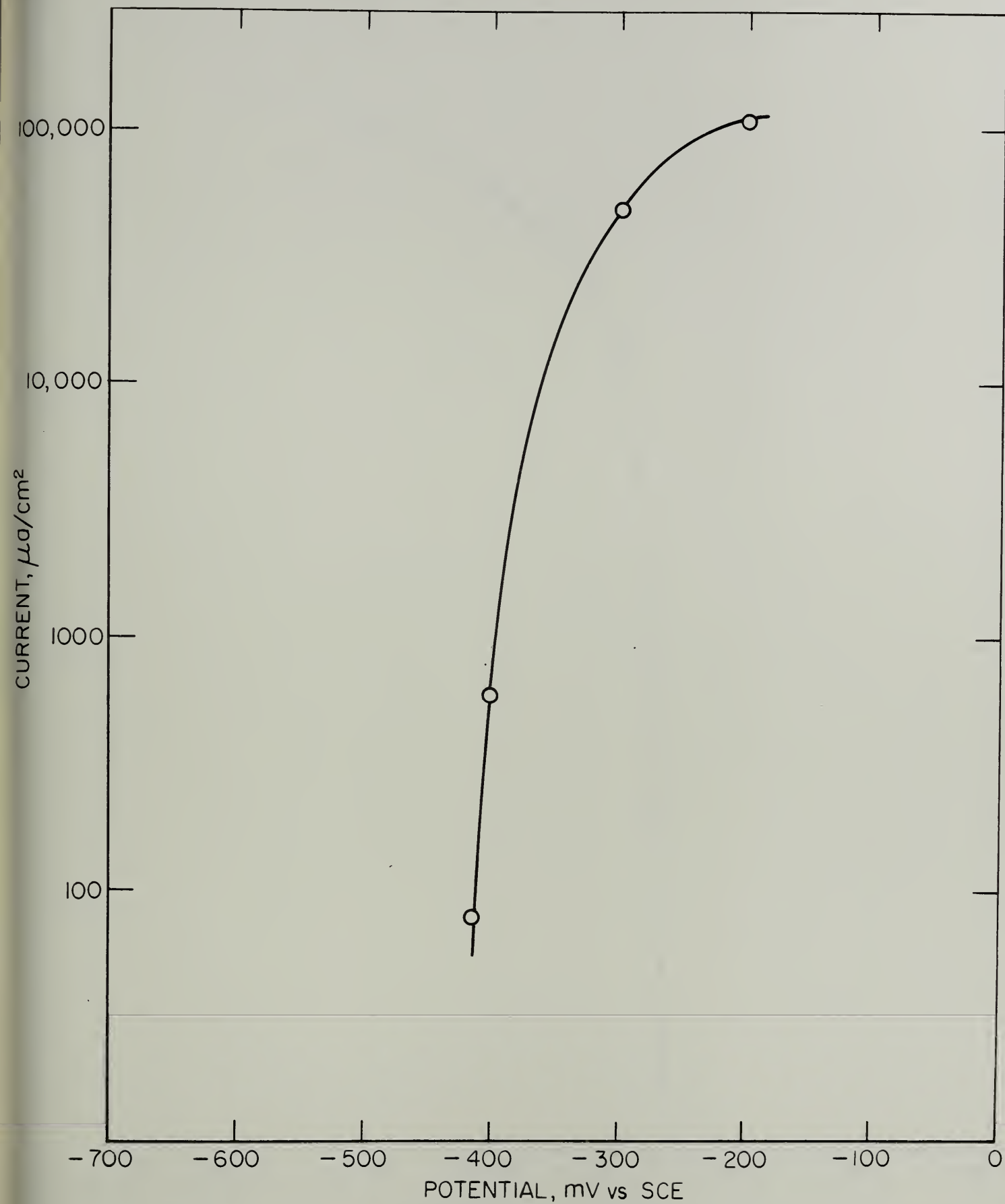


FIGURE 43

Anodic polarization curve for 7075-T651 in 0.3% NaCl -
3.0% $\text{K}_2\text{Cr}_2\text{O}_7$ - 3.0% CrO_3 .

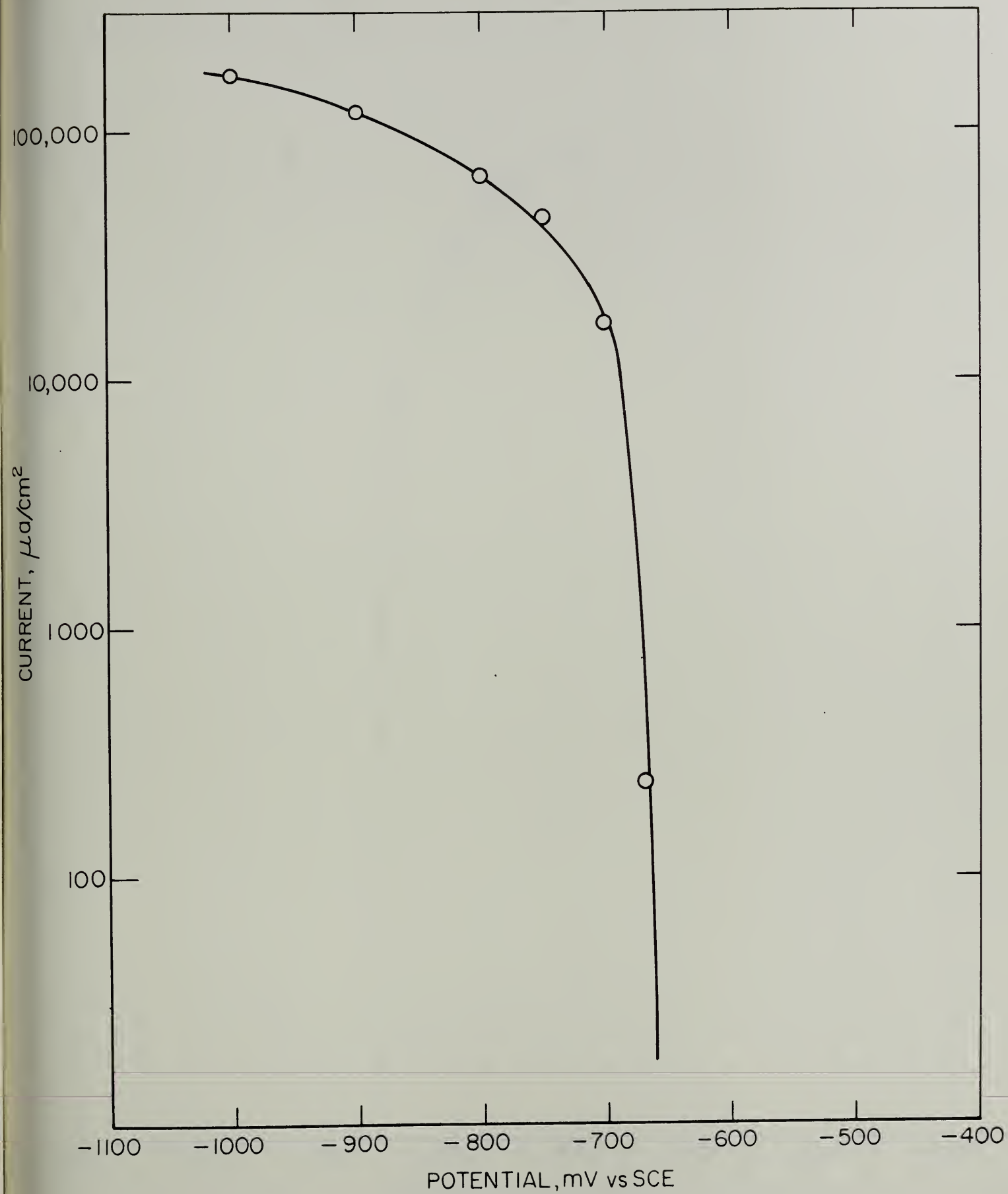


FIGURE 44

Cathodic polarization curve for 7075-T651 in 3.5% NaCl
(pH = 0.9 with HCl). Open circuit EMF = -670 mV vs SCE.

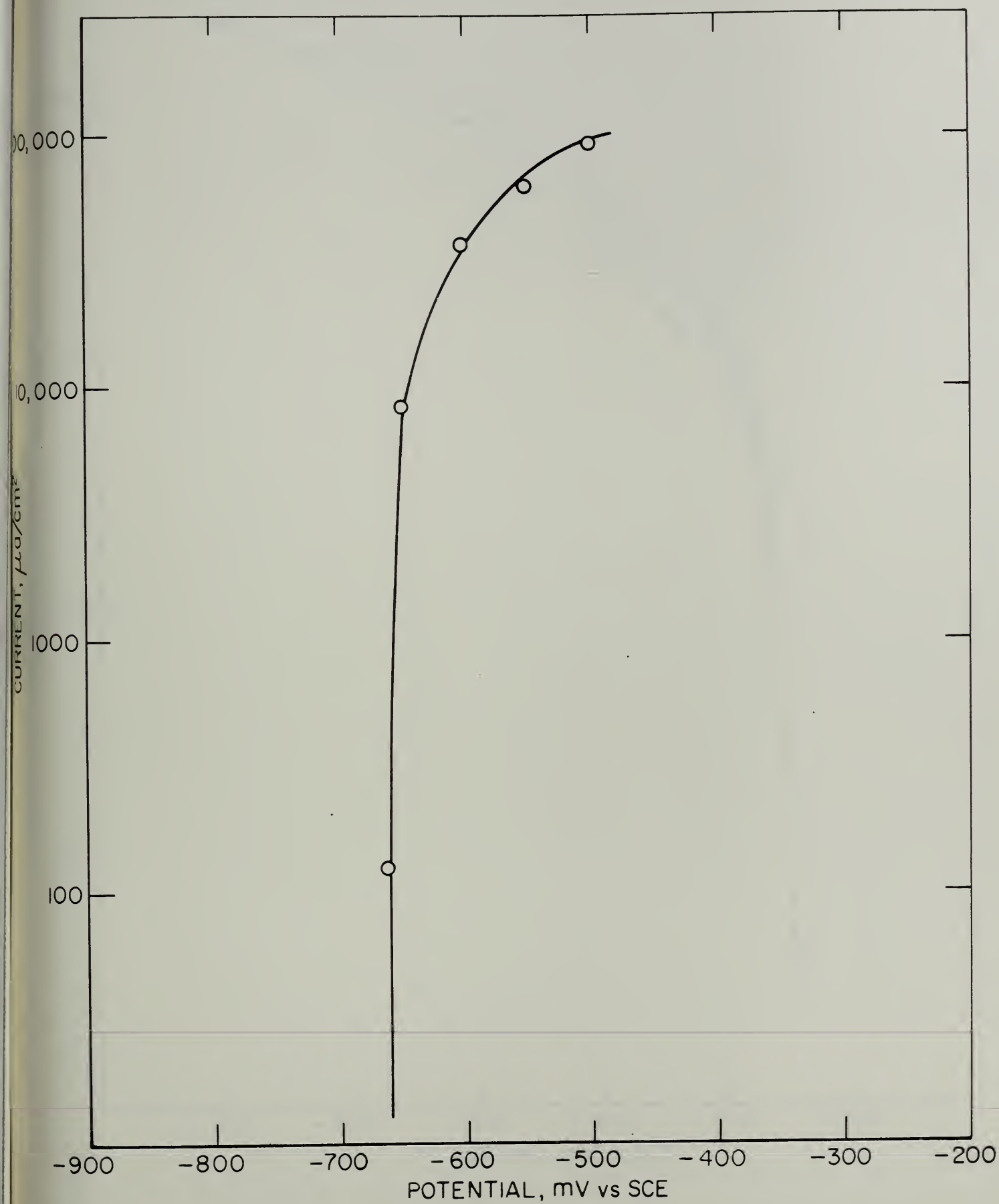


FIGURE 45

Anodic polarization curve for 7075-T651 in 3.5% NaCl
(pH = 0.9 with HCl).

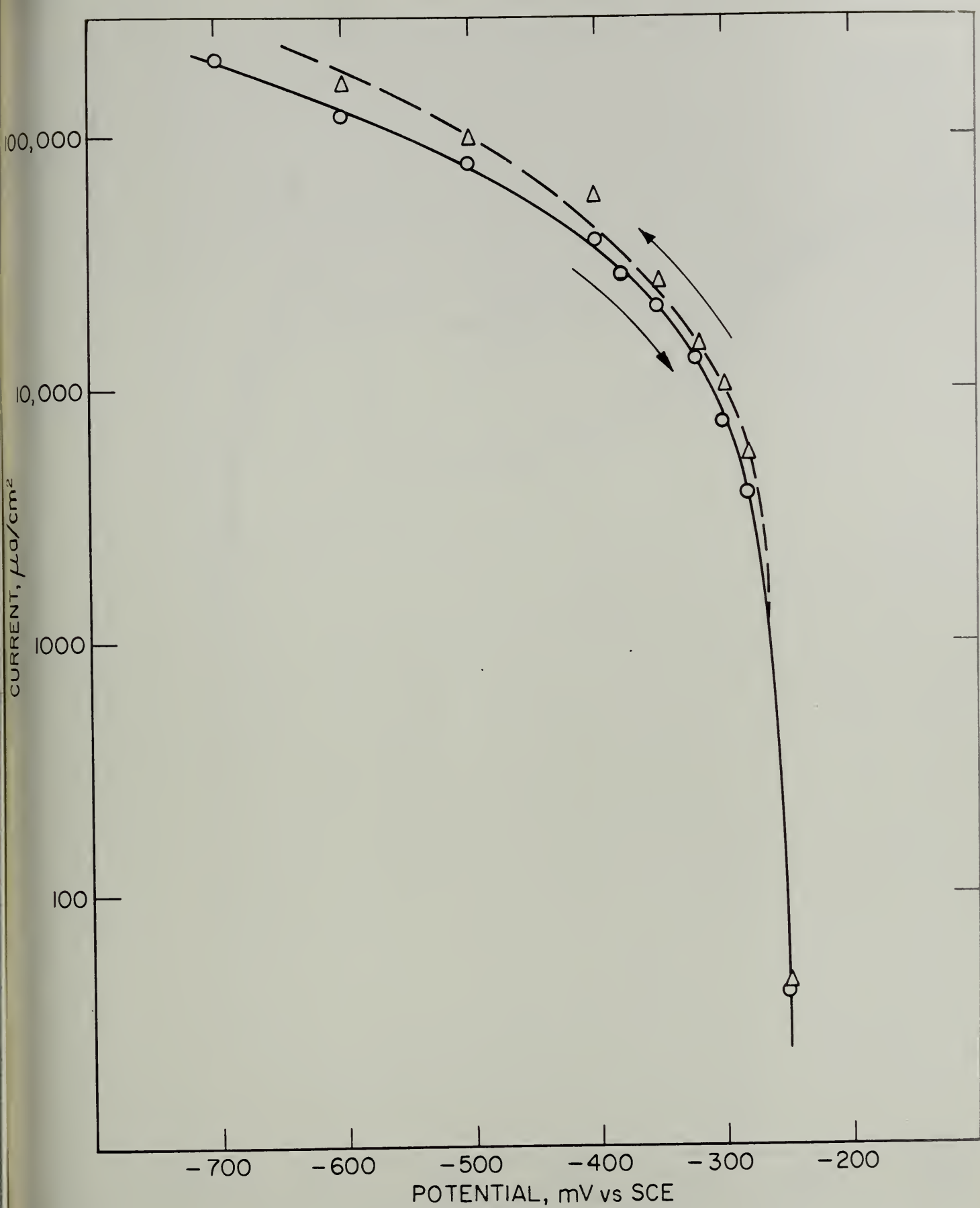


FIGURE 46

Cathodic polarization curve for 7075-T651 in 1.0N NaNO₃
(pH = 0.9 with HNO₃). Open circuit EMF = -260 mV vs SCE.

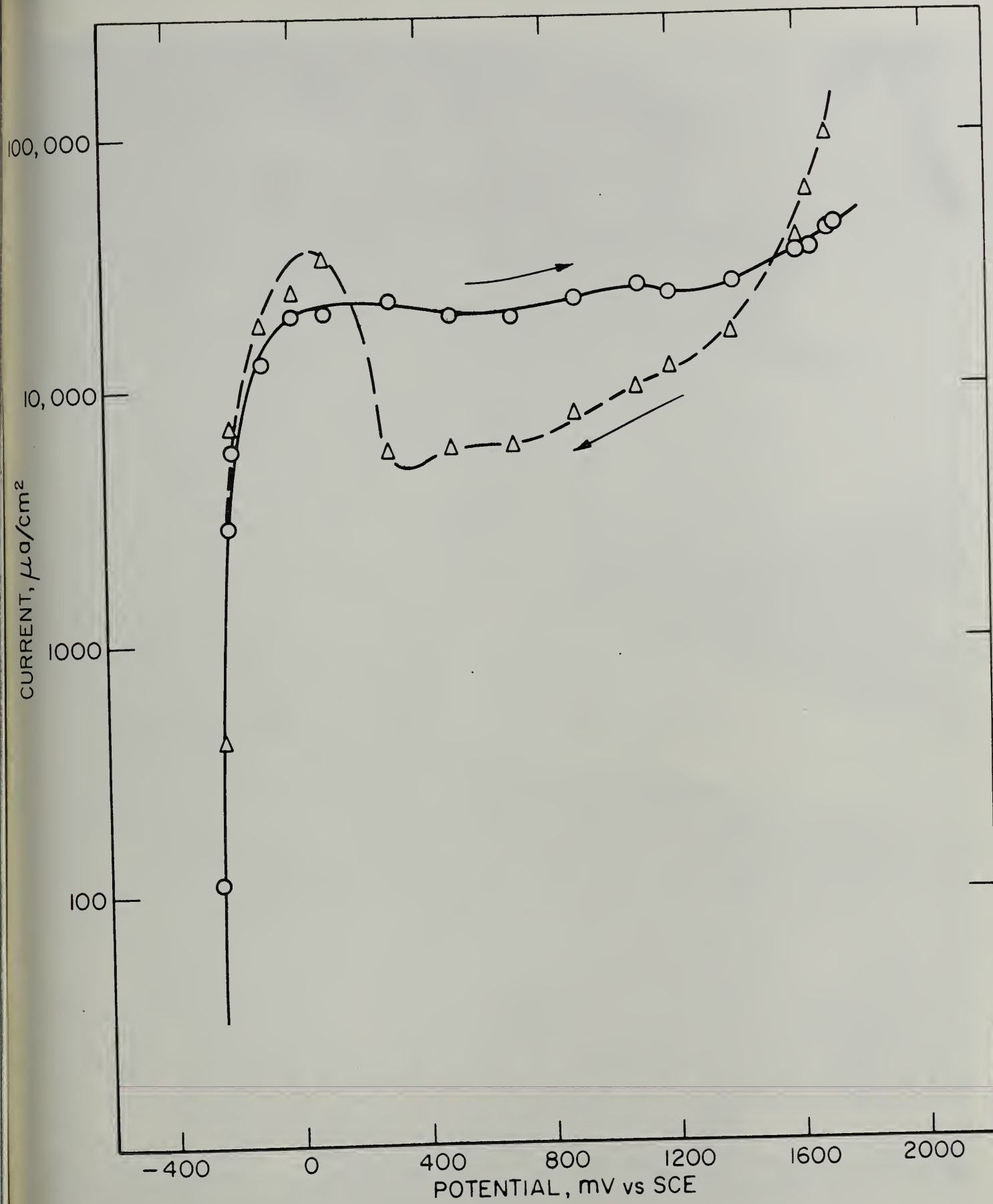


FIGURE 47

Anodic polarization curve for 7075-T651 in 1.0N NaNO_3
(pH = 0.9 with HNO_3).



FIGURE 48

Grain morphology in a long transverse section of a stress corroded 7075-T651 specimen. $M = 10,700$.



FIGURE 49

Longitudinal section of a 7075-T651 specimen illustrating precipitate distribution. $M = 30,000$.

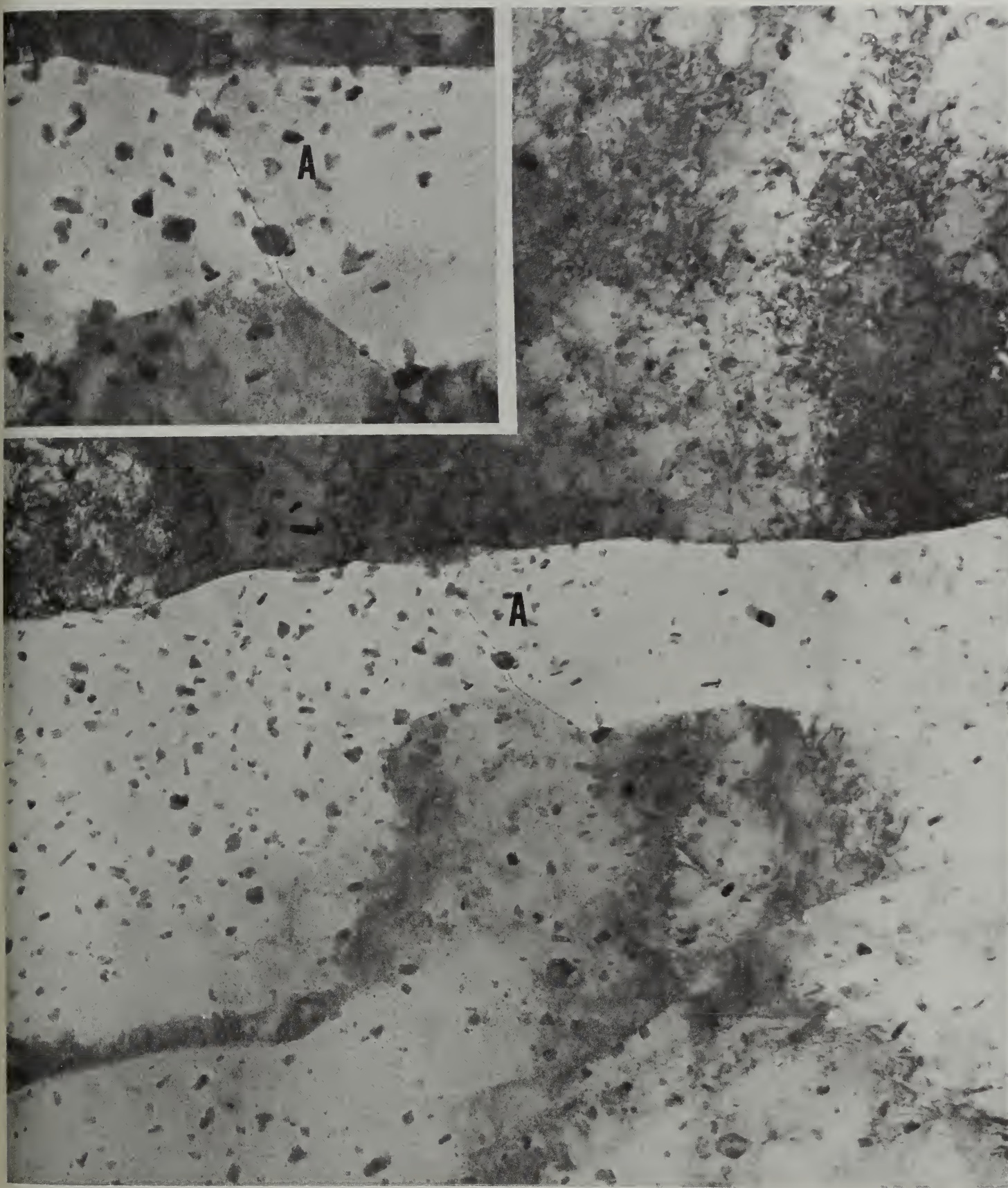


FIGURE 50

A long transverse section of a 7075-T651 specimen.
M = 34,000. The inset shows the area of a low
angle transverse boundary at M = 51,600.

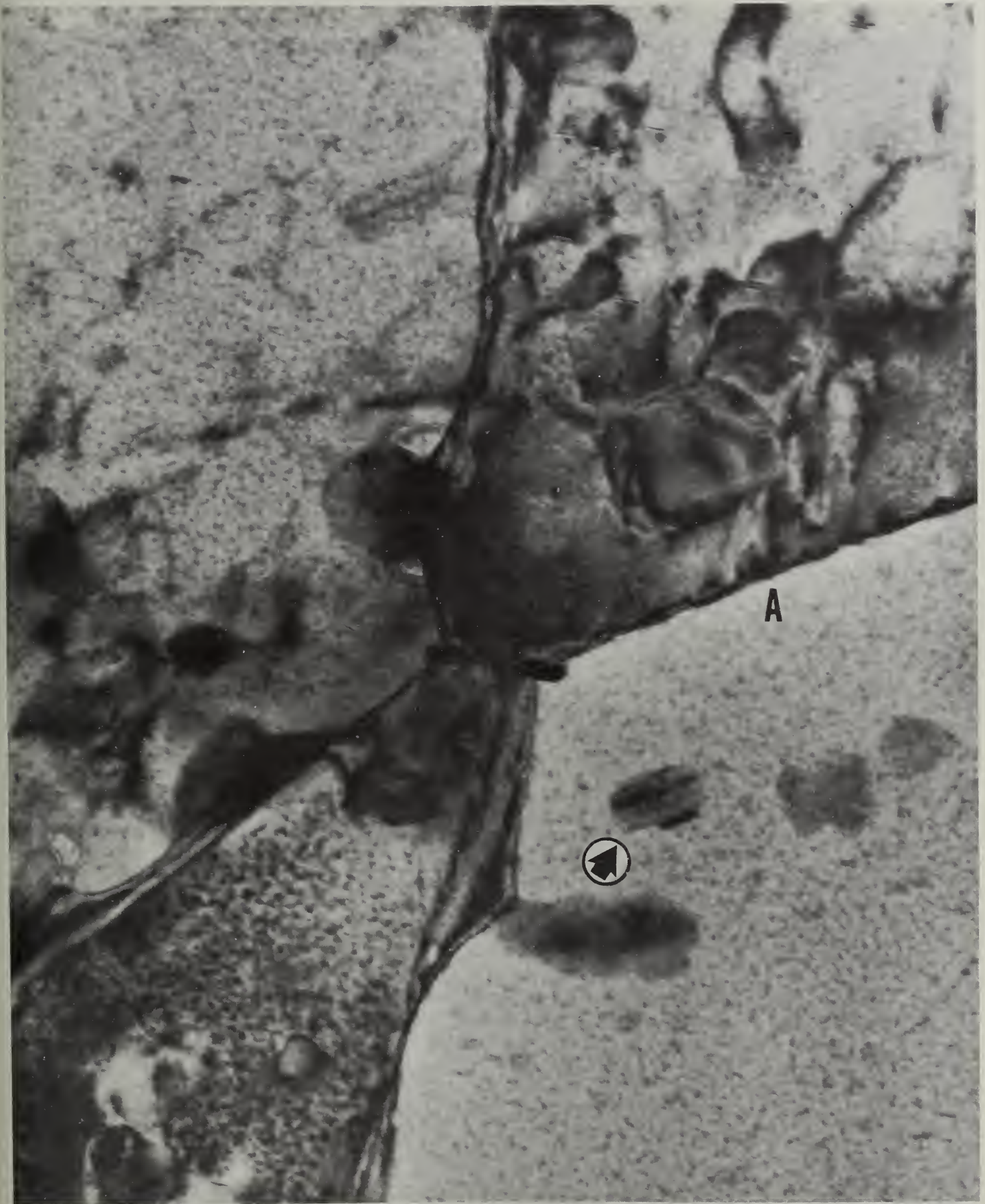


FIGURE 51a

Grain boundary and precipitate structures in the long transverse section of 7075-T651. $M = 268,000$.

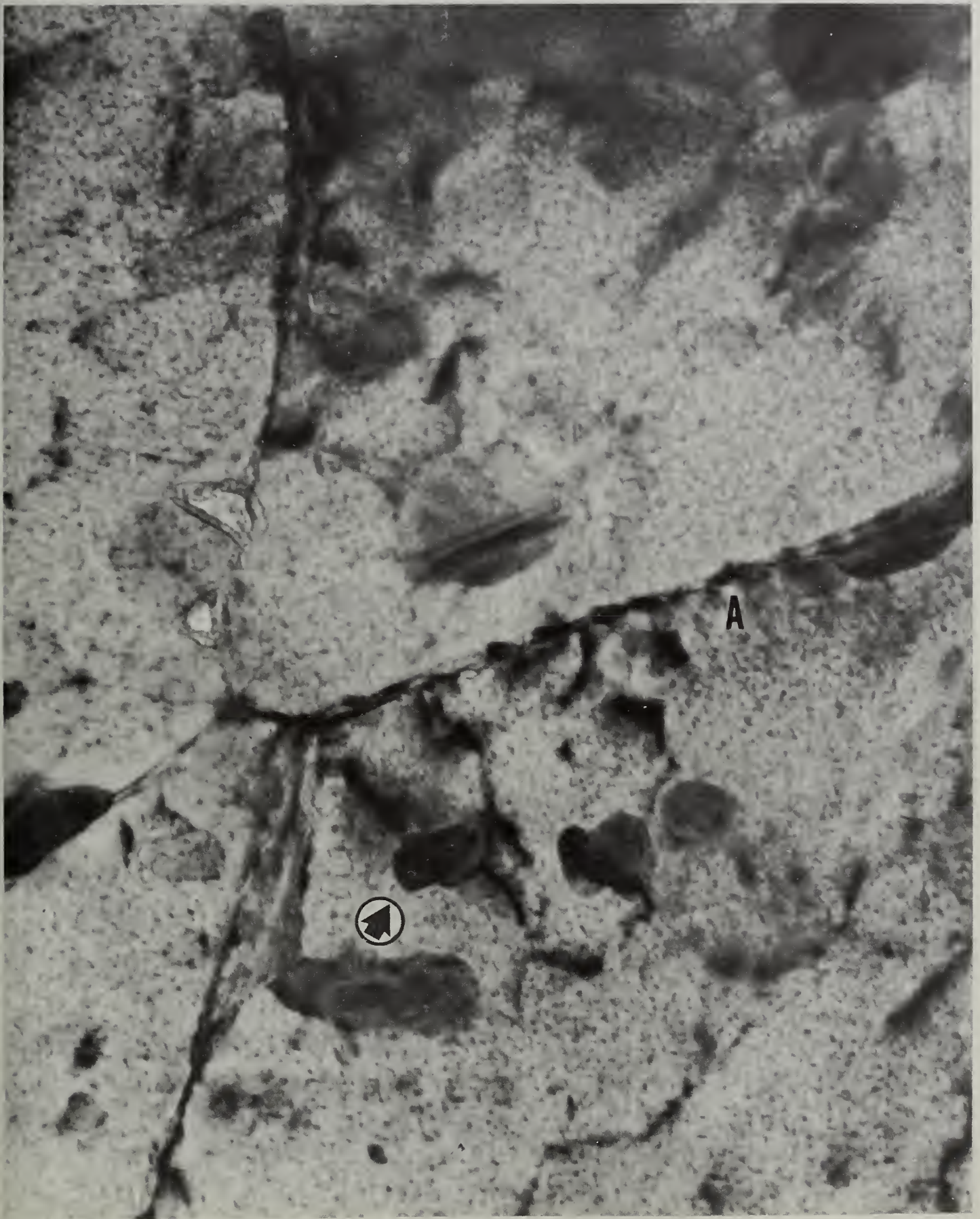


FIGURE 51b

Area of 51a tilted to show dislocation contrast.
M = 268,000.



FIGURE 52

Dislocation and precipitate interactions in a long transverse section of 7075-T651. $M = 92,000$.

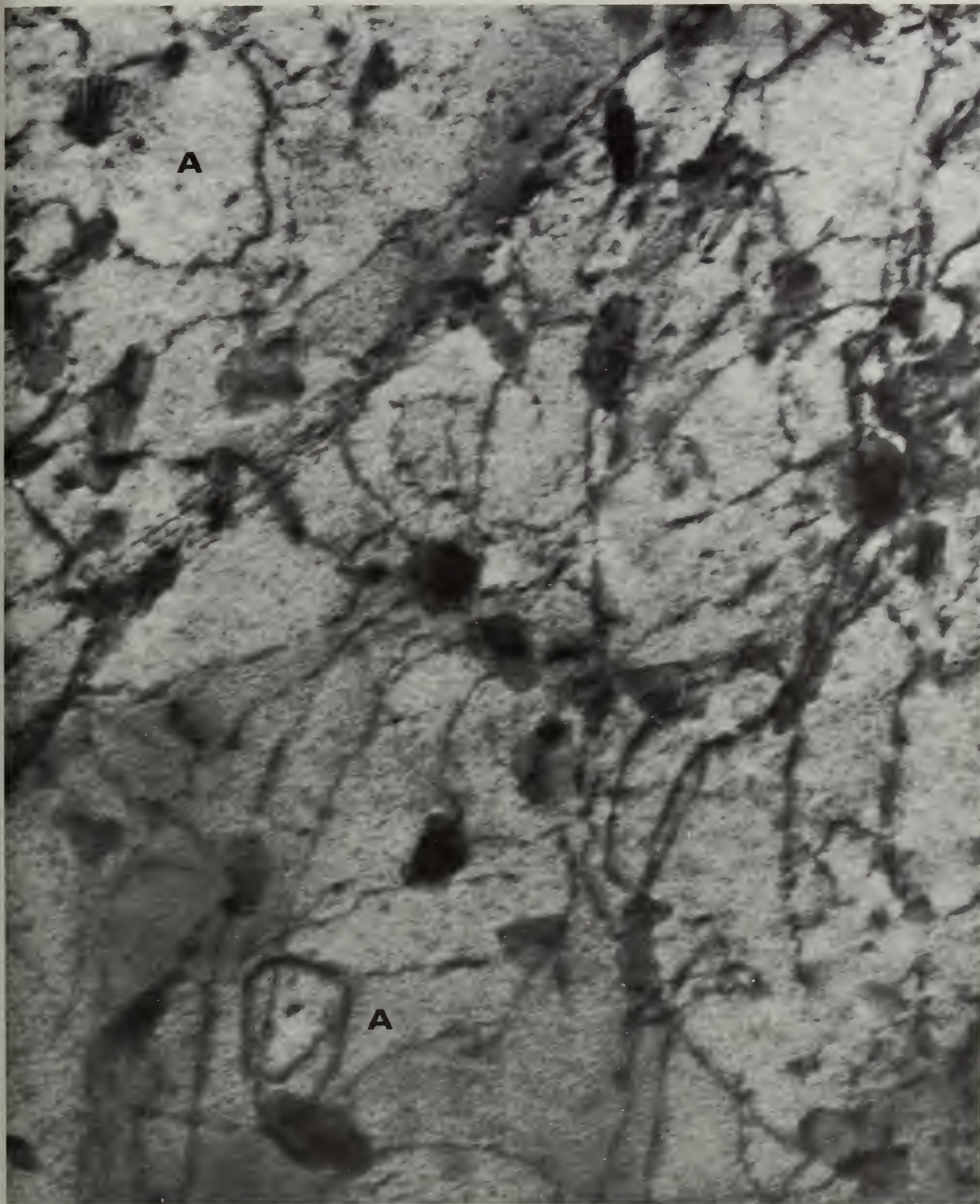


FIGURE 53

An area adjacent to a grain boundary in a long transverse section of a 7075-T651. $M = 155,000$.

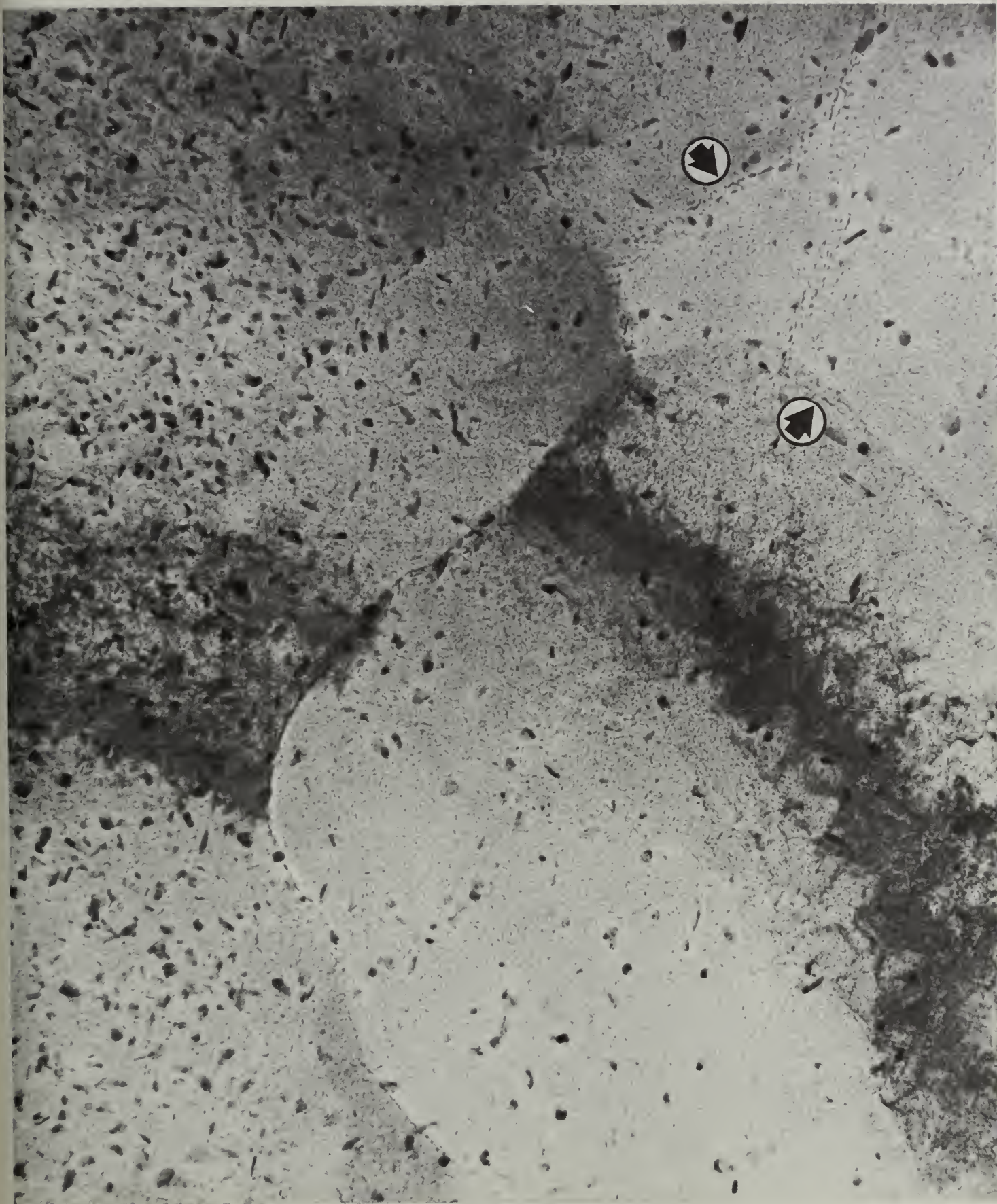


FIGURE 54

Grain and precipitate structures in a short transverse section of a 7075-T73 specimen. $M = 30,000$.

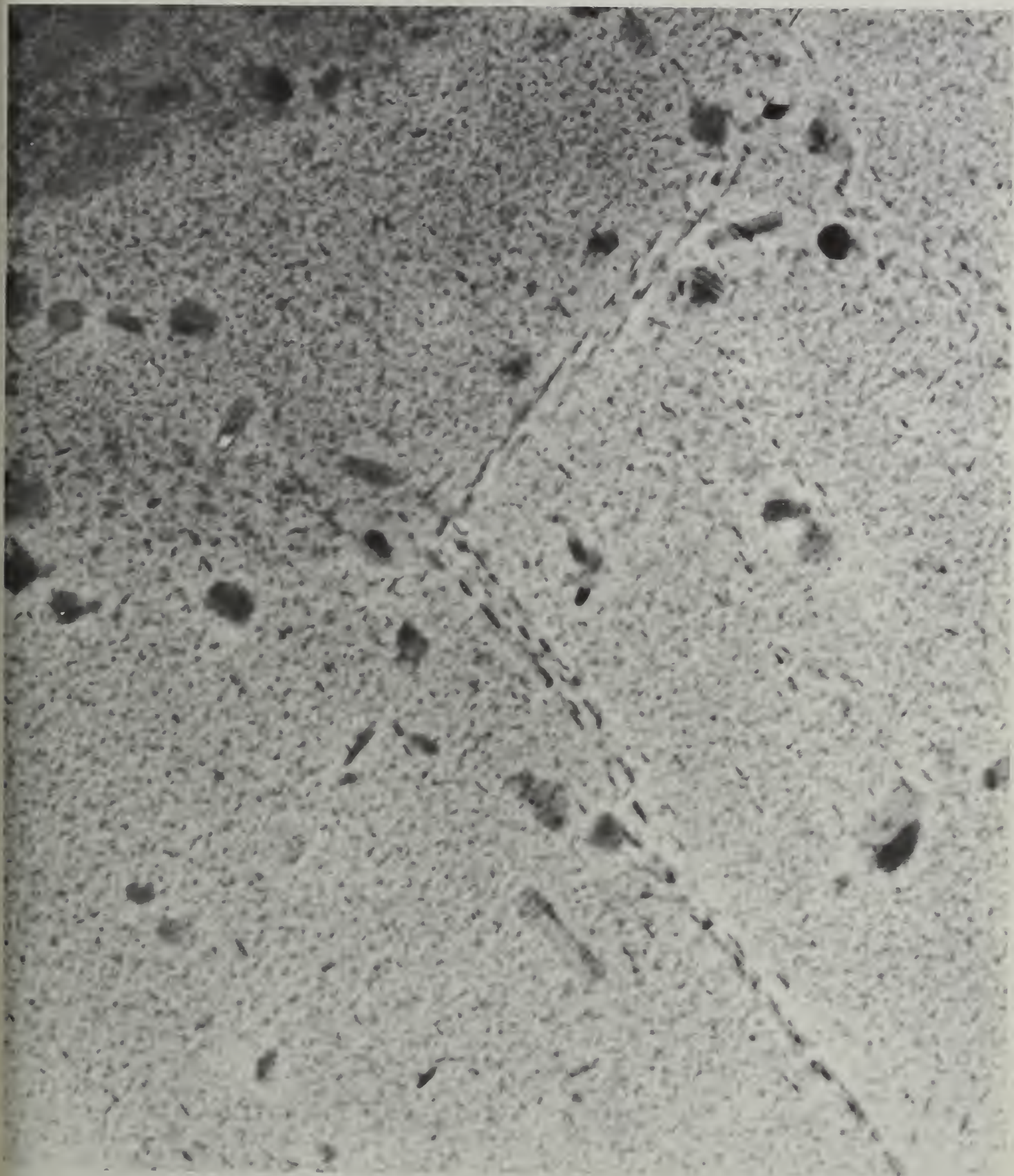


FIGURE 55

A triple grain junction region in the short transverse T73 specimen illustrating boundary precipitation and general precipitate growth. $M = 91,600$.

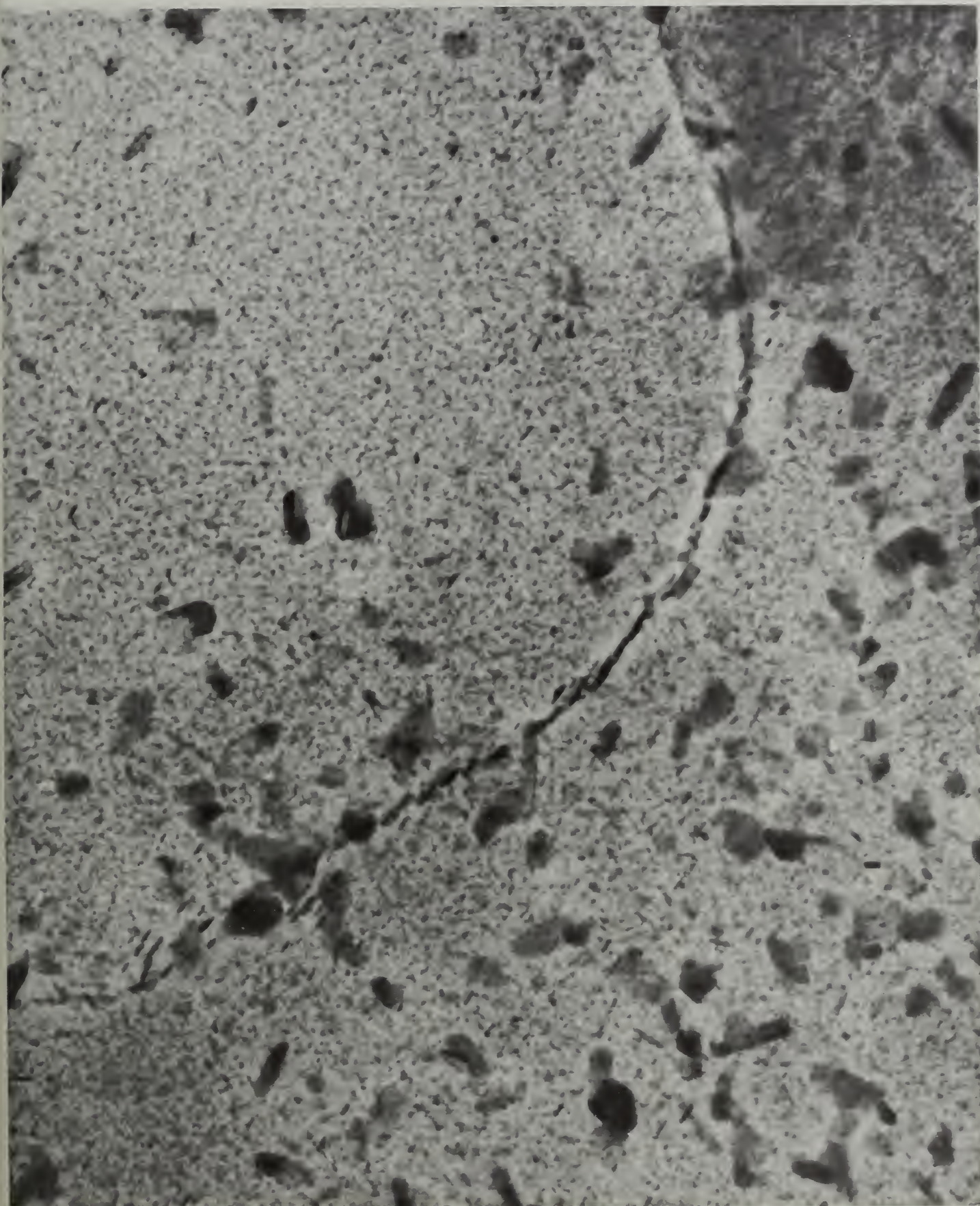


FIGURE 56

Another boundary region in the T73 condition specimen. $M = 91,300$.

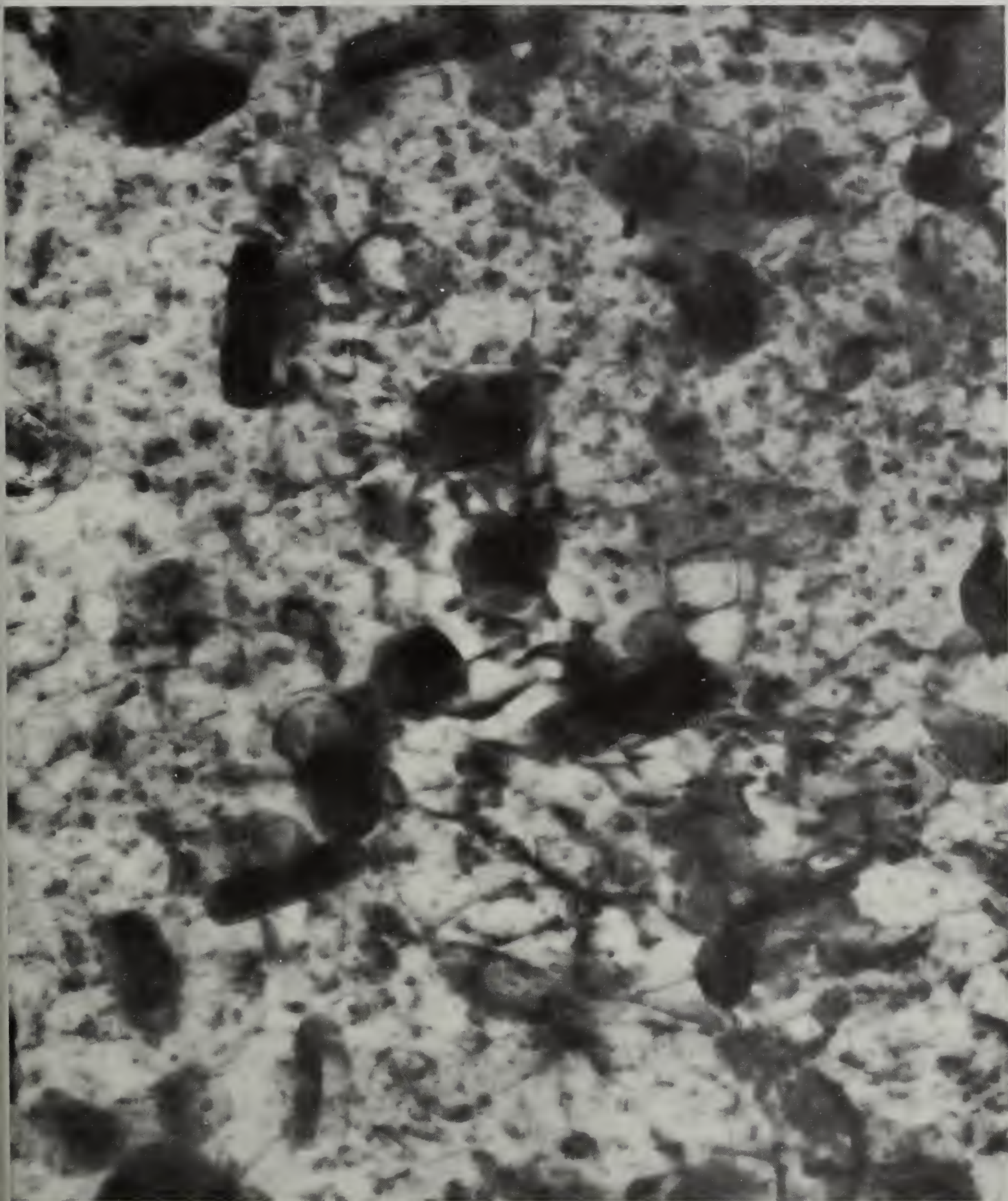


FIGURE 57

Dislocation-precipitate interactions in a short transverse section of the T73 specimen. $M = 268,000$.

